

การย่อยสลายไดยูรอนด้วยปฏิกิริยาไฟฟ้าเคมีชั้นสูงภายในเครื่องปฏิกรณ์ขนาดไมโคร



บทคัดย่อและแฟ้มข้อมูลฉบับเต็มของวิทยานิพนธ์ตั้งแต่ปีการศึกษา 2554 ที่ให้บริการในคลังปัญญาจุฬาฯ (CUIR)
เป็นแฟ้มข้อมูลของนิสิตเจ้าของวิทยานิพนธ์ ที่ส่งผ่านทางบัณฑิตวิทยาลัย

The abstract and full text of theses from the academic year 2011 in Chulalongkorn University Intellectual Repository (CUIR)
are the thesis authors' files submitted through the University Graduate School.

วิทยานิพนธ์นี้เป็นส่วนหนึ่งของการศึกษาตามหลักสูตรปริญญาวิศวกรรมศาสตรดุษฎีบัณฑิต

สาขาวิชาวิศวกรรมเคมี ภาควิชาวิศวกรรมเคมี

คณะวิศวกรรมศาสตร์ จุฬาลงกรณ์มหาวิทยาลัย

ปีการศึกษา 2558

ลิขสิทธิ์ของจุฬาลงกรณ์มหาวิทยาลัย

DEGRADATION OF DIURON VIA AN ELECTROCHEMICAL ADVANCED
OXIDATION PROCESS IN A MICROSCALE-BASED REACTOR

Mr. Worachate Khongthon



A Dissertation Submitted in Partial Fulfillment of the Requirements
for the Degree of Doctor of Engineering Program in Chemical Engineering

Department of Chemical Engineering

Faculty of Engineering

Chulalongkorn University

Academic Year 2015

Copyright of Chulalongkorn University

วรเชษฐ์ คงทน : การย่อยสลายไดยูรอนด้วยปฏิกิริยาไฟฟ้าเคมีขั้นสูงภายในเครื่องปฏิกรณ์ขนาดไมโคร (DEGRADATION OF DIURON VIA AN ELECTROCHEMICAL ADVANCED OXIDATION PROCESS IN A MICROSCALE-BASED REACTOR) อ.ที่ปริกษาวิทยานินพนธ์หลัก: รศ. ดร.วงศ์ ปวรจารย์, 182 หน้า.

การย่อยสลายไดยูรอนซึ่งเป็นยาปราบศัตรูพืชที่มีพิษซึ่งใช้กันอย่างแพร่หลายในหลายประเทศในน้ำถูกย่อยสลายได้ในเครื่องปฏิกรณ์ขนาดไมโครโดยใช้ปฏิกิริยาไฟฟ้าเคมีขั้นสูง ได้มีการใช้แผ่นแกรไฟต์และแผ่นเหล็กกล้าไร้สนิม เป็นขั้วแอโนดและแคโทด ตามลำดับ โดยผลของ ค่าพีเอช ค่าการนำไฟฟ้าของสารละลาย กระแสไฟฟ้า และความหนาของเครื่องปฏิกรณ์ ที่มีต่อการย่อยสลายไดยูรอนได้ถูกศึกษา ประมาณร้อยละ 90 ของการย่อยสลายไดยูรอนสามารถทำได้สำเร็จภายในเวลาที่สารอยู่ในเครื่องปฏิกรณ์เท่ากับ 100 วินาที ในเครื่องปฏิกรณ์ที่ป้อนกระแสไฟฟ้ากระแสตรงเท่ากับ 1 มิลลิแอมแปร์ นอกจากนี้การย่อยสลายไดยูรอนในน้ำที่ปนเปื้อนด้วยแอนไอออนได้ถูกศึกษาดูด้วยเช่นกัน ผลการทดลองบ่งบอกได้ชัดเจนว่าการย่อยสลายเกิดขึ้นหลักๆ ด้วยปฏิกิริยาระหว่างไดยูรอน กับอนุมูลไฮดรอกซิล ซึ่งเกิดขึ้นจากปฏิกิริยาแยกน้ำที่ขั้วแอโนด ถึงแม้ว่าปฏิกิริยารีดักชันของไดยูรอนจากการรีดิวซ์เกิดขึ้นด้วยก็ตาม การย่อยสลายไดยูรอนและการลดลงของปริมาณคาร์บอนในสารอินทรีย์ทั้งหมด (TOC) เพิ่มขึ้น เมื่อเพิ่มระยะเวลาที่สารอยู่ในเครื่องปฏิกรณ์ และค่ากระแสไฟฟ้าที่ป้อน แต่ในขณะเดียวกันการเพิ่มความหนาของเครื่องปฏิกรณ์ ค่าการนำไฟฟ้า และ ค่าพีเอช ของสารละลายกลับส่งผลให้ลดการย่อยสลายไดยูรอน ทั้งนี้การปนเปื้อนของไอออนในไดยูรอนยังลดการย่อยสลายไดยูรอนอีกด้วย โดยตัวแปรทั้งหมดที่ศึกษาส่งผลโดยตรงต่อปริมาณอนุมูลไฮดรอกซิล ที่เกิดขึ้นด้วยกระบวนการไฟฟ้าเคมีขั้นสูง นอกจากนี้การเกิดและการระบุโครงสร้างของสารมัธยันต์ได้ถูกศึกษาโดยใช้เครื่อง LC-MS/MS สารมัธยันต์ 15 ตัวถูกพบทั้งในสภาวะที่ไม่ปนเปื้อนและปนเปื้อนด้วยแอนไอออน สารมัธยันต์ใหม่ 2 ตัวถูกระบุได้ในสภาวะที่ปนเปื้อนด้วยไนเตรตไอออน แม้ว่าการย่อยสลายไดยูรอนเกิดสารมัธยันต์หลายตัว แต่อย่างไรก็ตามกลไกการเกิดปฏิกิริยาอันดับหนึ่งอย่างง่ายยังสามารถเป็นตัวแทนการย่อยสลายได้ดี ทั้งนี้เส้นทางการเกิดปฏิกิริยาและสมการทางคณิตศาสตร์ได้ถูกนำเสนอ ผลจากการคำนวณสอดคล้องกับข้อมูลการทดลองได้ดี โดยขั้นตอนการย่อยสลายส่วนใหญ่ในเส้นทางการเกิดปฏิกิริยาประมาณอยู่ในอัตราเดียวกัน แต่อัตราเร็วกว่าเมื่อเทียบกับ การย่อยสลายไดยูรอนด้วยกระบวนการออกซิเดชันขั้นสูงชนิดอื่นในระบบแบบดั้งเดิม

ภาควิชา วิศวกรรมเคมี

ลายมือชื่อนิสิต

สาขาวิชา วิศวกรรมเคมี

ลายมือชื่อ อ.ที่ปรึกษาหลัก

ปีการศึกษา 2558

5170616621 : MAJOR CHEMICAL ENGINEERING

KEYWORDS: DIURON / DEGRADATION / ELECTROCHEMICAL ADVANCED OXIDATION PROCESS / MICROREACTOR / ANIONS / REACTION PATHWAY

WORACHATE KHONGTHON: DEGRADATION OF DIURON VIA AN ELECTROCHEMICAL ADVANCED OXIDATION PROCESS IN A MICROSCALE-BASED REACTOR. ADVISOR: ASSOC. PROF. VARONG PAVARAJARN, Ph.D., 182 pp.

Degradation of diuron, which is a toxic herbicide widely used in many countries, in aqueous solution was done in a microscale-based reactor using electrochemical advanced oxidation process (EAOP). A graphite sheet and a stainless steel were used as an anode and a cathode, respectively. Effects of pH and conductivity of the solution, applied current, and height of the microchannel, on the degradation of diuron were investigated. About 90% degradation of diuron could be achieved within 100 s of residence time in the reactor that was applied with 1 mA direct current. Moreover, the diuron degradation in water contaminated with anions, was also studied. The experimental results clearly suggested that the degradation takes place mainly by the interaction between diuron and hydroxyl radical generated via dissociation of water at the anode, although direct reduction of diuron by supplied electrons was also observed. The diuron degradation and reduction of total organic carbon (TOC) increase with increasing residence time and applied current, while the increase in the thickness of microchannel, conductivity and pH result in the decrease in diuron degradation. The ion contamination in diuron solution also reduces the degradation. All parameters directly influence the amount of hydroxyl radicals generated via EAOP. Additionally, formation and identification of intermediates were also studied by LC-MS/MS. Fifteen intermediates were identified under no anion and anion contamination. Two new intermediates were identified under nitrate ion contamination. The degradation generates many reaction intermediates, however, a simple reaction model employing 1st kinetics could represent the degradation well. Reaction pathway and mathematical model is proposed. Simulation result shows a good agreement with experimental data. Most of the degradation steps in the degradation pathway proceed at roughly the same rate that is much faster than the degradation rate achieved by other AOPs in conventional scale.

Department: Chemical Engineering

Student's Signature

Field of Study: Chemical Engineering

Advisor's Signature

Academic Year: 2015

ACKNOWLEDGEMENTS

There has been much help and encouragement from others to make this study successful.

First and foremost I would like to thank my major advisor, Associate Professor Varong Pavarajarn for having me as one of his PhD students and for all of the extensive advice, encouragement, creative ideas, and opportunities that he has given me throughout my doctoral program. I also would like to express my sincere to Professor Goran N. Jovanovic who kindly hosted my research visit at Oregon State University. Moreover, I would also like to extend my appreciation to my thesis examination committee members; Associate Professor Sarawut Rimdusit, Associate Professor Tawatchai Charinpanitkul, Assistant Professor Apinan Soottitantawat and Dr. Nawin Viriya-empikul for their time and commitment to my doctoral program.

Further thanks go to all the professors in Chulalongkorn University, who provided me with valuable knowledge and experience during my graduate study.

This dissertation would not have been possible without all of my past and present group members in Center of Excellence in Particle Technology (CEPT), Chulalongkorn University.

This work was supported by the financial support from the Thailand Research Fund (TRF) through the Royal Golden Jubilee Ph.D. Program (Grant No. PHD/0124/2552) and Chulalongkorn University.

Finally, I would like to express the deepest appreciation and sincere gratitude to my father, mother, and brother for their endless love, enormous support, and encouragement throughout the years of my education. I would not have come this far without them.

CONTENTS

	Page
THAI ABSTRACT	iv
ENGLISH ABSTRACT	v
ACKNOWLEDGEMENTS.....	vi
CONTENTS.....	vii
CHAPTER I INTRODUCTION	1
CHAPTER II FUNDAMENTAL THEORY AND LITERATURE REVIEW	6
2.1 Diuron	6
2.2 Electrochemical advanced oxidation processes (EAOPs) for diuron degradation	8
2.2.1 Degradation of diuron by electrochemical advanced oxidation process (EAOP).....	8
2.2.2 Factors affecting to electrochemical advanced oxidation processes (EAOPs) efficiency	10
2.2.2.1 Electrode materials	10
2.2.2.2 Energy input (applied current, voltage and current density)	11
2.2.2.3 Solution pH.....	11
2.2.2.4 Liquid conductivity (ion contamination).....	12
2.2.2.5 Electrode gap.....	12
2.2.3 Intermediates and reaction pathway of diuron degradation	13
2.3 Microreaction technology	23
2.3.1 Intensification of heat and mass transport.....	23
2.3.2 Reduced size	23

	Page
2.3.3 Large surface to volume ratio	24
2.3.4 Production flexibility	24
2.3.5 Commercial applications	24
2.4 Mathematical model and simulation	26
CHAPTER III EXPERIMENTAL.....	27
3.1 Materials and chemicals	27
3.1.1 Chemicals.....	27
3.1.2 Apparatus	28
3.1.2.1 Microreactor	28
3.1.2.2 DC power supply	30
3.1.2.3 Syringe pump.....	30
3.1.2.4 Protection resistor	33
3.2 Analytical methods.....	34
3.2.1 High performance liquid chromatography (HPLC).....	34
3.2.2 Liquid chromatography – mass/mass spectrometer (LC-MS/MS)	35
3.2.3 TOC analyzer.....	36
3.2.4 UV-Visible spectrophotometer	36
3.2.5 pH and conductivity meter	37
3.3 Electrochemical degradation of diuron and reference standard compounds in microreactor.....	38
3.4 Mathematical and simulation model	40
3.4.1 Mathematical model	40
3.4.1.1 Momentum balance	40

	Page
3.4.1.2 Mass balance	44
3.4.1.3 Diffusion coefficients	45
3.4.2 Numerical method	46
3.4.2.1 COMSOL Multiphysics	46
3.4.2.2 Model development	47
3.4.2.3 Optimization	51
CHAPTER IV RESULTS AND DISCUSSION	53
4. 1 Degradation of diuron via electrochemical advanced oxidation process in microreactor.....	53
4.1.1 Characteristic of diuron degradation by EAOP in a microreactor	53
4.1.2 Effect of applied current	63
4.1.3 Microchannel thickness	66
4.1.4 Initial solution pH and conductivity	71
4.1.5 Ion contamination.....	77
4.1.5.1 Effect of nitrate and sulfate ion on diuron degradation	77
4.1.5.2 Effect of nitrate and sulfate ion on total organic carbon (TOC) removal	87
4. 2 Identification Intermediate products and reaction pathway of diuron degradation via electrochemical advanced oxidation process in a microreactor.....	90
4.2.1 The degradation of 3 reference standard compounds	95
4.2.2 Identification of main intermediates and degradation pathway of diuron during electrochemical advanced oxidation process	97

	Page
4.2.2.1 No anion contamination	97
(1) The intermediate products of diuron	97
(2) The intermediate products of 3 reference standard compounds	104
(3) Overall reaction pathway	106
4.2.2.2 Anion contamination	108
(1) Nitrate and nitrite ion contamination.....	108
(2) Sulfate and persulfate ion	113
(3) Overall reaction pathway	116
4. 3 Mathematical model and simulation for diuron degradation in EAOP microreactor.....	117
4.3.1 Mathematical model for diuron degradation and reference standard compounds	117
4.3.2 Mathematical model for pathway of diuron degradation in EAOP microreactor	124
CHAPTER V CONCLUSIONS AND RECOMMENDATIONS	129
5.1 Summary of results	129
5.2 Conclusions.....	129
5.3 Recommendations	131
REFERENCES.....	133
APPENDICES.....	142
APPENDIX A CALIBRATION DATA ANALYSIS.....	143
APPENDIX B PROCEDURE OF CHEMICAL PREPARATION	148

	Page
APPENDIX C LIQUID CHROMATOGRAPHY–MASS/MASS SPECTRUM (LC-MS/MS) DATA.....	152
APPENDIX D CALCULATION OF DIFFUSION COEFFICIENTS.....	162
APPENDIX E INPUT PARAMETERS AND VARIABLES IN NUMERICAL MODEL	164
APPENDIX F PROCEDURE OF OPTIMIZATION OF NUMERICAL MODEL	170
APPENDIX G TOXICITY TEST	179
APPENDIX H PUBLICATIONS.....	181
VITA	182



CHAPTER I

INTRODUCTION

Several pesticides and herbicides are used worldwide in many agricultural and aquacultural activities. Thailand is also the one agricultural country that involves using several pesticides and herbicides. Due to run-off of them still exists in environment, the occurrence of environmental problem are dramatically risen [1]. Diuron or 3-(3, 4-dichlorophenyl)-1, 1-dimethyl urea is one of the most commonly herbicide that used to eliminate and control unwanted weed [2]. It is classified to be phenylurea herbicides which are carcinogenic and genotoxic compound [3]. Since its properties, strong toxicity, great bio-recalcitrant with great chemical stability, long half-life in soil with over 370 days and slowly degradation in nature, it can slowly penetrates through soil contaminating in underground water and surface water at a ppm level [4-7]. Therefore, the contamination of diuron in environment becomes very serious. Especially, as diuron was degraded, many intermediates are generated, which some intermediates are more toxic than parents [4, 6, 8]. The last decades, environmental problems of diuron have been mostly published by several researchers [9]. Figure 1.1 shows the relative frequency of studies dealing with different pesticide classes defined in Directive 2013/39/EU treated, which diuron is considered the most studied pesticides for treatment.

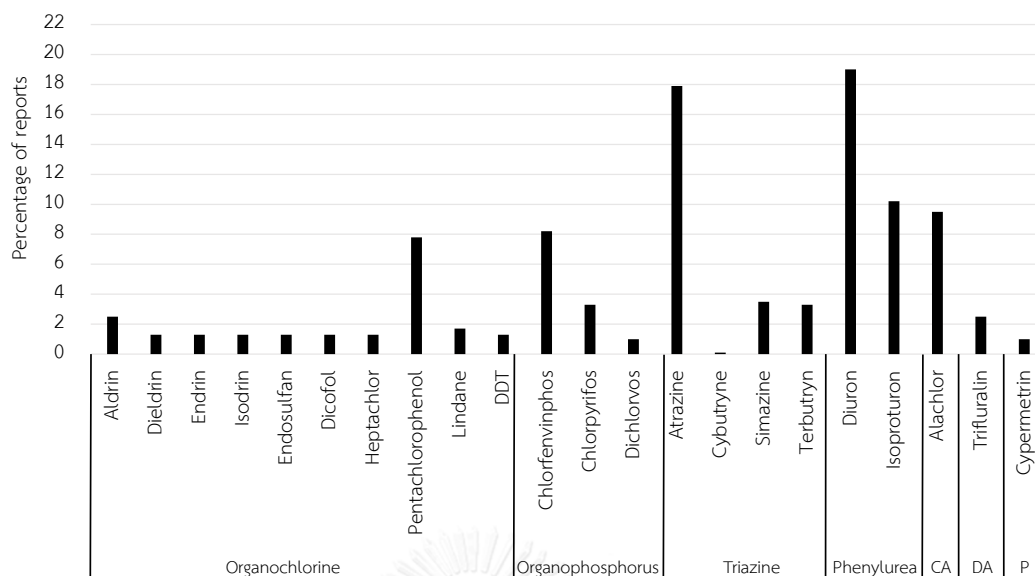


Figure 1.1 shows the relative frequency of studies dealing with different pesticide classes defined in Directive 2013/39/EU treated [9]

Nowadays, many reports have been published for the methods of removal diuron including adsorption [10], biological treatment [11] and advanced oxidation processes (AOPs) [3, 12, 13]. Due to high degradation efficiency of AOPs, recognized to be tools for destruction recalcitrant compounds or at least for transformation them into biodegradable [9]. Recently, electrochemical advanced oxidation processes (EAOPs), which is classified to be AOPs, are also being developed for many types of organic pollutant in water treatment application [14-17]. EAOPs is classified to be in miscellaneous of different types of AOPs as shown in figure 1.2 [9]. However, there are few researchers that have studied the degradation of diuron by EAOPs [18-20]. These technique generally produces in situ hydroxyl radical ($\cdot\text{OH}$), are formed via dissociation of water (oxidation of water), at an anode surface which radicals react and mineralize organic compounds. Hydroxyl radicals have high standard redox potential ($E_0(\cdot\text{OH}/\text{H}_2\text{O}) = 2.8 \text{ V/SHE}$).

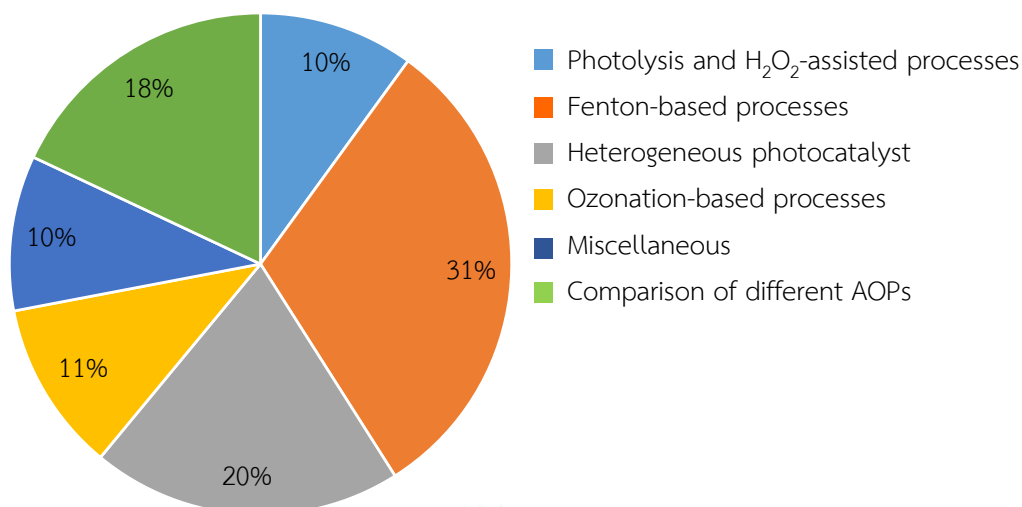


Figure 1.2 Relative frequency of reports of different types of AOPs to treat priority substances in the field of water policy, according to the Directive 2013/39/EU [9].

Efficiency of EAOPs in water treatment strongly depends on many parameters which are applied potential, electrode material, solution conductivity, solution pH and additives (salts and ions) [21, 22]. Many types of anode electrodes are applied to EAOPs [14, 15, 22]. Carbon and graphite also has been considered to be anode for EAOPs due to it is cheap and greatly produced hydroxyl radical under supplied voltage in range 2.7-4.0 V [23]. Under low current density of electrode condition ($\leq 5 \text{ mA/cm}^2$), low corrosion effects on anode surface was observed which this type electrode can be operated for several working hour [24].

Generally, there are common anions contaminated in drinking water source (nitrate and sulfate ion) releasing form household activities, agricultural activities and industrial effluents [21, 25]. Ion is one of the important parameter influences to degradation and formation intermediates which there are a few researchers have studied using AOPs [26-28].

Over the past decade, microfluidic technology has been increasingly interested applying to chemical reaction processes which it is well known that the microreactor shows many advantages over conventional scales to improve the efficiency of chemical reaction including (i) an increase in surface-to-volume ratio, (ii) negligible mass and heat transfer resistances, (iii) easy control of residence time, and (iv) enhanced control of reaction conditions [29]. Generally, the efficiency of the conventional electrochemical process depends on mass transfer of substrate to the surface of electrode [30]. Low current efficiencies are usually achieved when a high abatement of the organic pollutants is required, mostly due to the fact that, the rate determining step in the electrochemical conversion of the pollutant is its mass transfer towards electrodes whose rate is extremely reduced at low pollutant concentrations [31]. Therefore, applying electrochemical oxidation in microreactor could solve the problem, which significantly enhance efficiency of degradation although no supporting electrolyte [31, 32].

The prime of this research are to investigate efficiency of diuron degradation via electrochemical advanced oxidation process in microreactor and to investigate reaction pathway and identify intermediate compounds during diuron degradation. Furthermore, mathematical model is also developed to simulate reaction rate constants and concentration profiles of diuron and its intermediates for describing reaction pathway.

The thesis consisted of 5 main chapters as shown below:

Chapter I gives motivation and introduction of this work.

Chapter II describes fundamental knowledge and theory of diuron, its intermediates and the degradation of diuron by electrochemical advanced oxidation process (e.g. its characteristic, mechanism of EAOP and factors affected to EAOP efficiency). Moreover, the definition and advantages of microreactor over conventional reactor are presented. Literature review of previous work related with this work is also provided in this chapter.

Chapter III provides chemicals, microreactor apparatus, experimental set up, analytical methods and electrochemical degradation of diuron procedure.

Chapter IV describes experimental results and discussion of this research.

Chapter V gives overall conclusions and recommendations of this work.



CHAPTER II

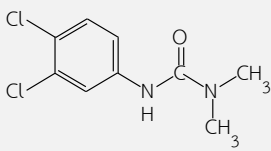
FOUNDAMENTAL THEORY AND LITERATURE REVIEW

This chapter provides fundamental theory and literature review relating of diuron properties, intermediates formed during diuron degradation, reaction pathway. Additionally definition of electrochemical advanced oxidation processes (EAOPs) and microreactor will be described. Finally, mathematical and simulation model for simulating diuron degradation via EAOP in microreactor will be described.

2.1 Diuron

Diuron or 3-(3,4-dichlorophenyl)-1,1-dimethylurea) is commonly herbicide classified in the family of phenylurea compound. It is widely used for elimination or control grass and broadleaf weed by inhibiting photosynthesis in a wide variety of agricultural activities [3]. Properties of diuron are highly toxic, bio-recalcitrant and chemically stable with half-life in soil over 370 days [4, 33]. Due to diuron is slightly soluble, non-volatile compound and slowly degraded over 3-4 months under solar irradiation, it can gradually penetrate through soil leading to contaminate in surface and underground water [33]. Moreover, during diuron degradation, aromatic amines are known to be one of the degradation products, which often results in toxic intermediate compounds that can induce cancer [34]. Moreover, in Europe-wide survey, diuron was detected in 70% of European river samples so it is considered a priority substance [35]. Recently, Directive 2013/39/EU also considers diuron as first priority substances [9]. Therefore, diuron contamination in environment became very serious. Physical properties of diuron are shown in table 2.1.

Table 2.1. Physicochemical properties of diuron.

Properties	Data
Chemical structure	
Molecular formula	$C_9H_{10}Cl_2N_2O$
Molecular weight	233.10
Melting point	158 – 159°C
Vapor pressure	0.0041 Pa at 30°C
Appearance	 <p>White crystalline solid</p>
Synonyms	3-(3,4-dichlorophenyl)-1,1-dimethylurea, Cekiuron, Crisuron, Dailon, Diater, Di-on, Direx, , Diurex, Karmex, Unidron,Uridalk, Weedex
Solubility	42 mg/l in water at 20°C
Toxicity	The concentrated material may cause irritation to the eyes and mucous membrane, but a 50% water paste was not irritating to the intact skin of mammal
Half-life	Over 370 days in soil

2.2 Electrochemical advanced oxidation processes (EAOPs) for diuron degradation

Nowadays, many reports have been published for the removal of diuron in aqueous solution including adsorption [10], biological treatment [11] and advanced oxidation processes (AOPs) [3, 12, 13]. Due to high degradation efficiency of AOPs, recognized to be tools for destruction recalcitrant compounds or at least for transformation them into biodegradable [9]. Advanced oxidation processes have been defined as water treatment processes that involve an input of energy (either chemical, electrical or radioactive) into the water matrix to produce highly reactive species, which then attack and destroy the organic compounds. Most advanced oxidation processes for water and wastewater treatment are based on generation of hydroxyl radicals to initiate oxidations. Many techniques are classified to be AOPs applying to waste water treatment, which are Ultraviolet photolysis, ozone oxidation, Fenton reaction, photocatalysis and electrical discharge [8, 13, 28, 36, 37]. Among the AOPs, Electrochemical advanced oxidation processes (EAOPs), has been studied as a successful technology for the degradation of several organic compounds including diuron [18-20]. The difference between photocatalytic reaction and electrochemical oxidation is the mechanism of production of hydroxyl radical. The hydroxyl radical was induced by light under photocatalytic reaction while hydroxyl radical was induced by electrical source under electrochemical oxidation at anode [9].

2.2.1 Degradation of diuron by electrochemical advanced oxidation process (EAOP)

Electrochemical advanced oxidation processes, pollutants can be removed by (i) direct electrolysis, where pollutants exchange electrons directly with the anode surface without involvement of other substances, or (ii) indirect electrolysis, where organic pollutants do not exchange electrons directly with the anode surface but rather through

the mediation of some electroactive species regenerated there, which act as intermediaries for electrons shuttling between the electrode and the organic compounds [24]. Indirect electrolysis can be a reversible or an irreversible process, and the redox reagent can be electrogenerated by either anodic or cathodic process. Process selection depends on the nature and structure of the electrode material, experimental conditions, and electrolyte composition [24]. In this work, graphite sheet was selected to be anode, which are classified as inactive electrodes. Inactive electrode are electrode materials whose atoms do not change oxidation state during electrochemical reactions, which hydroxyl radical ($\cdot\text{OH}$) generally produces via dissociation of water (discharge of water) at an anode surface as shown in equation 2.1 [38]. Hydroxyl radicals, are unselectively and very powerful, rapidly react and mineralize diuron compounds due to its high standard redox potential ($E^0 (\cdot\text{OH}/\text{H}_2\text{O}) = 2.8 \text{ V/SHE}$). Additionally, hydroxyl radical interaction together results in the formation of hydrogen peroxide (H_2O_2) near to the electrode's surface as shown in equation 2.2 [39, 40]. Thus, the degradation of diuron is competing for hydroxyl radicals with the production of hydrogen peroxide reaction as shown in equation 2.3. Figure 2.1 shows mechanism of diuron degradation via EAOP in microreactor.



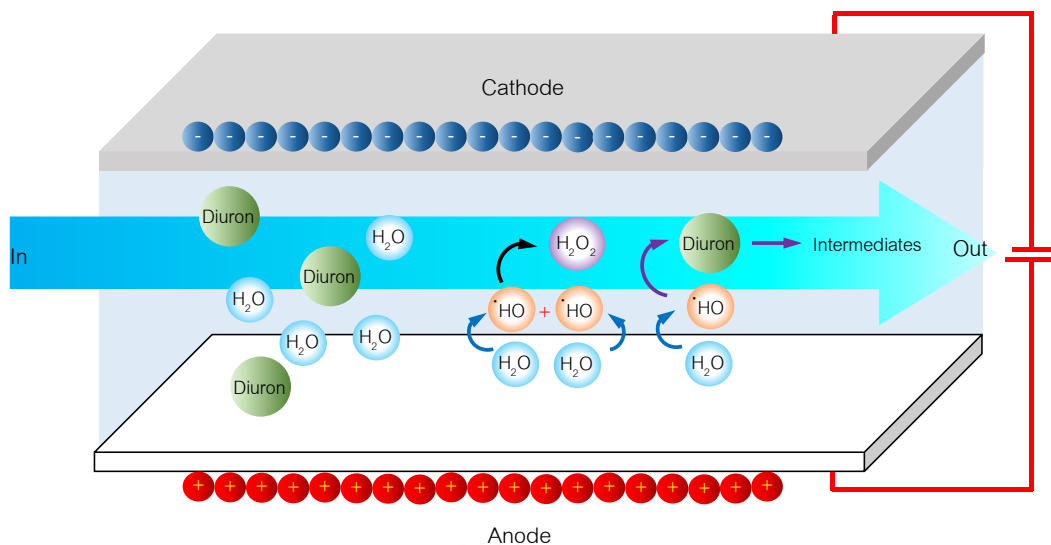


Figure 2.1. Mechanism of diuron degradation via EAOP

2.2.2 Factors affecting to electrochemical advanced oxidation processes (EAOPs) efficiency

There are several operating variables that influence the electrochemical oxidation of organic pollutants, as listed in the following:

2.2.2.1 Electrode materials

Many types of anode electrodes are applied to EAOPs [14, 15, 22]. Traditionally, anode materials used for water treatment such as boron-doped diamond (BDD) [17-19], dimensionally stable anode (DSA) [41] and carbon or graphite [23]. The electrode material must have the following properties [30]: (i) high physical and chemical stability; resistance to erosion, corrosion and formation of passivation layers, (ii) high electrical conductivity, (iii) catalytic activity and selectivity and (iv) low cost/life ratio. The use of electrode materials that are inexpensive and durable must be favored.

Carbon and graphite also has been considered to be anode for EAOPs due to it is cheap and greatly produced hydroxyl radical under supplied voltage in range 2.7-4.0 V [23]. Under low current density of electrode condition ($\leq 5 \text{ mA/cm}^2$), low corrosion effects on anode surface was observed which this type electrode can be operated for several working hour [24]. Drawback of graphite sheet is due to graphite sheet is not quit hard when thickness (electrode gap) is too small, graphite surface (anode) could contact with cathode surface resulting in short circuit.

2.2.2.2 Energy input (applied current, voltage and current density)

Energy input is considered as an important operating parameter for electrochemical oxidation of organics in term of both mechanistic study and cost effectiveness analysis. In electrochemical oxidation, the capability of electron transfer and generation of oxidizing agents ($\cdot\text{OH}$), significantly depend on the energy input. Increasing energy input enhances electrochemical oxidation, which have been reported by several researchers [15, 17, 42]. Although high energy input increases the electrochemical oxidation of many pollutants, consumption of energy spontaneously increases. Thus, the optimum condition need to be considered.

2.2.2.3 Solution pH

Solution pH is one important factor for electrochemical oxidation of organic pollutants, which depends on types of the target pollutants, supporting electrolytes and electrodes. In general, the removal efficiency of organic pollutants via electrochemical oxidation tends to increase in the lower pH range including degradation of diuron [19]. One reason to explain is the $\cdot\text{OH}$ exhibits higher oxidative potential in the lower pH range following Nernst relationship as shown in equation 2.4 [43].

$$E^0(\cdot OH_{aq}/H_2O) = 2.59 - 0.059pH \quad 2.4$$

Additionally, more hydroxyl radicals are generated at low pH [39], while the hydroxyl radical behaves as a weak acid and reacts with OH⁻ ion to form O⁻ in a basic solution [44]. As a result, decreased amount of hydroxyl radicals are available at high pH.

2.2.2.4 Liquid conductivity (ion contamination)

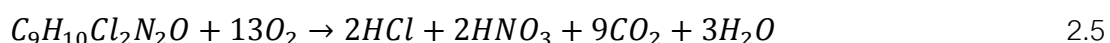
Solution conductivity is one of the important factors to electrochemical oxidation. In general, solution conductivity depends on types and concentrations of ions contaminated in solution. Increasing ion concentrations spontaneously increases solution conductivity. In nature, there are common anions contaminated in drinking water source (nitrate and sulfate ion) releasing from household activities, agricultural activities and industrial effluents [21, 25]. These ions are mainly considered to be hydroxyl scavenger reducing organic degradation efficiency [45], which sulfate ion acted as higher order of hydroxyl radical scavenger than nitrate ion [17, 46]. Additionally, the effect of the conductivity seems to be less pronounced when the solution is high conductivity leading to low oxidation [47].

2.2.2.5 Electrode gap

Normally, the efficiency of the electrochemical process depends on mass transfer of substrate and electron to the surface of electrode [30]. Decreasing distance between electrodes, higher degradation of organic compound was obtained due to more effective mass transfer [32].

2.2.3 Intermediates and reaction pathway of diuron degradation

As diuron is degraded, it generated many by-product compounds which have higher toxic effect than parent [8, 35, 48]. It is hence of interest not only to monitor the degradation of the parent compound but also to identify the intermediate compounds formed. The complete oxidation of diuron was proposed as followed in equation 2.5 [3].



Intermediates and reaction pathways of diuron were reported by many researchers by advanced oxidation processes (AOPs), which hydroxyl radical is mainly induced to form intermediate products. The one of main pathway is the diuron degradation yields mainly 2 hydroxychloro-products via hydroxylation, through a substitution of a chlorine atom by OH simultaneously, which dechlorination and hydroxylation take place [8, 49, 50]. The next pathway involved a series of oxidation processes that eliminated alkyl groups at side chain of diuron molecule, which is demethylation process [49]. Additionally, it was reported that C atom on methyl group and C atom connected with Cl atom on aromatic ring of diuron molecule are the favorable positions that hydroxyl radical preferred to attack because of the lower barrier energy comparing with C atom at another positions [4, 51]. In addition, dechlorination of diuron alone is taken place by electrophilic substitution after transferring of electrons results in the formation of reduction products [8]. The last step of diuron degradation involved oxidative opening of the aromatic ring after demethylation, hydroxylation and dechlorination take place, leading to small organic ions and inorganic species [3]. Therefore, it could be concluded that the main pathways of diuron degradation by AOPs as following: (i) demethylation, (ii) hydroxylation and (iii) dechlorination or dehalogenation

alone. The example of intermediate products and reaction pathways of diuron degradation are shown in figure 2.2, 2.3 and 2.4.

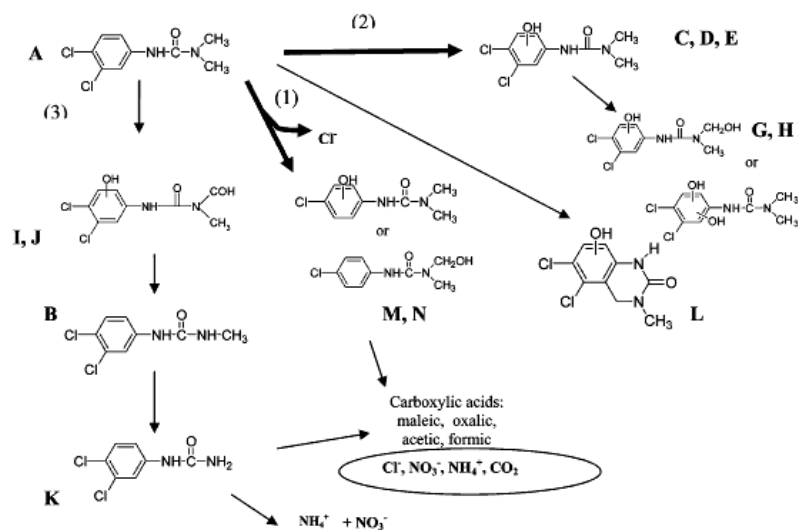


Figure 2.2 The reaction pathway of diuron pathway by photocatalytic reaction was proposed by Carrier et. al. (2009) [4]

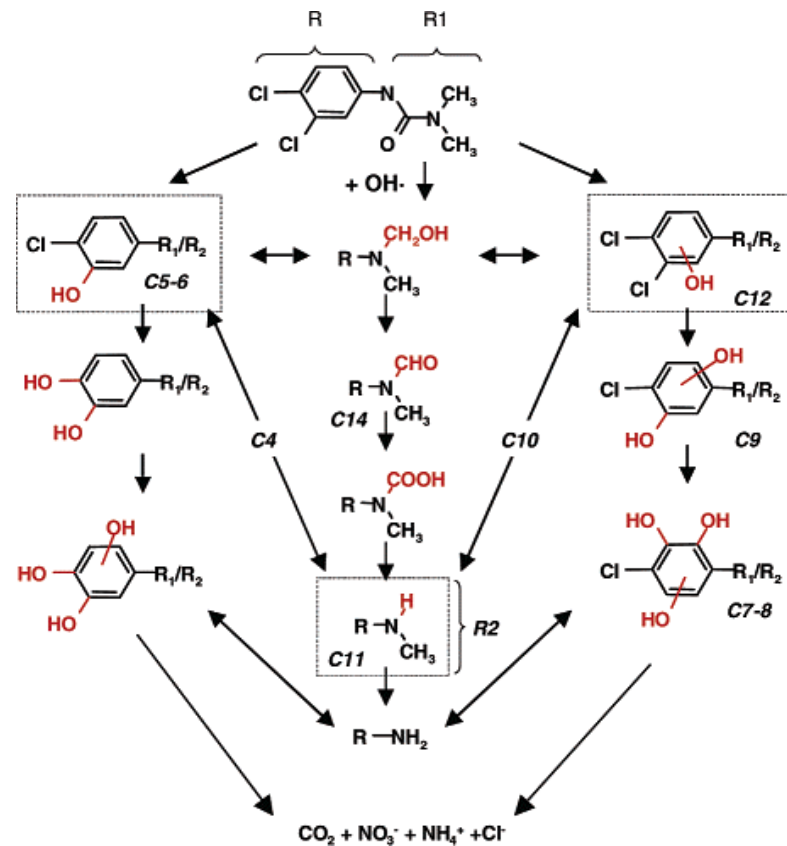


Figure 2.3 Proposed degradation pathway of diuron using photocatalysis (TiO_2 and photo-Fenton) by Malato et. al. (2003) [6]

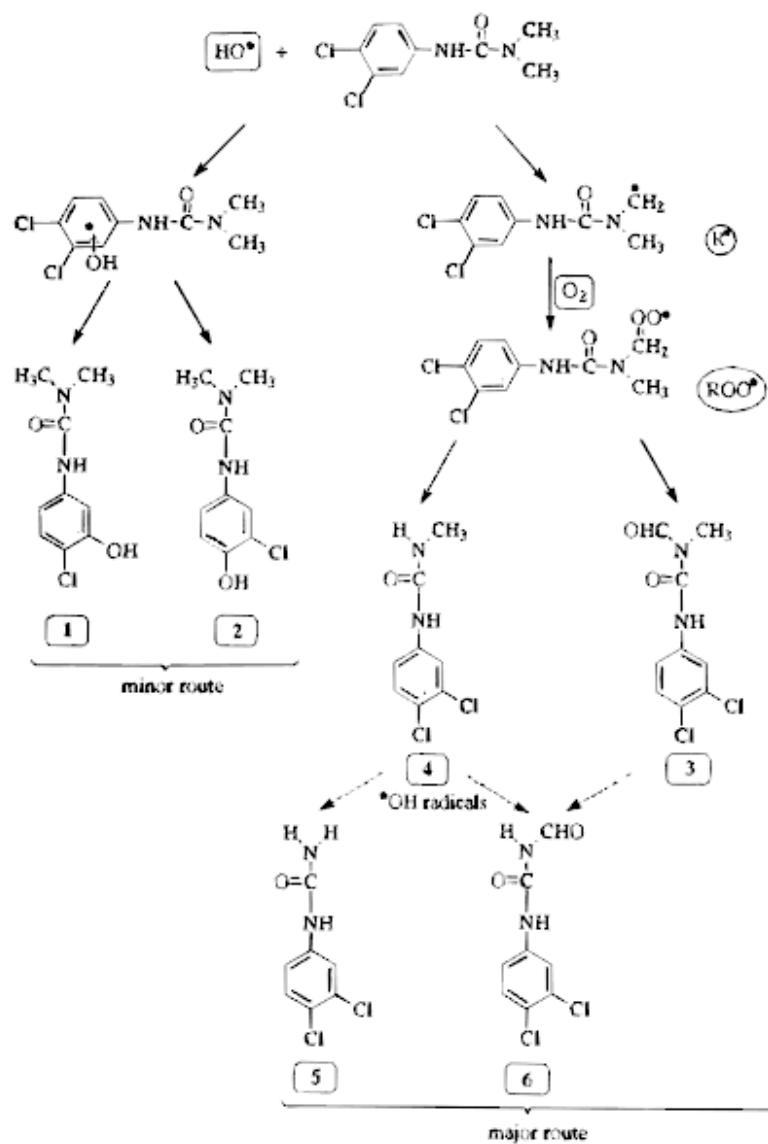


Figure 2.4 Routes of photodegradation of diuron induced by iron (III) is proposed by

Mazellier et. al. (1997) [36]

Furthermore, it has been reported that ion contamination influences to the formation of intermediates via AOPs [52, 53]. Nitrate products are identified generated by nitrate and nitrite-induced phototransformation of monuron via photodegradation [52]. The reaction pathway of monuron degradation contaminated by nitrate and nitrite ion (NO_3^- and NO_2^-) is shown in figure 2.5. Moreover, contamination of nitrate and nitrite ions influence to the formation of nitrate-products during phenol degradation under electrical discharge as shown in figure 2.6 [53]. In the present, several researchers reported structure of possible intermediates generated during diuron degradation identified in advanced oxidation processes (AOPs) including nitrate-products as shown in table 2.2.



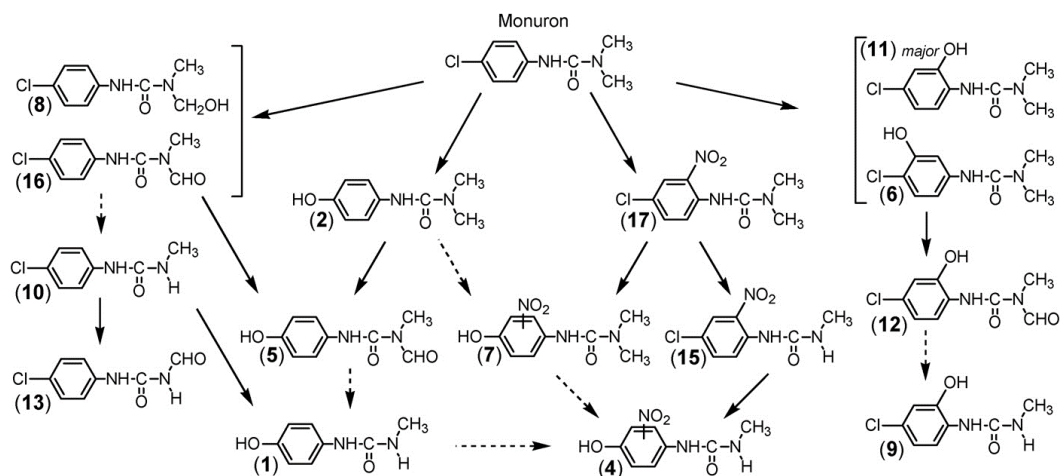


Figure 2.5 Pathways of monuron photo-induced degradation by nitrate and nitrite ion is

proposed by Nelieu et. al. (2008) [52]

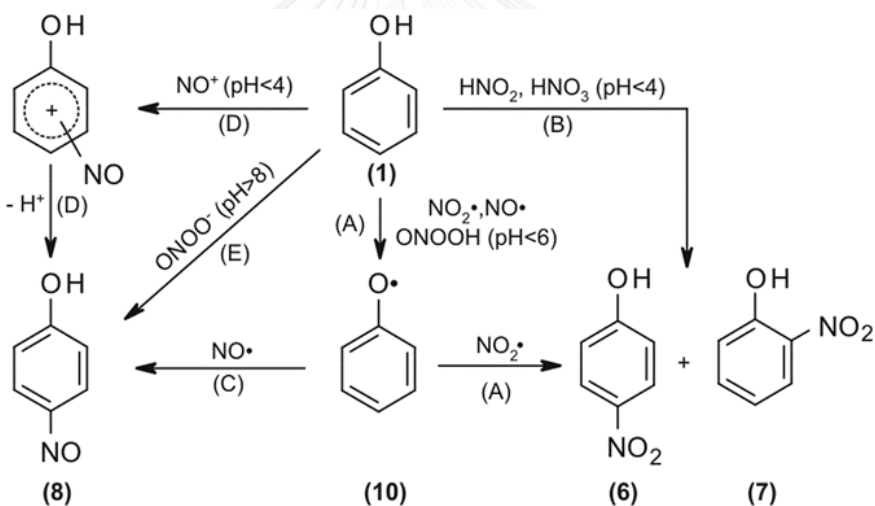
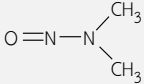
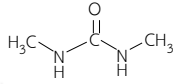
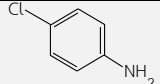
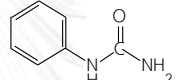
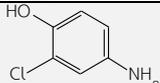
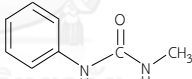
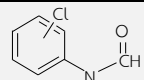
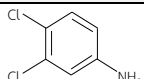
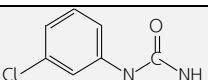
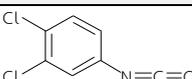
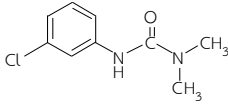
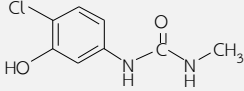
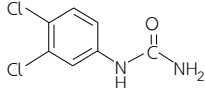
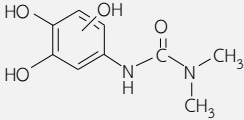
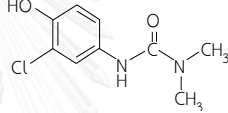
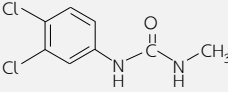
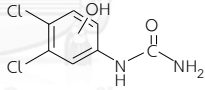
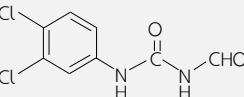
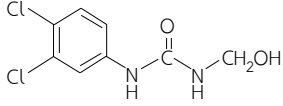
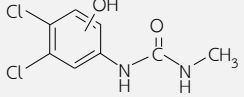
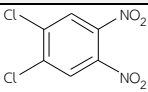


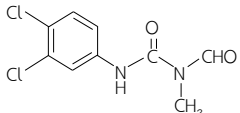
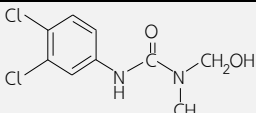
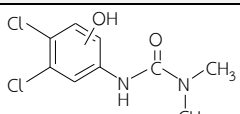
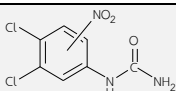
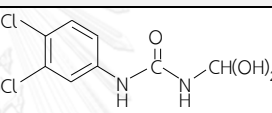
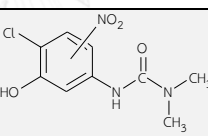
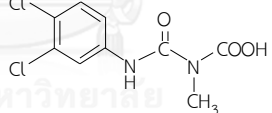
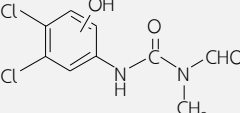
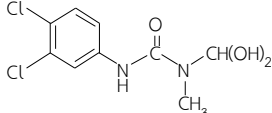
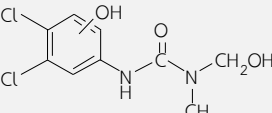
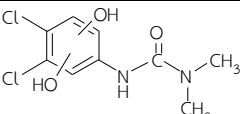
Figure 2.6 Possible reaction pathways of phenol degradation to form nitrated products is

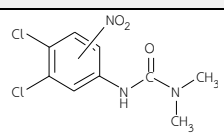
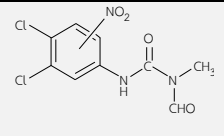
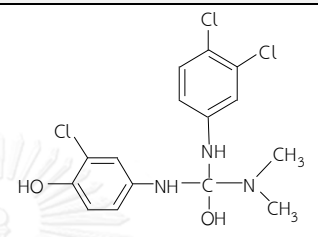
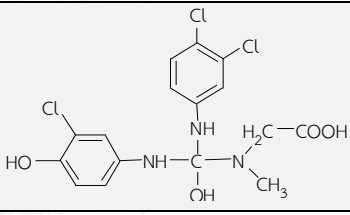
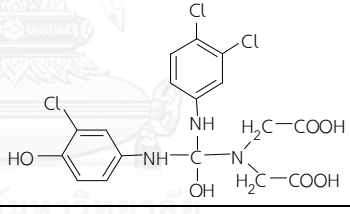
proposed by Luke et. al. (2014) [53]

Table 2.2 Structure of possible intermediates generated during diuron degradation identified in advanced oxidation processes (AOPs).

Molecular mass (avg.)	Molecular formula	Structure	Ref.
74.08	$C_2H_6ON_2$		[54]
88.11	$C_3H_8ON_2$		[6]
127.57	C_6H_6ClN		[55]
136.15	$C_7H_8ON_2$		[55]
143.57	C_6H_6OCIN		[3]
150.18	$C_8H_{10}N_2O$		[12]
156.59	C_7H_7NOCl		[4]
162.02	$C_6H_5ONCl_2$		[3, 4, 8, 48, 49]
170.60	$C_7H_7ON_2Cl$		[55]
188.01	$C_7H_7N_2O_2Cl$		[48, 54]

Molecular mass (avg.)	Molecular formula	Structure	Ref.
198.65	$C_9H_{11}ON_2Cl$		[8]
200.62	$C_8H_9O_2N_2Cl$		[6, 12, 36]
205.04	$C_7H_6ON_2Cl_2$		[5, 36]
213.21	$C_9H_{13}O_2N_2Cl$		[12]
214.65	$C_9H_{11}O_2N_2Cl$		[3, 6, 8, 12, 13, 36]
219.07	$C_8H_8ON_2Cl_2$		[3-6, 12, 13, 36]
222.05	$C_7H_7O_2N_2Cl_2$		[6, 49]
232.62	$C_8H_6O_2N_2Cl_2$		[3, 5, 6, 36]
235.07	$C_8H_8O_2N_2Cl_2$		[5, 8]
236.07	$C_8H_9O_2N_2Cl_2$		[12]
237.00	$C_6H_2O_4N_2Cl_2$		[54]

Molecular mass (avg.)	Molecular formula	Structure	Ref.
247.08	$C_9H_8O_2N_2Cl_2$		[6, 8, 13, 49]
249.05	$C_9H_{10}O_2N_2Cl_2$		[5, 6, 8, 13, 49]
250.10	$C_9H_{11}O_2N_2Cl_2$		[3, 4, 8, 12]
251.04	$C_7H_6O_3N_3Cl_2$		[56]
251.06	$C_8H_8O_3N_2Cl_2$		[13, 49]
260.65	$C_9H_{11}O_4N_3Cl$		[56]
263.08	$C_9H_8O_3N_2Cl_2$		[8, 13]
264.08	$C_9H_9O_3N_2Cl_2$		[4, 8, 36]
265.09	$C_9H_{10}O_3N_2Cl_2$		[49]
266.10	$C_9H_{11}O_3N_2Cl_2$		[8]
267.11	$C_9H_{12}O_3N_2Cl_2$		[4, 6]

Molecular mass (avg.)	Molecular formula	Structure	Ref.
279.10	$C_9H_{10}O_3N_3Cl_2$		[56]
293.08	$C_9H_8O_4N_3Cl_2$		[56]
376.66	$C_{15}H_{16}O_2N_3Cl_3$		[57]
420.68	$C_{16}H_{16}O_4N_3Cl_3$		[57]
464.68	$C_{17}H_{16}O_6N_3Cl_3$		[57]

2.3 Microreaction technology

Over the past decade, microfluidic technology has been increasingly interested applying to chemical reaction proposes which it is well known that the microreactor shows many advantages over conventional scales chemistry to improve the efficiency of chemical reaction [29, 58].

Microfluidic technology can be described as the study, development, and application of devices whose operation is based on the scale of 100-1000 μm . The widely accepted term “microreactors” in this technology is usually defined as miniaturized reaction systems fabricated by using, at least partially, methods of microtechnology and precision engineering. The characteristic dimensions of the internal structures of microreactors like fluid channel typically range from the sub-micrometer to the sub-millimeter level. The construction of microreactors generally is performed in a hierarchic manner, comprising an assembly of units composed of subunits and so forth [59].

Originating from chemical engineering principles, there are fundamental advantages associated with miniaturized reaction vessels that make microreactors more favorable. Advantages of microreaction technology are described below [59]:

2.3.1 Intensification of heat and mass transport

Due to short diffusional distances, conversion rates can be significantly enhanced in microsystems. This was exemplarily verified for the intensification of heat transfer of thermally coupled high-temperature reactions by recent calculations.

2.3.2 Reduced size

Due to the reduction of the linear dimensions, the volume of microreactors is significantly decreased compared to conventional large-scale reactors. Hardware mass

can also be reduced by 5-50 times. Reduction of the size also contribute to shifting size-energy trade-offs toward higher efficiency.

2.3.3 Large surface to volume ratio

As a consequence of the decrease in fluid layer thickness, the corresponding surface-to-volume ratio of the fluid entity is also notably increased. Specific surfaces of microchannels amount to 10,000 to 50,000 $\text{m}^2 \cdot \text{m}^{-3}$, whereas typical laboratory and production vessels usually do not exceed 1000 $\text{m}^2 \cdot \text{m}^{-3}$ and 100 $\text{m}^2 \cdot \text{m}^{-3}$. This increase not only benefits to heat transfer, but also can be utilized catalytic reactors.

2.3.4 Production flexibility

Rather than by scaling-up, an increase in throughput in microreactors is achieved by a numbering-up approach. The functional unit of a microreactor is multiply repeated. Fluid connection between these units can be achieved by using distribution lines and flow equi-partition zones, most likely hierarchically assembled. This numbering-up strategy results in higher flexibility in adapting production rate to varying demand since a certain number of systems can be switched off or further systems may be simply added to the production plant without influence on other components. A plant design based on a large number of small reaction system can be modified to perform a variety of reactions by changing the piping network. This flexibility may be supported by a considerably broader range of operating conditions of a microreactor compared with a macroscopic system.

2.3.5 Commercial applications

Due to reduced size of reactors, less space, materials and energy are required for microreactors, and operation time can be reduced to seconds, milliseconds, in some

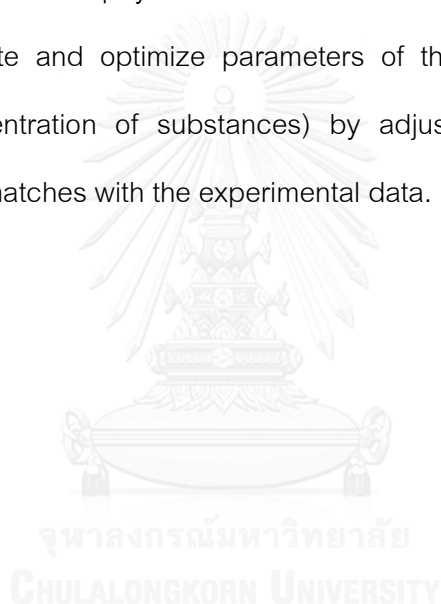
cases even nanoseconds. These result in lower capital investment, operating cost and cost of transportation of material and energy. In addition, the numbering-up strategy allows simple and inexpensive replication of microreactor units, and avoids complexity and intensively increasing cost on large-scale production. Besides, techniques like replacing batch with continuous processes, distributed production and integration of microtechnology with other systems can be applied to reduce the contact time, which also contribute to lowering the cost.

These properties can improve efficiency of reaction as well. So, microreaction systems have been examined for wide range of applications of organic chemistry. Nowadays, however, there are still few researches on EAOPs. It is interested in study diuron degradation using EAOP in microreactor.



2.4 Mathematical model and simulation

The mathematical model is developed to describe the chemical reaction flow in microreactor for diuron degradation and formation of intermediates via electrochemical oxidation in microreactor. This model can be used as an analytical tool for kinetics parameter estimation and used as a design tool for optimal microreactor design. The kinetic rate equations were combined with mass transport equations, in which simulates the reaction rate constants and concentration of diuron and its products. All equations are implemented in COMSOL Multiphysics software 4.2. Moreover, COMSOL-Matlab LiveLink were used to estimate and optimize parameters of the process kinetics (e.g. rate constants and concentration of substances) by adjusting the parameter until the mathematical model matches with the experimental data.



CHAPTER III

EXPERIMENTAL

This chapter describes the detail of experimental procedure in works. It consists of 4 main sections: (i) materials including chemicals and apparatus of experimental set up, (ii) analytical methods and (iii) electrochemical advanced oxidation process of diuron degradation procedure in microreactor and (iv) mathematical and simulation model.

3.1 Materials and chemicals

3.1.1 Chemicals

Standard diuron or, 3-(3,4-dichlorophenyl)-1,1-dimethyl urea (99.5% purity) was purchased from Sigma Aldrich. 3-(3,4-dichlorophenyl)-1-formyl-1-methylurea, 3-(3-chlorophenyl)-1, 1-dimethylurea and 3, 4-dichloro-aniline, which were used as reference standard compounds, also purchased from Sigma Aldrich. Sodium persulfate ($\text{Na}_2\text{S}_2\text{O}_8$) was purchased from Panreac. Sodium nitrite (NaNO_2) was purchased from Carlo Erba. Sodium nitrate (NaNO_3) and sodium sulfate (Na_2SO_4) were purchased from UNIVAR. Hydrogen peroxide (30% w/w, solution in water) also was purchased from Carlo Erba. All of chemicals were used in analytical grade. Acetonitrile was used in analysis was high-performance liquid chromatography (HPLC) grade and liquid chromatography-mass spectroscopy (LC-MS) grade.

3.1.2 Apparatus

The experimental of microscale-base reaction system in this work consists of following parts: microreactor, DC power supply, syringe pump and protection resistor. Schematic and photograph of microreactor and experimental set up are shown in figure 3.1 and 3.2.

3.1.2.1 Microreactor

The microreactor used in this work consists of 4 main parts which are stainless steel housing plates, 2 electrodes (anode and cathode), Teflon spacer and gasket. Figure 3.3 and 3.4 show the components of microreactor, front view and side view of reactor. List of following parts are shown below.

(1) Stainless steel housing plates consists of two flat plates (top and bottom plate), which were ordered from International Crystal Labs (Garfield, NJ). The housing plates, consists of one inlet and one outlet on the bottom plate, which use to prevent leaking of microreactor.

(2) Anode and cathode are made from graphite sheet stuck with stainless steel plate and bare stainless steel plate, respectively. Dimension of graphite sheet is 2.3 cm x 3.8 cm x 1 mm while the dimension of stainless steel plate is 2.3 cm x 3.8 cm x 2.5 mm. Two electrodes are connected with metal rod on the back of each plate to connect with DC power supply and protection resistor.

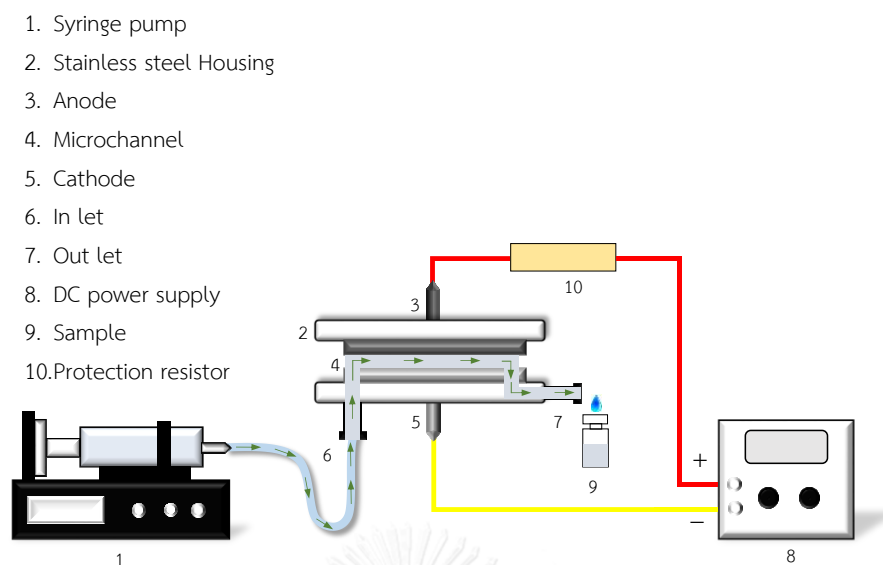


Figure 3.1 Schematic of experimental set up of electrochemical oxidation in microreactor

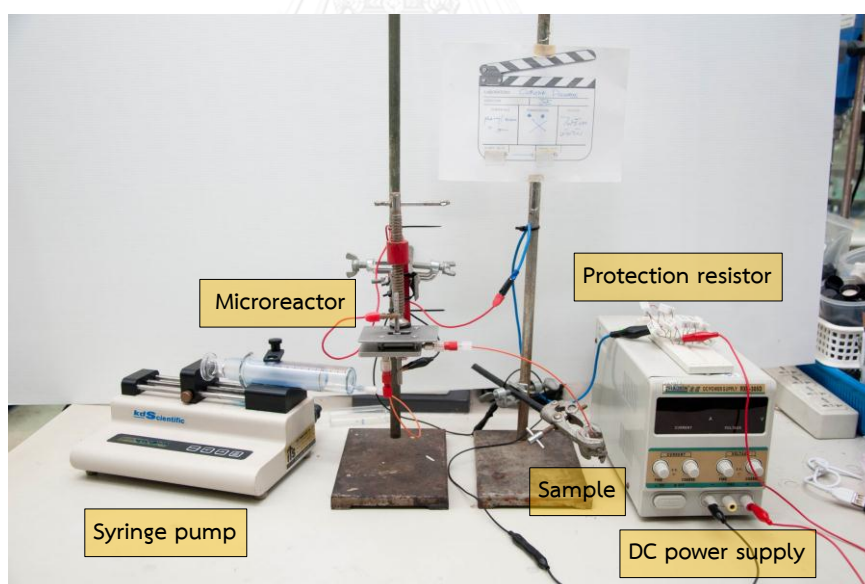


Figure 3.2 Photograph of experimental set up

(3) Spacer is made from Teflon sheet which is predetermined opening for making gap (microchannel) between 2 electrodes. The dimension of Teflon sheet is 2.3 cm x 3.8 cm x 250 μm while the dimension of inside opened zone is 10 mm x 21 mm x 250 μm . To vary the thickness of microchannel, double or triple layers of Teflon sheets are used to create 500 and 750 μm of microchannel thickness.

(4) Gasket is made from neoprene which use to cushion and to form seals and insulations between the electrodes and housing plates. The dimensions of gasket are 38.5 mm x 19.5 mm x 2 mm.

3.1.2.2 DC power supply

Regulated DC power supply (Thaoxin, RXN 305D) is used to supply DC current and potential across the electrodes to initiate electrochemical reaction. Figure 3.5 illustrates DC power supply.

3.1.2.3 Syringe pump

A KD Scientific single syringe pump (model: KDS-100) is used to deliver reactant solution to the microreactor as shown in figure 3.6. To control of mean residence time, total flow rate of reactant is varied by adjustment volumetric flow rate to the syringe pump.

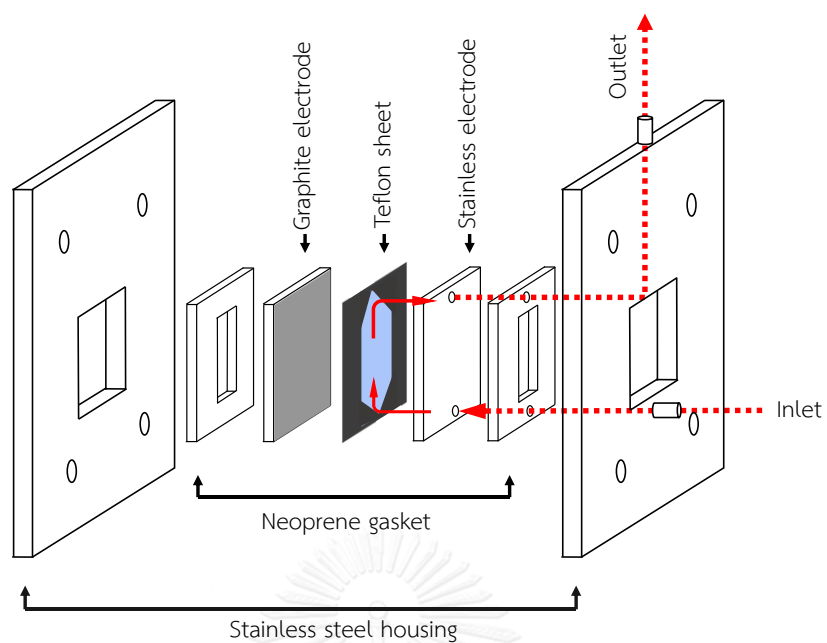


Figure 3.3 Assembly of electrochemical oxidation microreactor

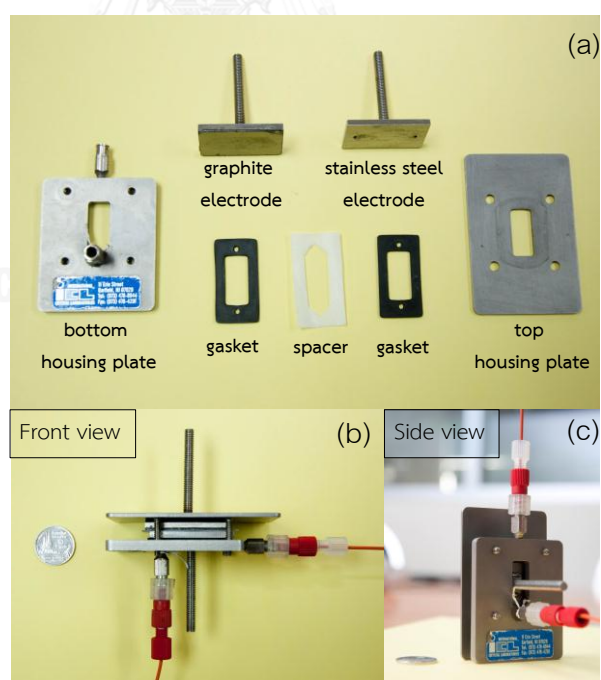


Figure 3.4 Components of microreactor (a), front view (b) and side view (c)



Figure 3.5 A photograph of DC power supply.



Figure 3.6 A photograph of syringe pump.

3.1.2.4 Protection resistor

During electrochemical oxidation process, short circuit in system maybe occurs, protection resistor is used to prevent this situation to keep DC power supply be safe. Protection resistor consists of parallel of resistors which total resistance is $4.88\text{ k}\Omega$. Figure 3.7 shows protection resistor in this study.

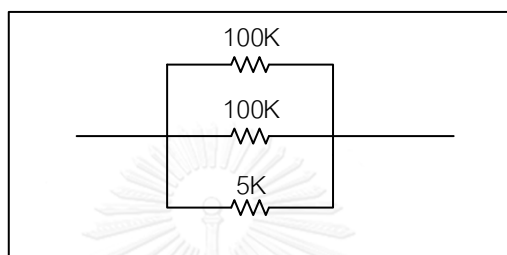


Figure 3.7 An electrical circuit of protection resistor.

3.2 Analytical methods

3.2.1 High performance liquid chromatography (HPLC)

To measure concentration of diuron and 3 reference standard compounds, High performance liquid chromatography (HPLC) is used. A Shimadzu HPLC (Model: Class 10VP) is performed which equipped with reverse-phase C18 column (phenomenex, Luna 5 μ C18(2) 100 $^{\circ}$ A, 250 x 4.6 mm.) equipped with a multiple wavelength UV diode array detector as shown in figure 3.8. The detection wavelengths are 240, 250 and 254 nm. The mobile phase is consisted of 70% (v/v) acetonitrile and 30% (v/v) deionized water, total flow rate is 1.5 mL \cdot min $^{-1}$ and retention time for all analyzed compounds is set to be 6 min. The column temperature is kept at 30 $^{\circ}$ C. Injection volume is 20 μ L with auto-sampling injection.



Figure 3.8 A photograph of high performance liquid chromatography

3.2.2 Liquid chromatography – mass/mass spectrometer (LC-MS/MS)

Identification of intermediate structures formed during diuron degradation was done by liquid chromatography with mass/mass spectrometer (LC-MS/MS). Mass spectroscopy (MS) is performed with amaZon SL Ion Trap LC/MS (Bruker Daltonics) in ESI-MS analyze mode (Nebulizer pressure: 20 psi; Drying gas flow rate: $6 \text{ L} \cdot \text{min}^{-1}$; Drying gas temperature: $220 \text{ }^\circ\text{C}$). MS spectra are acquired in UltraScan mode between m/z 70 - 1,000 in both of positive and negative ionization. Liquid chromatography system (Dionex Ultimate 3000 Rapid Separation) equipped with reverse-phase C18 column (phenomenex, Luna 2.5μ C18(2) - HST, $100 \times 2.0 \text{ mm.}$). $10 \mu\text{L}$ volume of injection is made on column, which is maintained column temperature at $40 \text{ }^\circ\text{C}$ with auto sampling injection. The mobile phase consist of 60% acetonitrile (v/v) and 40% water (v/v) with total flow rate of $0.200 \mu\text{L} \cdot \text{min}^{-1}$ and retention time is 10 min. Figure 3.9 shows a photograph of liquid chromatography with mass/mass spectroscopy (LC-MS/MS).

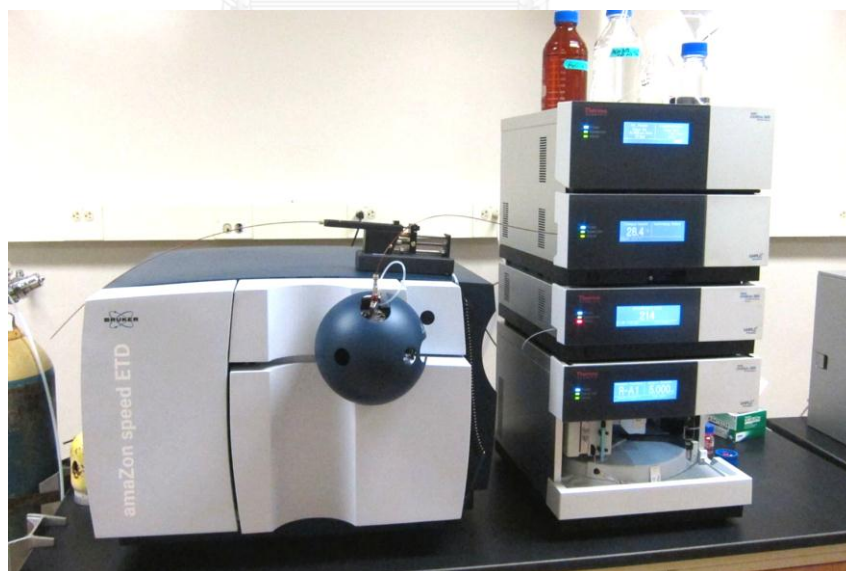


Figure 3.9 A photograph of liquid chromatography with mass/mass spectroscopy (LC-MS/MS)

3.2.3 TOC analyzer

Total organic carbon concentration (TOC) is determined by TOC analyzer (Shimadzu, Model: TOC-VCPH) as shown in figure 3.10. Before TOC measuring, the samples are purge by nitrogen gas to remove CO₂ for 20 min.



Figure 3.10 A photograph of TOC analyzer

3.2.4 UV-Visible spectrophotometer

UV-Visible spectrophotometer (Shimadzu, Model: UV-1700) is used to measure concentration of hydrogen peroxide and nitrite ion by a colorimetric method [60, 61], nitrate ion [62], sulfate ion by turbidimetric test [63] and persulfate ion by Ferrous Ammonium Sulfate (FAS) method [64, 65]. Detailed measurement procedure of hydrogen peroxide and all ions are addressed in *Appendix B*. Figure 3.11 shows a photograph of UV-Visible spectrophotometer.



Figure 3.11 A photograph of UV-Visible spectrophotometer

3.2.5 pH and conductivity meter

Conductivity and pH of solution during electrochemical process were measured by conductivity and pH meter (Mettler Toledo). Figure 3.12 shows a photograph of pH and conductivity meter.



Figure 3.12 A photograph of pH meter (a), and conductivity meter (b)

3.3 Electrochemical degradation of diuron and reference standard compounds in microreactor

In the experiment, 10 ppm of diuron and 3 reference standard compounds was prepared in deionized water to be reactant. Reactants are fed into the microchannel at controlled speed via a syringe pump. To vary mean residence time in range of 25, 50, 75 and 100s, volumetric flow rate of solution was changed by adjustment the total flow rate in range $7.56 - 1.89 \text{ ml}\cdot\text{h}^{-1}$ to syringe pump. The solution samples coming out of the reactor was periodically collected and analyzed in reaction time at least 3 samples to be sure that steady state conditions were achieved. Before starting to apply current to the reactor, reactant solutions were flown through the reaction system into microchannel for 1 h making sure that adsorption of the reactants on graphite sheet took place. DC power supply was used supplying direct current (DC) across the gap between the electrodes. Most of the experiments were repeated at least twice, giving rise to a good reproducibility of results. Table 3.1 shows all experimental conditions in this study.

Table 3.1 List of experimental conditions

condition	Value
1. Mean residence time (s)	25, 50, 75 and 100
2. Applied current (mA)	0.5, 1 and 2
3. Microchannel thickness (μm)	250, 500 and 750
4. Initial pH of solution by adding 0.1 M of HCl and NaOH	3, 7 and 10
5. Initial conductivity of solution ($\mu\text{S/cm}$) by adding 0.01 M of NaCl	6.7, 140, 500 and 1000
6. Ion contaminations (M)	0.0013, 0.005 and 0.05
7. Reference compounds	<ul style="list-style-type: none"> • 10 ppm of init. conc. • 25, 50, 75 and 100s of residence time • 1 mA of applied current) • 250 μm of thickness
<ul style="list-style-type: none"> • 3-(3,4-dichlorophenyl)-1-formyl-1-methylurea • 3-(3-chlorophenyl)-1, 1-dimethylurea • 3, 4-dichloro-aniline 	

3.4 Mathematical and simulation model

To clearly understand behavior of diuron degradation and 3 reference compound via electrochemical degradation in microreactor, simulation model was studied. In this study, COMSOL Multiphysics was used to build a numerical model describing the performance of the microreactor for diuron degradation, and its extensive interface COMSOL-Matlab LiveLink is used to determine the reaction rate constants in this process.

3.4.1 Mathematical model

3.4.1.1 Momentum balance

The flow of the incompressible fluid is governed by the continuity and The Navier–Stokes equations.

Assumption:

- (i) The fluid is Newtonian and incompressible
- (ii) The flow is laminar and isothermal
- (iii) Steady state condition is operated
- (iv) No velocity in y and z direction, v_y and $v_z = 0$
- (v) Velocity doesn't change along the z direction
- (vi) The Gravity is neglect, g_x , g_y and $g_z = 0$

We assume that electrodes are both very wide and very long so that the formulation of the problem can be approximated to a 2-dimension (2D). Figure 3.13 shows scheme of momentum balance in a microreactor.

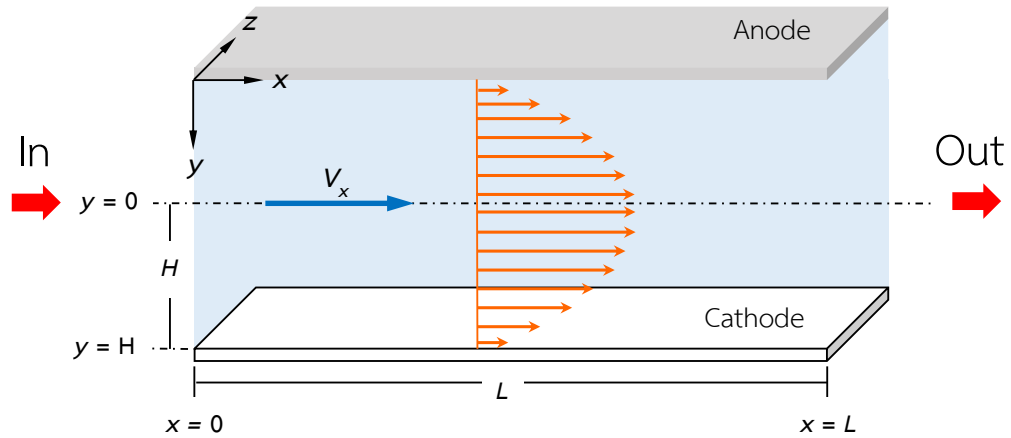


Figure 3.13 Scheme of momentum balance in a microreactor

Continuity and The Navier–Stokes equations in 2D-rectangular coordinates (x - y) is given in equation 3.1 and 3.3 – 3.5.

Continuity equation

$$\frac{\partial v_x}{\partial x} + \frac{\partial v_y}{\partial x} + \frac{\partial v_z}{\partial x} = 0 \quad 3.1$$

After applying assumptions, equation 3.1 became to equation 3.2: v_y and $v_z = 0$

$$\frac{\partial v_x}{\partial x} = 0 \quad 3.2$$

The Navier–Stokes equation

Applying The Navier–Stokes equation in rectangular co-ordinates

In x-direction

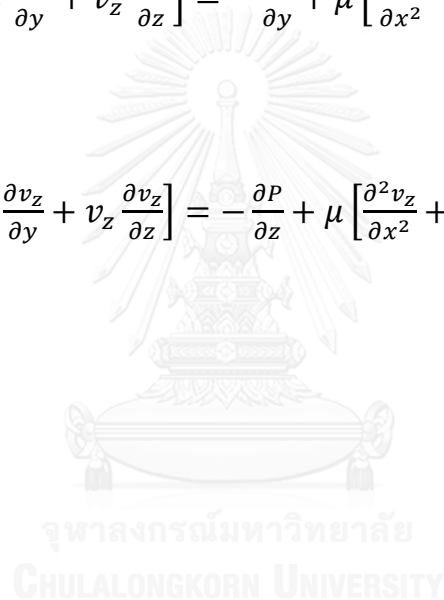
$$\rho \left[\frac{\partial v_x}{\partial t} + v_x \frac{\partial v_x}{\partial x} + v_y \frac{\partial v_x}{\partial y} + v_z \frac{\partial v_x}{\partial z} \right] = -\frac{\partial P}{\partial x} + \mu \left[\frac{\partial^2 v_x}{\partial x^2} + \frac{\partial^2 v_x}{\partial y^2} + \frac{\partial^2 v_x}{\partial z^2} \right] + \rho g_x \quad 3.3$$

In y-direction

$$\rho \left[\frac{\partial v_y}{\partial t} + v_x \frac{\partial v_y}{\partial x} + v_y \frac{\partial v_y}{\partial y} + v_z \frac{\partial v_y}{\partial z} \right] = -\frac{\partial P}{\partial y} + \mu \left[\frac{\partial^2 v_y}{\partial x^2} + \frac{\partial^2 v_y}{\partial y^2} + \frac{\partial^2 v_y}{\partial z^2} \right] + \rho g_y \quad 3.4$$

In z-direction

$$\rho \left[\frac{\partial v_z}{\partial t} + v_x \frac{\partial v_z}{\partial x} + v_y \frac{\partial v_z}{\partial y} + v_z \frac{\partial v_z}{\partial z} \right] = -\frac{\partial P}{\partial z} + \mu \left[\frac{\partial^2 v_z}{\partial x^2} + \frac{\partial^2 v_z}{\partial y^2} + \frac{\partial^2 v_z}{\partial z^2} \right] + \rho g_z \quad 3.5$$



After simplification, Navier-Stoke equations became to equation 3.6 - 3.8

$$\frac{\partial P}{\partial z} = \mu \frac{\partial^2 v_x}{\partial y^2} \quad 3.6$$

$$\frac{\partial P}{\partial y} = 0 \quad 3.7$$

$$\frac{\partial P}{\partial z} = 0 \quad 3.8$$

After applying boundary conditions to equation (3.6) - (3.8), expression of velocity profile would be in equation 3.9

Boundary conditions

$$\text{At } x = 0, P = P_0 \quad \text{At } x = L, P = P_L$$

$$\text{At } y = 0, \frac{\partial v_x}{\partial y} = 0 \quad \text{At } y = H, v_x = 0$$

The velocity profile

$$v_x(y) = \frac{y^2 - H^2}{2} \left(\frac{P_L - P_0}{\mu L} \right) \quad 3.9$$

3.4.1.2 Mass balance

The convection–diffusion equation for liquid phase mass transfer in rectangular coordinates was developed. Figure 3.14 shows scheme of material balance in a microreactor. Material balance equation is developed as shown in equation 3.10.

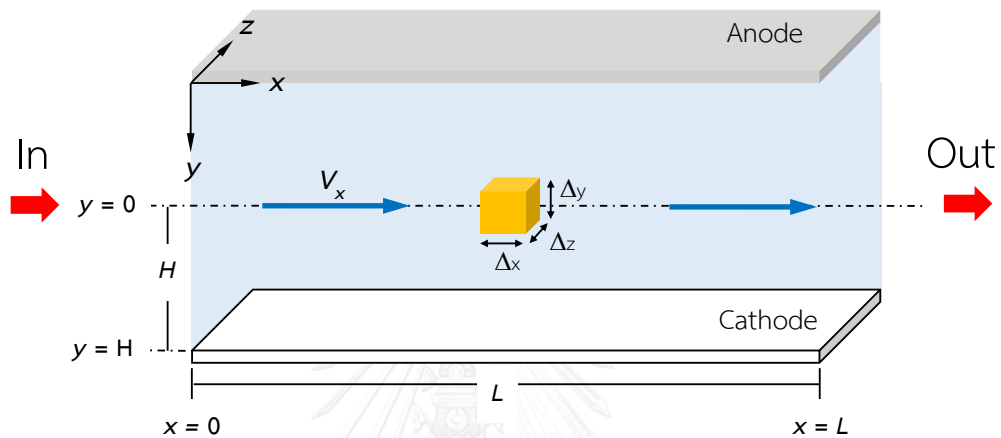


Figure 3.14 Scheme of material balance in a microreactor

$$(\text{Convection} + \text{Diffusion})_{\text{in}} - (\text{Convection} + \text{Diffusion})_{\text{out}} + \text{Generation} = \text{Accumulation} \quad 3.10$$

Assumptions

- (i) No convection in y-direction, $v_y = 0$
- (ii) No convection and diffusion in z-direction, $v_z = 0$ and $N_{i,z} = 0$
- (iii) Steady state process
- (iv) Diluted solution, $\frac{C_i}{C} \ll 1$

After taking element analysis and assumptions to equation 3.10. And then, taking limit to zero, so it became to equation 3.11.

$$\frac{\partial}{\partial x}(-v_x C_i) - \frac{\partial N_{i,x}}{\partial x} - \frac{\partial N_{i,y}}{\partial y} + R_i = 0 \quad 3.11$$

General flux equation for a dilute mixture (see equation 3.12) was applied to equation (3.11), material balance equation was developed to be equation 3.13

$$N_i = D_i \nabla C_i + \frac{C_i}{C} \sum_{i=1}^n N_i \quad 3.12$$

$$-v_x \frac{\partial C_i}{\partial x} + D_i \frac{\partial^2 C_i}{\partial x^2} + D_i \frac{\partial^2 C_i}{\partial y^2} + R_i = 0 \quad 3.13$$

The following boundary conditions were chosen for microreactor system

$$\text{At } x = 0, C_i(0, y) = C_{i,0} \quad \text{At } x = L, \frac{\partial C_i(L, y)}{\partial x} = 0$$

$$\text{At } y = 0, \frac{\partial C_i(x, 0)}{\partial y} = 0 \quad \text{At } y = H, \frac{\partial C_i(x, H)}{\partial y} = 0$$

3.4.1.3 Diffusion coefficients

Values of diffusion coefficients for diuron and 3 reference standard compounds in water at room temperature were calculated by Wilke-Chang correlation (see *Appendix D*).

3.4.2 Numerical method

3.4.2.1 COMSOL Multiphysics

COMSOL Multiphysics is a finite element analysis software program that provides the means to model engineering designs and simulate potential failure modes. The program allows exploration of various assumptions, design geometries and boundary conditions, and enables users to visually and quantitatively analyze the implications of different design decisions. Its simulation environment facilitates all the steps in the modeling process—defining geometry, meshing, specifying physics, solving, and then visualizing results. It also serves as a platform for the application specific modules. A number of predefined physics interfaces lead to a quick model set-up. In this study, COMSOL Multiphysics is used to build a numerical model describing the performance of EAOP microreactor for diuron degradation in aqueous solution, and its extensive interface COMSOL-Matlab LiveLink is used to optimize the reaction rate constants in this process.

3.4.2.2 Model development

Defining geometry

Due to the width of microreactor is much larger than the thickness, which there was no convection and diffusion in the direction along the width of reactor, a 2D space dimension was used to describe our microreaction system. The actual reactor size is 0.25 x 21 mm (thickness x length), a 2D rectangular space was built in COMSOL as shown in figure 3.15.

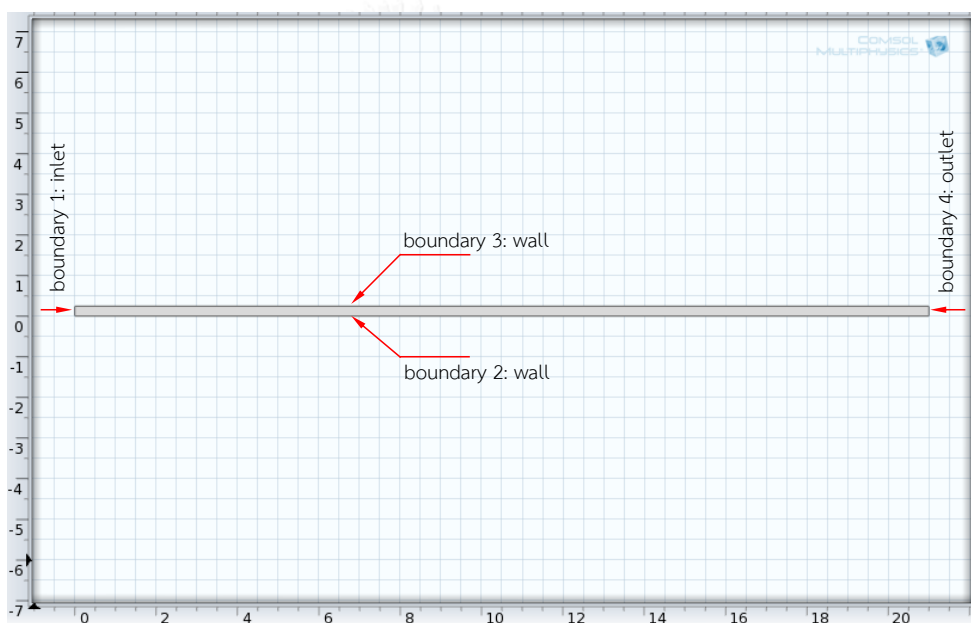


Figure 3.15 Geometry of microreactor in COMSOL

Parameters

All used constants for solving the model were defined here, including linear velocity, outlet pressure, initial concentration of diuron, diffusion coefficient of diuron and 3 reference standard intermediate compounds. The detailed table of parameters is shown in *Appendix E*.

Variables

All variables required by the model are defined here, including reaction rates of diuron and 3 reference standard intermediate compounds. The detailed table of variables is shown in *Appendix E*.

Physics models

Two physics models are used in the numerical model: (i) Laminar Flow model to simulate the velocity profile of the flow and (ii) Transport of Diluted Species model to simulate the concentration profiles of diuron and its products. The detailed table of node properties setting in two physics models is shown in *Appendix E*.

Meshing

A mesh setting with maximum element size of 0.012 mm and minimum element size of 0.0034 mm is satisfied for this model. The meshing of the geometry is shown below in figure 3.16.

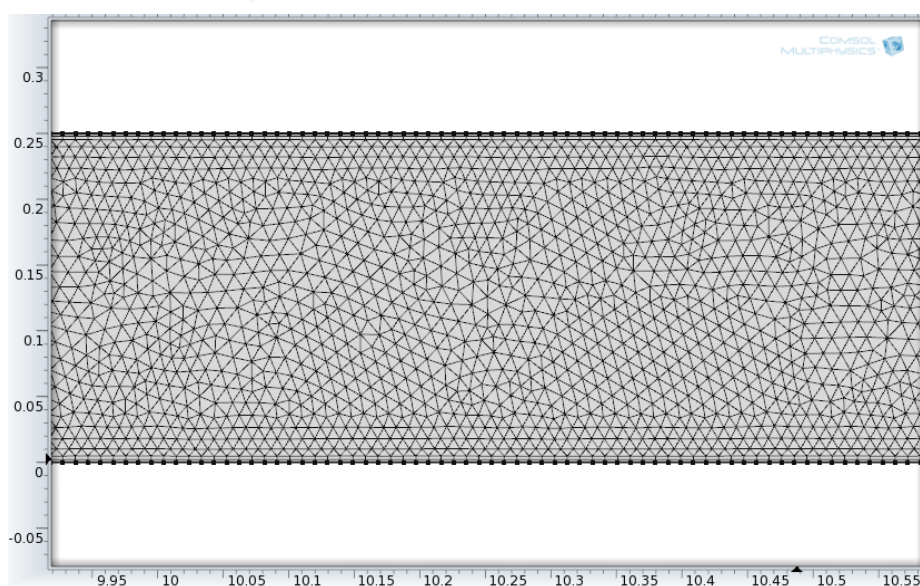


Figure 3.16 Meshing of the geometry in microreactor.

Solving and visualizing results

The velocity profile and concentration profiles are shown as shown in figure 3.17 and 3.18 and, respectively. The velocity profile shows there is no disruption between the two parallel plates and is proved as laminar flow. In the concentration profiles, diuron continuously consumed so its profile goes all the way down along the reactor.



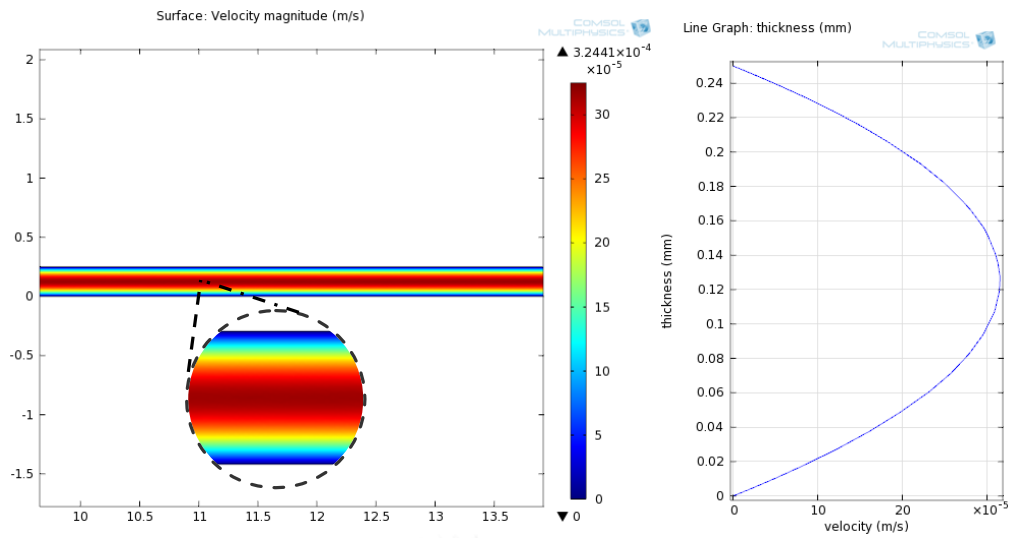


Figure 3.17 The velocity profile of diuron in the reactor

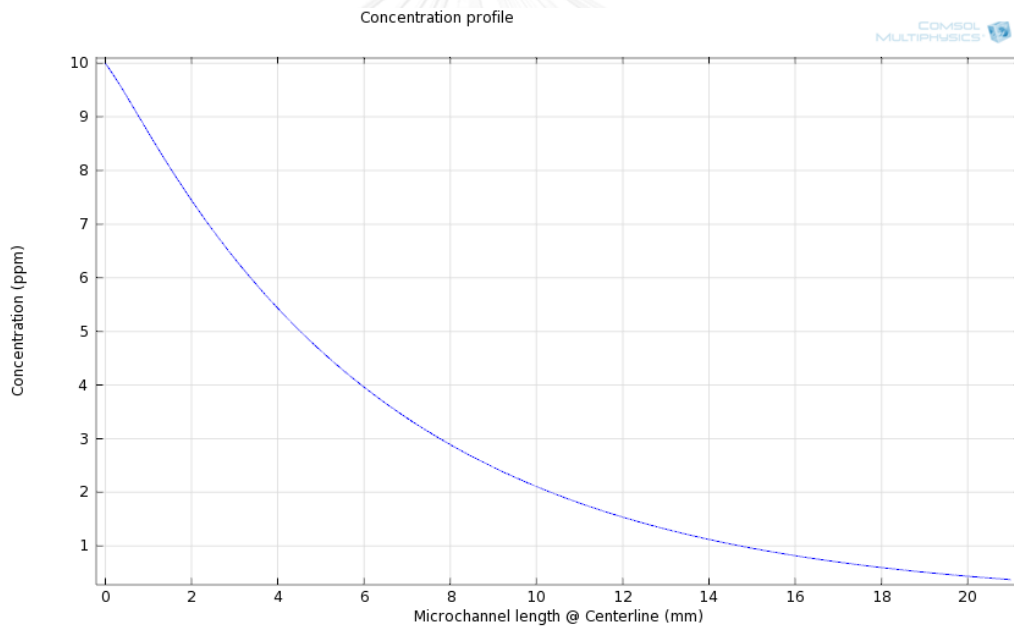
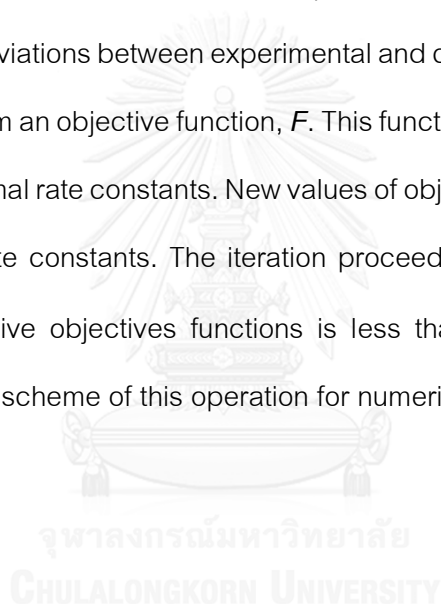


Figure 3.18 The concentration profile of diuron at a horizontal cutline through middle of the reactor

3.4.2.3 Optimization

COMSOL and MATLAB optimization routine was used for determining the rate constants of the reactions. A MATLAB optimization subroutine 'fminsearch', which is based on simplex search method was used for optimization. The simulation program read the initial values of the rate constants, which were determined by the trial and error method. The rate equations, a system of simultaneous differential equations, of the reaction were solved to get the analytical concentration of the reactant at the outlet of microreactor. The simulation results were compared with experimental results at each measured point. All deviations between experimental and calculated values were squared and summed up to form an objective function, F . This function was fed into an optimization routine to find the optimal rate constants. New values of objective function were calculated for each set of the rate constants. The iteration proceeds until the absolute difference between two successive objectives functions is less than a predefined tolerance, ϵ . Figure 3.19 shows the scheme of this operation for numerical model optimization.



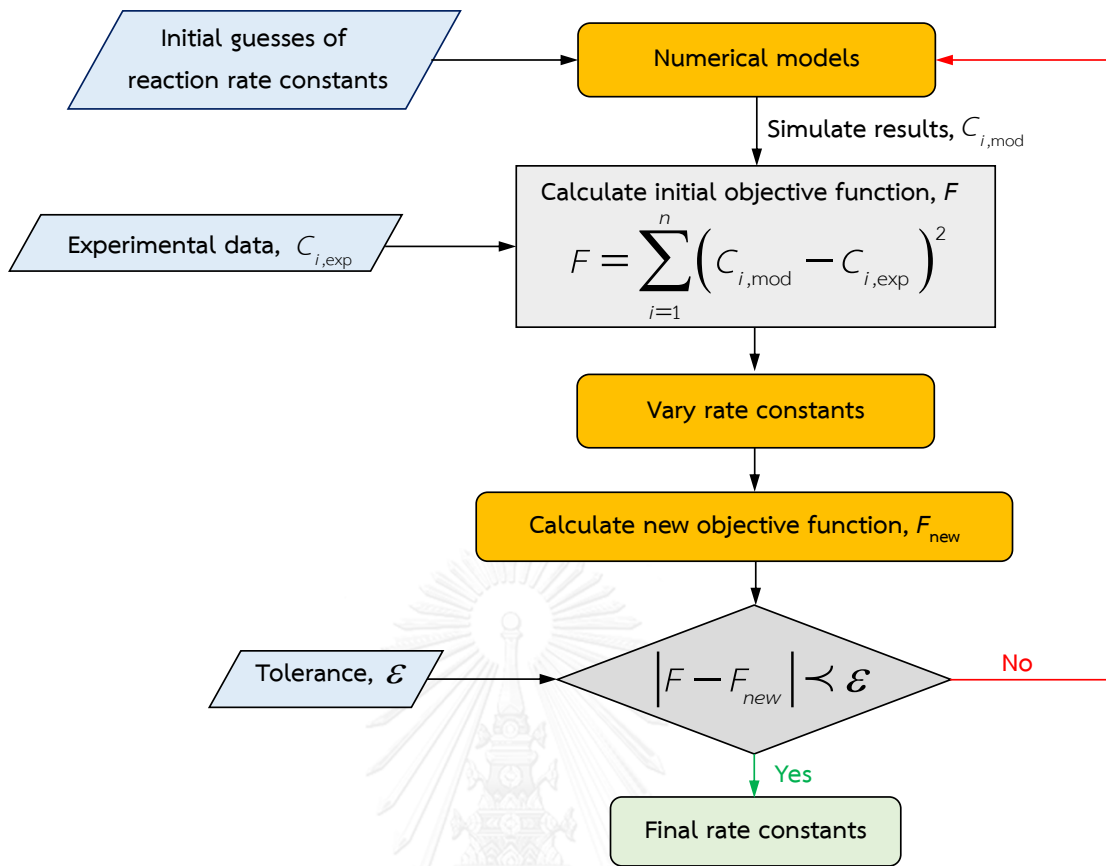


Figure 3.19 Schematic of shows the operation for numerical model optimization
numerical model optimization

CHAPTER IV

RESULTS AND DISCUSSION

The diuron degradation was successfully done using electrochemical advanced oxidation process (EAOP) in microreactor. In this chapter consists of 3 main parts which are (1) degradation of diuron via EAOP in microreactor which various parameters will be discussed, (2) intermediate products and reaction pathway of diuron degradation via electrochemical microreactor and (3) mathematical model and simulation.

4. 1 Degradation of diuron via electrochemical advanced oxidation process in microreactor

Characteristic of electrochemical advanced oxidation process for diuron degradation was discussed. The effect of mean residence time, applied current, thickness of microchannel, initial pH solution, initial liquid conductivity and contamination of ions on the degradation of diuron via EAOP in microreactor are also studied.

4.1.1 Characteristic of diuron degradation by EAOP in a microreactor

Once the direct current or potential was applied to the system, degradation of diuron takes place. The steady-state concentration of diuron at the outlet of the microreactor is lower than the inlet concentration. Hydrogen peroxide (H_2O_2) is also detected in the product stream. The formation of hydrogen peroxide has been suggested as the result of association of reactive hydroxyl radicals, which are formed by dissociation of water (oxidation) at the anode surface as shown in equation 4.1 [39, 40]. Due to lifetime of hydroxyl radical is short, there are a few hydroxyl radical diffuses to cathode to hardly providing reduction. Therefore, the equation 4.1 is not reversible reaction. It should be noted that, due to low applied current density, the corrosion of the graphite surface

was so small that it did not interfere with the measurement of hydrogen peroxide by the colorimetric method. This was verified by a separate experiment where the product stream was added with sodium carbonate (Na_2CO_3), which is an efficient scavenger for hydrogen peroxide [66]; the signal detected from the product after having passed through the reactor is exactly the same as that from the input solution. Table 4.1 shows concentration of hydrogen peroxide before and after adding sodium carbonate. It should be noted that due to low current density was supplied that was probably not enough to occur water splitting.

Table. 4.1 Table 4.1 shows concentration of hydrogen peroxide before and after adding sodium carbonate

Residence time (s)	H_2O_2 conc. in DI water (ppm)	SD	H_2O_2 conc. in DI water after adding Na_2CO_3 (ppm)	SD
Stock solution	0.030	± 0.004	0.030	± 0.005
0	0.050	± 0.004	0.051	± 0.003
100	0.670	± 0.27	0.052	± 0.01

When pure deionized water was supplied to the microreactor operated at 1 mA with current density of 0.157 mA/cm^2 and mean residence time of 25 s, the concentration of hydrogen peroxide detected was 0.34 ppm. However, if 10 ppm of diuron was presented in the solution, the concentration of hydrogen peroxide decreased to 0.27 ppm, which suggests that portion of hydroxyl radicals interacts with diuron and induces the degradation of diuron. The concentrations of hydrogen peroxide in pure deionized water and diuron solution is shown in figure 4.1. Thus, the degradation of diuron is competing

for hydroxyl radicals with the production of hydrogen peroxide reaction equation 4.2 and 4.3.

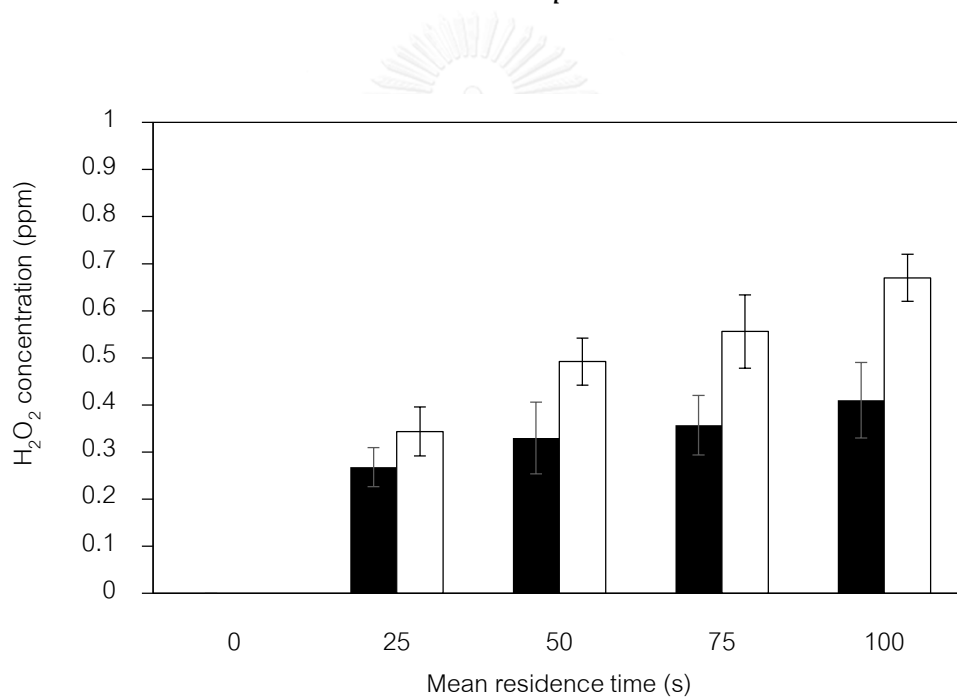


Figure 4.1 Concentration of hydrogen peroxide detected at the outlet of the microreactor operating under applied current of 1 mA; (□) in pure deionized water and (■) in 10 ppm diuron solution

As the mean residence time in the reactor is increased, the concentration of hydrogen peroxide in the exit stream (in the experiment with pure water) is increased; Figure 4.1. This implies that greater amount of hydroxyl radicals are generated within the reactor. As expected, the extent of diuron degradation also increases with the increased residence time because it is exposed to the reactive species for longer period of time. The degradation of diuron under the applied current of 1 mA is increased from 68% to 91% when the residence time is increased from 25 s to 100 s as shown in figure 4.2.

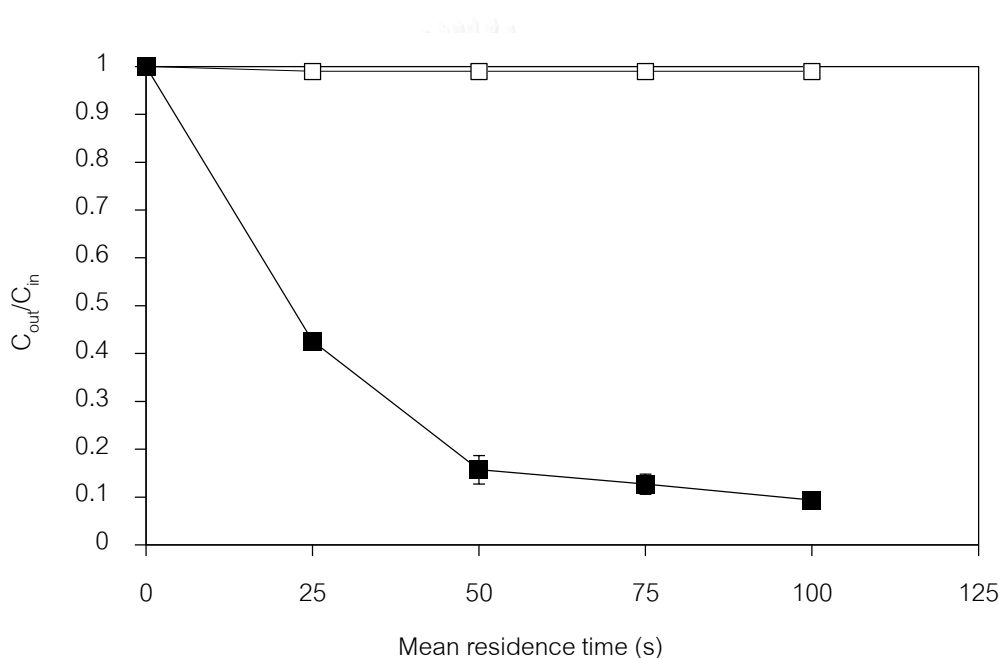


Figure 4.2 Diuron degradation with/without applied current: (□) no applied potential and (■) applied potential

Moreover, it was found, in the control experiment, that the concentration of hydrogen peroxide at the outlet of the reactor remains the same even when the feed is purged with N_2 to remove majority of dissolved oxygen. Another experiments were conducted by bubbling oxygen to pure deionized water to make saturated oxygen in pure water before applying electrical source. The results showed that no significantly difference

of hydrogen peroxide concentration was observed when compared with hydrogen peroxide concentration was formed under pure deionized water with purged N_2 . It indicated that O_2 concentration was not enough to supply to form H_2O_2 on cathode (O_2 reduction). The values of the concentration of hydrogen peroxide in pure deionized water (with purging N_2 , O_2 and no purging) are shown in table 4.2.

Table 4.2 Formation of hydrogen peroxide in different conditions (100s of mean residence time, 250 μm of thickness and 1mA of applied current)

H_2O_2 conc. in DI water (ppm)	H_2O_2 conc. in DI water after purge with N_2 (ppm)	H_2O_2 conc. in DI water after purge with O_2 (ppm)
0.67 ± 0.05	0.67 ± 0.27	0.62 ± 0.07

Furthermore, the experimental results confirm that the degradation of diuron by hydrogen peroxide, within residence times investigated, is negligible. No diuron degradation was observed when hydrogen peroxide was intentionally added to the solution passing through the reactor without applying the potential. Other reactions to convert to hydroxyl radical to another species are shown as equation 4.4 - 4.5 [17, 67]. However, hydrogen peroxide is mainly produced from recombination of hydrogen peroxide, which is good represent hydroxyl radical [68]. Additionally, collected sample was measured immediately after collecting preventing decomposition of hydrogen peroxide. Therefore, we can safely conclude that hydrogen peroxide is not an active species, which directly participates in diuron degradation. It should be noted that hydrogen peroxide is one of oxidant agent which the relative oxidation power is lower than hydroxyl radical. The relative oxidation power of hydroxyl radical is 2.8 V while that of hydrogen peroxide is 1.77 V [67]. Due to low oxidation power, applied current density and

low formed concentration of hydrogen peroxide in solution as shown in figure 4.1, however, hydrogen peroxide hardly affect to diuron degradation. Figure 4.2 also represents that no diuron degradation is observed when no electrical current is supplied, which indicated that diuron degradation was initiated by electrical source. It should also be noted that the concentration of hydrogen peroxide detected in the experiment with diuron solution becomes significantly lower than the value detected in the experiment with pure water at long residence times. Therefore, these measurements/observations indicate that an increased amount of hydroxyl radicals participates in diuron degradation as the process progresses. Moreover, figure 4.3 shows time on stream of diuron degradation during EAOP. It suggests that before 1 h of time on stream, steady state condition already takes place in continuous microscale-based system at all mean residence time. Due to advantages of microreactor in EAOPs, steady state condition easily reaches.



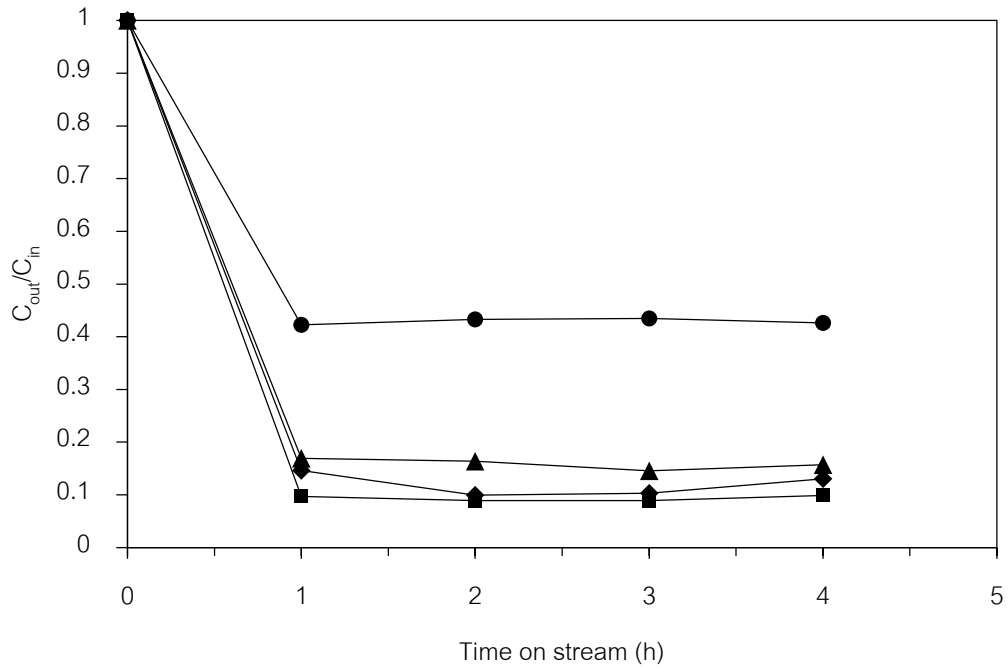


Figure 4.3 Time on stream of diuron degradation under various mean residence time: (●) 25s, (▲) 50s, (◆) 75s and (■) 100s; 250 μm of thickness and 1mA of applied current

It has been reported the degradation of organic compounds using EAOP including diuron in aqueous solution can be assumed to be pseudo first order kinetic reaction [19]. In order to determine the reaction rates of diuron degradation, the experimental data were fitted by the following equation 4.6.

$$\ln\left(\frac{C_{in}}{C_{out}}\right) = kt \quad 4.6$$

where C_{in} , C_{out} , t and k is the inlet concentration of diuron (ppm), the outlet concentration of diuron (ppm), mean residence time (s) and the rate constant (s^{-1}), respectively. The diuron degradation was found to be well represented by the pseudo first order kinetics with $2.69 \times 10^{-2} \text{ s}^{-1}$ of the reaction rate constants with $R^2 = 0.9$ under 1 mA of applied

current and 250 μm of microchannel thickness. It should be noted that many works reported that the degradation efficiency increased with decreasing the initial diuron concentration by AOPs [13, 69]. Therefore, initial concentration of diuron was fixed in this work.

As diuron is degraded toward its mineralization, the concentration of total organic carbon (TOC) of the solution is decreased. However, the decrease in TOC is not as much as the decrease in diuron concentration as shown in figure 4.4. At the residence time of 100 s, about 90% of diuron is degraded, but the TOC in the solution is decreased only by about 60%. It is indicated that reaction intermediates are formed during the degradation of diuron. The mineralization current efficiency (MCE) was also calculated via equation 4.7 [70].

$$\text{MCE}(\%) = \frac{n \cdot F \cdot V_s \cdot \Delta(\text{TOC})_{\text{exp}}}{4.32 \times 10^7 \cdot m \cdot I \cdot \bar{t}} \times 100 \quad 4.7$$

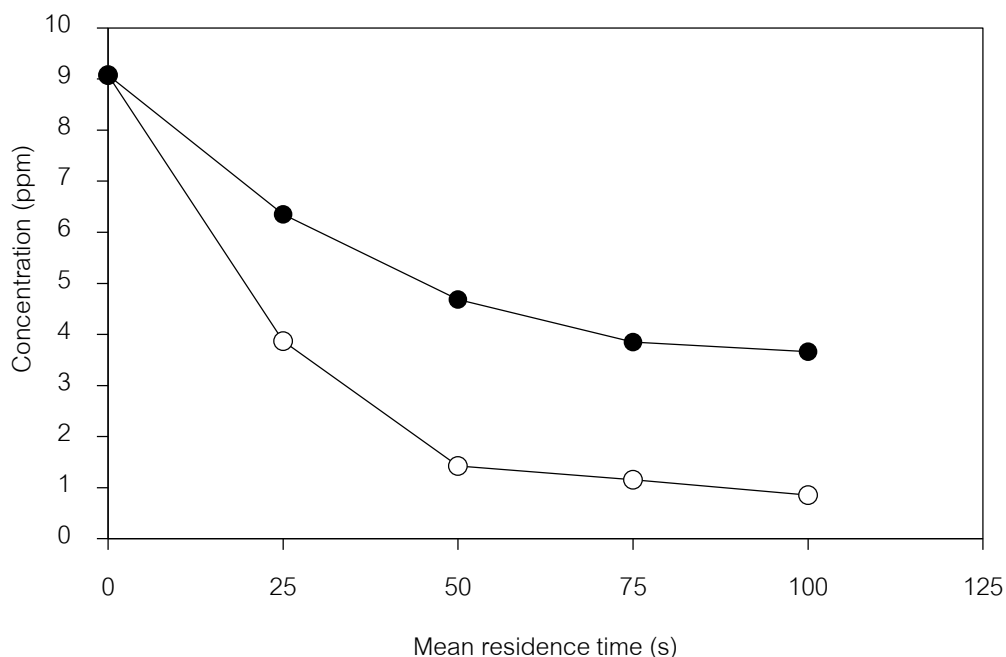
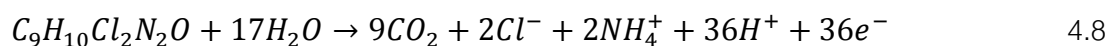


Figure 4.4 Effect of mean residence time on diuron degradation and reduction of total organic carbon: (○) diuron concentration and (●) TOC concentration

In this equation, I is the applied current (A); \bar{t} is the mean residence time in the reactor (h); F is the Faraday constant ($96,487 \text{ C}\cdot\text{mol}^{-1}$); V_s is the reactor volume (L); $\Delta(\text{TOC})_{\text{exp}}$ is the experimental TOC decay ($\text{mg}\cdot\text{L}^{-1}$); 4.32×10^7 is a conversion factor ($3600 \text{ s}\cdot\text{h}^{-1} \times 12,000 \text{ mg carbon}\cdot\text{mol}^{-1}$) and m is the number of carbon atoms of diuron (i.e., 9 atoms). The number of electrons consumed per each diuron molecule (n) was taken to be 36 for the complete mineralization leading to carbon dioxide, chloride and ammonium ions as shown in equation 4.8. The energy consumption per unit TOC (EC_{TOC}) was also calculated from equation 4.9 [71, 72]. In this equation, E_{cell} is the applied potential (V).



$$EC_{TOC}(\text{kWh}^{-1}) = \frac{E_{cell} \cdot I \cdot \bar{t}}{V_s \cdot (\Delta TOC)_{exp}} \quad 4.9$$

For diuron degradation via EAOP under the applied current of 1 mA in this work, the value of MCE is 21.1%, 16.2%, 12.7% and 9.8%, while that of EC_{TOC} is 0.16, 0.21, 0.27 and 0.35 $\text{kWh} \cdot \text{g}^{-1}(\text{TOC})$, when the residence time is 25, 50, 75 and 100 s, respectively. The MCE and EC_{TOC} values are shown in table 4.3. The results suggest that the degradation of recalcitrant intermediates requires larger amount of energy for total mineralization than diuron. Nevertheless, it should be pointed out that the degradation process investigated in this work requires one order of magnitude lower of EC_{TOC} than that reported for the conventional EAOP systems [18]. Hence significant increase in the mineralization current efficiency is observed. This is one of the important advantages of the microscale-based reaction system.

Table 4.3 Values of MCE and EC_{TOC} of diuron degradation via electrochemical advanced process.

Residence time (s)	%MCE	EC_{TOC} ($\text{kWh} \cdot \text{g}^{-1} \text{TOC}$)
25	21.1	0.16
50	16.2	0.21
75	12.7	0.27
100	9.8	0.35

4.1.2 Effect of applied current

Energy input is one of the important parameters affecting characteristic of the oxidation in EAOPs [15, 24]. As the applied current is increased, the extent of diuron degradation is increased, as shown in figure 4.5. Under the mean residence time of 100 s, the percentage of diuron degraded is 69.7%, 90.6%, and 97.5%, when the applied current is 0.5, 1, and 2 mA (current density of 0.157, 0.313 and 0.637 mA·cm⁻²), respectively under 250 μm of microchannel thickness. The concentration of hydrogen peroxide in diuron solution also increased with increasing applied current as in figure 4.6. This is a result from increased amount of hydroxyl radicals induced by increased applied current [15, 18], which is also observed through the increase in concentration of hydrogen peroxide detected when pure water is supplied to the system (see figure 4.7).

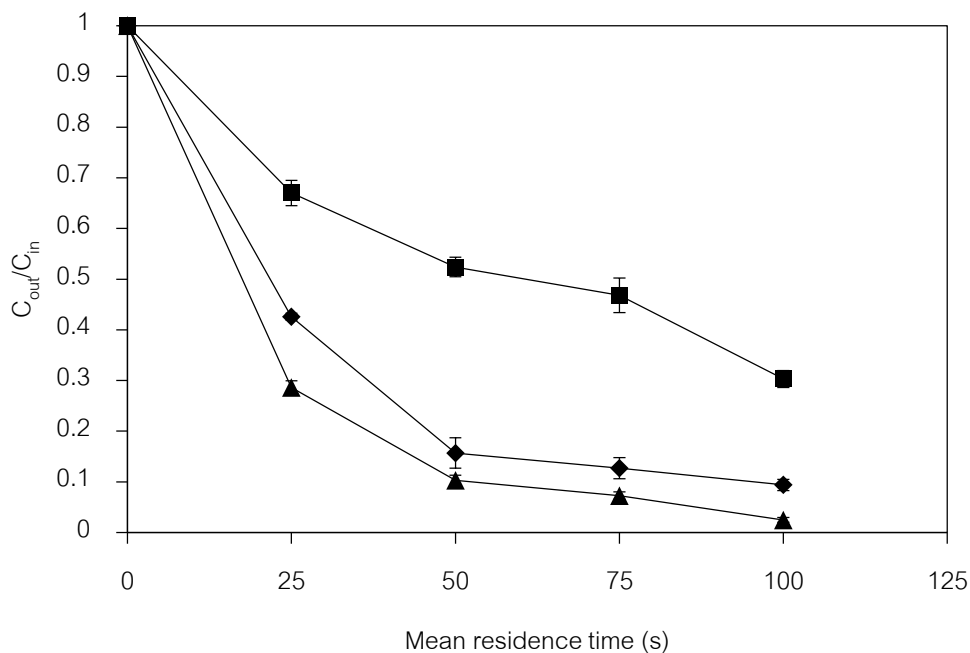


Figure 4.5 Effect of applied current on diuron degradation: (■) $I = 0.5$ mA, (◆) $I = 1$ mA and (▲) $I = 2$ mA

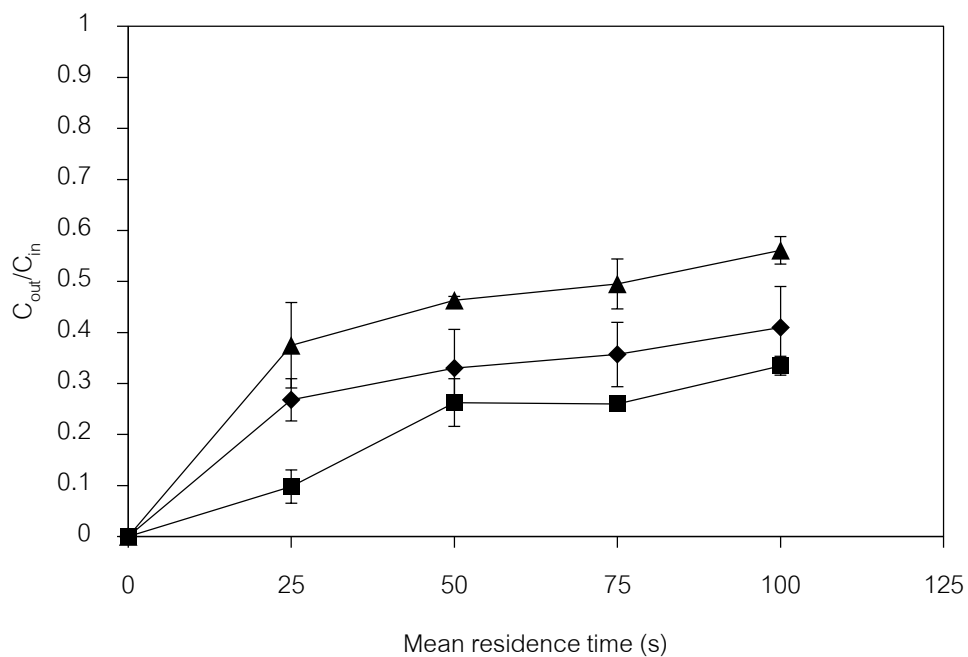


Figure 4.6 Amount of hydrogen peroxide detected in diuron solution during EAOP: (■)

I = 0.5 mA, (◆) I = 1 mA and (▲) I = 2 mA

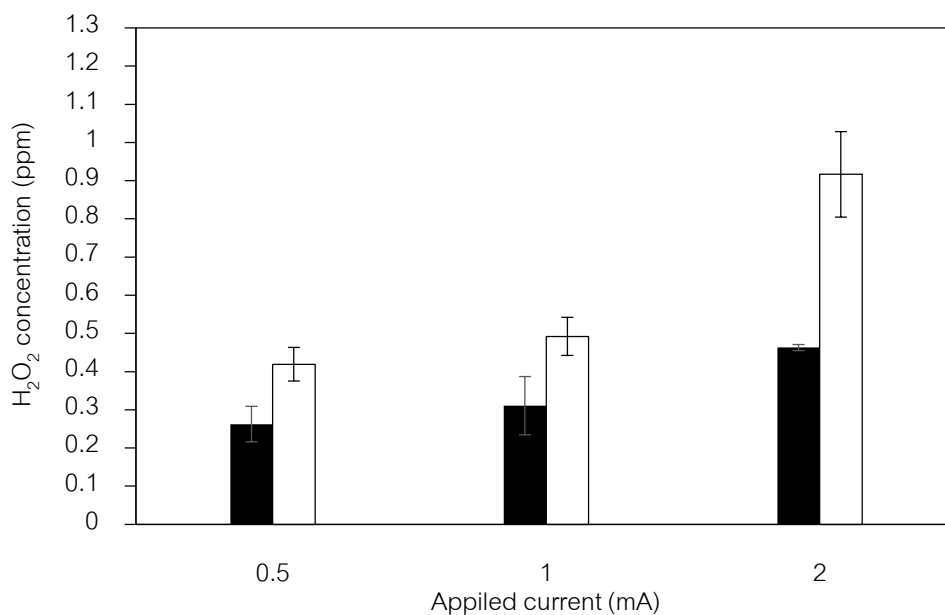


Figure 4.7 Formed hydrogen peroxide in system: (□) in pure deionized water and (■) in 10 ppm diuron solution: at 250 μ m of microchannel thickness and 50 s of residence time

Then, the data obtained at several residence times were also fitted to the pseudo first order model with $R^2 > 0.9$. Good fits were obtained as seen in figure 4.8, which indicated that the change in the applied current does not affect the order of the reaction. The reaction rate constant is 1.17×10^{-2} , 2.69×10^{-2} , and $3.79 \times 10^{-2} \text{ s}^{-1}$ when the applied current is 0.5, 1 and 2 mA, respectively. While the extent of diuron degradation is higher under higher applied currents, the enhancement in the degradation becomes less pronounced as the applied current exceeds 1 mA because of the competing radical-radical interaction [15, 73]. The production of hydrogen peroxide in pure deionized water at 2 mA of applied current was also much higher difference when compared with the production at 0.5 mA and 1 mA as shown in figure 4.7.

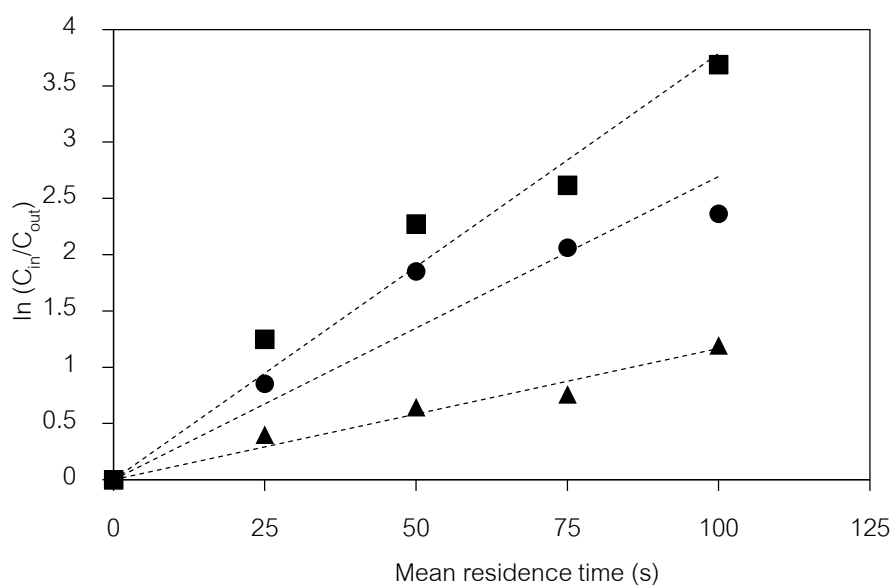


Figure 4.8 Pseudo first order kinetic plot of diuron degradation via EAOP under 0.5, 1 and 2 mA of applied current: (■) = 0.5 mA, (●) = 1 mA and (▲) = 2 mA

4.1.3 Microchannel thickness

The influence of microchannel thickness on diuron degradation was firstly studied by varying the gap between anode and cathode in the range of 250 to 750 μm , at fixed current of 1 mA. The mean residence time was also fixed at 100 s. As the height of the microchannel was increased to 750 μm , the flow rate of the solution had to be increased to keep the mean residence time constant. Although the thickness and flow rate were changed, however, linear velocity did not change. Since the applied current was fixed, the total number of electron supplied to the reactor was presumed to be unchanged. As a consequence, the number of electrons per volume of liquid processed in the microreactor was proportionally decreased. Also, the concentration of hydroxyl radical in the reactor should decrease as fluid flow rate and reactor volume increase. This is confirmed by the decrease in concentration of hydrogen peroxide detected in the experiments using pure deionized water, as shown in figure 4.9. Thus, as the concentration of the hydroxyl radical is decreased, diuron degradation is expected to decrease when the thickness of the microchannel is increased as shown in figure 4.9. The experimental results show that the degradation efficiency is decreased more drastically than expected. It is also interesting to point out that the concentration of hydrogen peroxide formed while diuron is degraded in a large (750 μm high) reactor is not substantially different than the value detected in the blank experiment. These observations indicate that, when the thickness of the microchannel is widened, majority of the hydroxyl radicals formed by the electrochemical reaction recombine to form hydrogen peroxide rather than interacting with diuron.

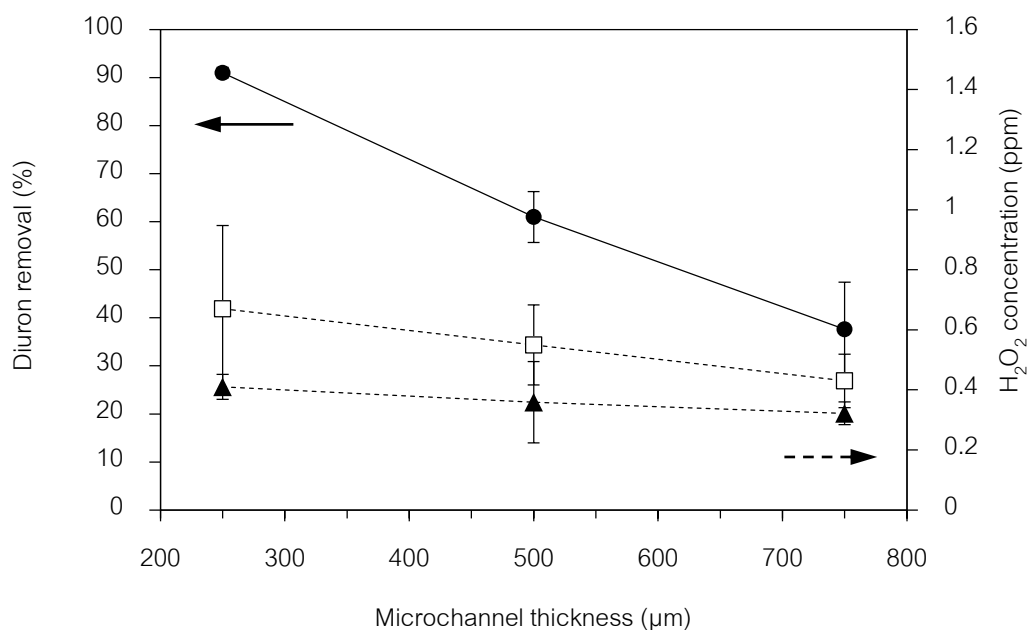


Figure 4.9 Effect of channel thickness on the degradation of diuron (●) and amount of hydrogen peroxide generated when pure water (□) and when diuron solution (▲) was supplied to the reactor. The reactor was operated under constant applied current of 1 mA

To further understand the effect of the microchannel height, another set of experiments were conducted. The gap between the electrodes was increased from 250 to 750 μm as previously indicated, but the applied current was also increased so that the number of charge per unit volume of the reactor, i.e., electron density, remained unchanged. The results are shown in figure 4.10. It is found that the concentration of hydrogen peroxide generated from pure water, which reflects the amount of hydroxyl radical produced in the system, is increased as the gap is widened. This is a result from the fact that the increase in the applied current in this case was accompanied by significant increase in applied potential, which subsequently increases the chance for dissociation of water to form hydroxyl radicals. Interestingly, however, the degradation of diuron in the large microchannel is still significantly less than that in 250-μm channel although the concentration of hydroxyl radical produced is proportionally increased.

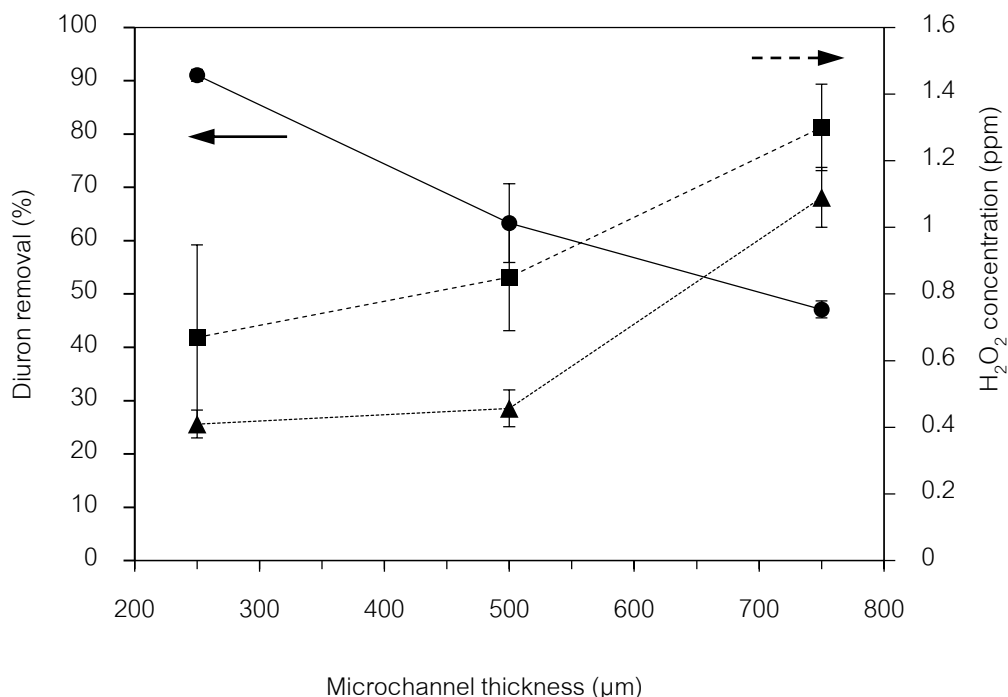


Figure 4.10 Effect of channel thickness on the degradation of diuron (●) and amount of hydrogen peroxide generated when pure water (■) and when diuron solution (▲) was supplied to the reactor under a condition of constant electron density

These results remind us that hydroxyl radicals are formed on the anode surface where they are present at higher concentrations rather than deeper in the bulk of the reactor toward the cathode. Hence, in the microreactor with a substantial height (750 μm), diuron near the cathode is not effectively degraded. This effect is negligible when the gap between the electrodes is small (250 μm) simply because the diffusion mechanism is adequate to transport hydroxyl radicals relatively quickly from the anode to the cathode and to transport diuron in the opposite direction.

Not only, microchannel thickness affected to diuron degradation, but also influenced to TOC removal as shown in figure 4.11. The increase microchannel thickness also decreased TOC removal. Moreover, the degradation of diuron still are pseudo first order reaction even changing thickness of microchannel which reaction rate constants are 2.69×10^{-2} , 0.98×10^{-2} and $0.52 \times 10^{-2} \text{ s}^{-1}$ at 250, 500 and 750 μm under 1 mA of applied current as shown in figure 4.12.



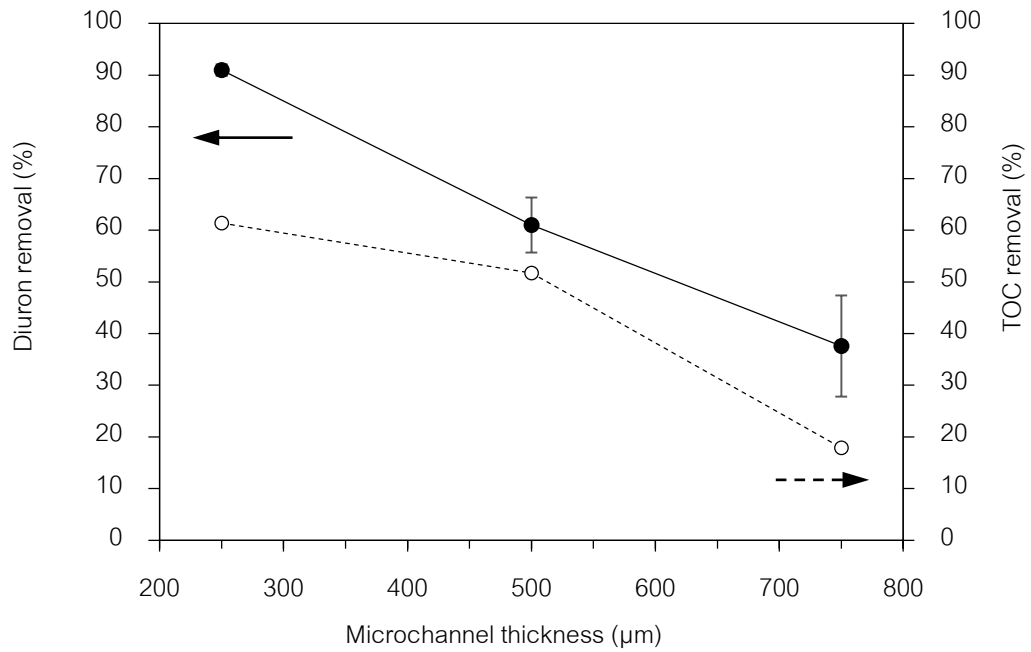


Figure 4.11 Effect of microchannel thickness on TOC removal

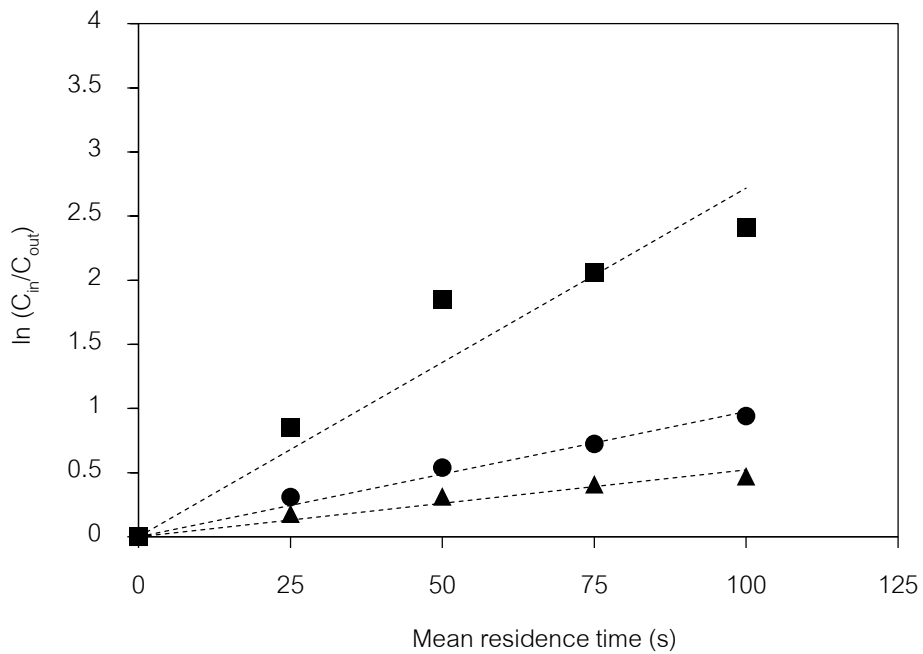


Figure 4.12 Pseudo first order kinetic plot of diuron degradation via EAOP under 1 mA of applied current: (■) 250 μm , (●) 500 μm and (▲) 750 μm of μm -thickness.

4.1.4 Initial solution pH and conductivity

It is well known that pH of solution plays an important role in the degradation of various organic compounds by oxidation processes. In this work, initial pH of the solution fed into the reactor was varied from strong acid (i.e., pH of 3.0), neutral (i.e., pH of 7.0) to strong base (i.e., pH of 10.0) by adjusting conductivity of the solution to 140 $\mu\text{S}/\text{cm}$ and on use buffer to control pH during running experiment. The results in figure 4.13 indicate that the degradation of diuron is more effective under acidic condition, which is similar to the results from other EAOP methods [37]. Under the applied current of 1 mA and residence time of 100 s, the degradation reaches 95.5% when the initial pH is 3.0, while the degradations of the solution with pH value of 7.0 and 10.0 are 88.3% and 82.2%, respectively. It should also be noted that pH of the solution is slightly decreased while the conductivity is slightly increased as diuron in the solution is degraded into acidic organic products.

The degradation efficiency is increased in acidic solution because more hydroxyl radicals are generated at low pH, as shown by the results in figure 4.14. It is consistent with the report that electrochemical generation of hydroxyl radicals via water discharge reaction in EAOPs is favored at pH lower than 9 [39]. Moreover, in a basic solution, the hydroxyl radical behaves as a weak acid and reacts with OH^- ion to form O^- [44]. As a result, decreased amount of hydroxyl radicals are available at high pH. The hydroxyl radical generated via dissociation of water, was produced quit excess. Therefore decrease in hydroxyl radical was not enough to drive forward the dissociation of water when OH^- react with hydroxyl radical in basic solution. Furthermore, the hydroxyl radical reacts readily with carbonate ion, which is one of the products from diuron degradation [1], when pH value is higher than 7 [74, 75]. Thus, the efficiency of diuron degradation is decreased in the basic solution.

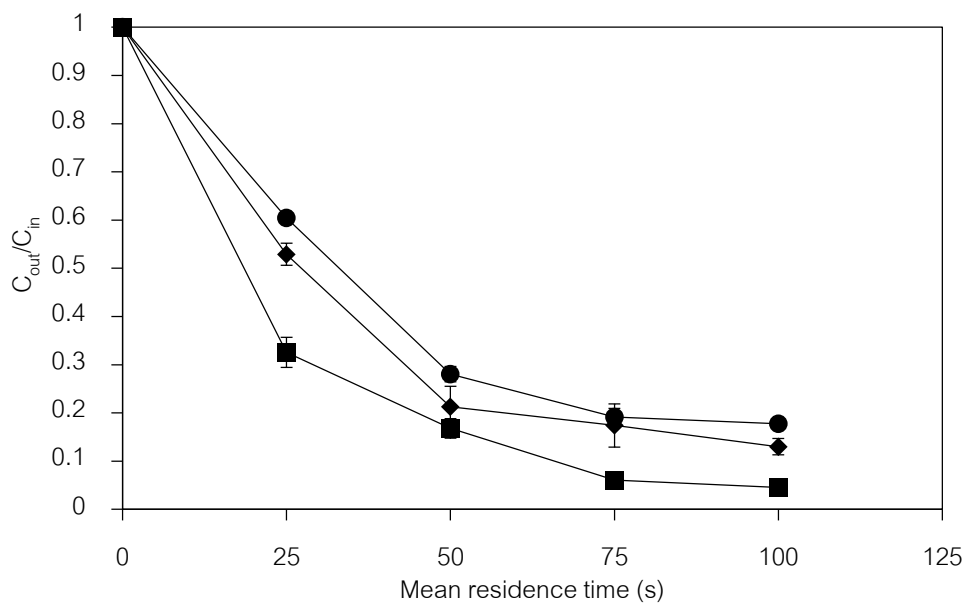


Figure 4.13 Effect of initial solution pH on diuron degradation: (■) pH=3.0, (◆) pH = 7.0 and (●) pH = 10.0

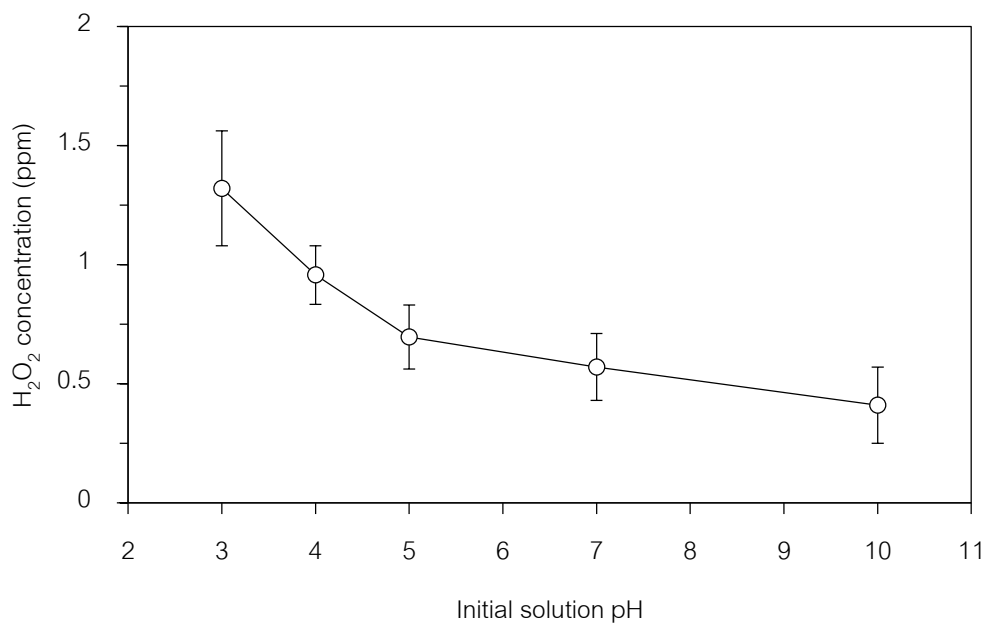


Figure 4.14 Formed hydrogen peroxide in pure deionized water under various pH of solution

Figure 4.15 shows effect of solution conductivity on the diuron degradation. When the conductivity of the solution is increased in the range from 6.7 to 1,000 $\mu\text{S}/\text{cm}$, efficiency of the degradation is decreased because the formation of active radicals is decreased as confirmed by the results shown in figure 4.16. The concentration of hydrogen peroxide in pure deionized water/diuron solution decreased with increasing initial solution conductivity. The effect of the conductivity seems to be less pronounced when the solution has conductivity higher than 500 $\mu\text{S}/\text{cm}$, which agrees with the previous report [47]. It should be noted that sodium chloride was used to adjust conductivity of the solution. The presence of chloride ion, which is a scavenger of hydroxyl radicals [76], also affects the degradation of diuron. Authors have reported that increasing in chloride ion increased degradation rate [41]. However, our results showed that in the presence of chloride ion decreased degradation rate due to the effect of solution conductivity effect were predominant, since very low concentration of chloride ion was added (0.001 – 0.009 M corresponding to 140 – 1000 $\mu\text{S}/\text{cm}$) which probably chloro-active species are formed in low concentration.

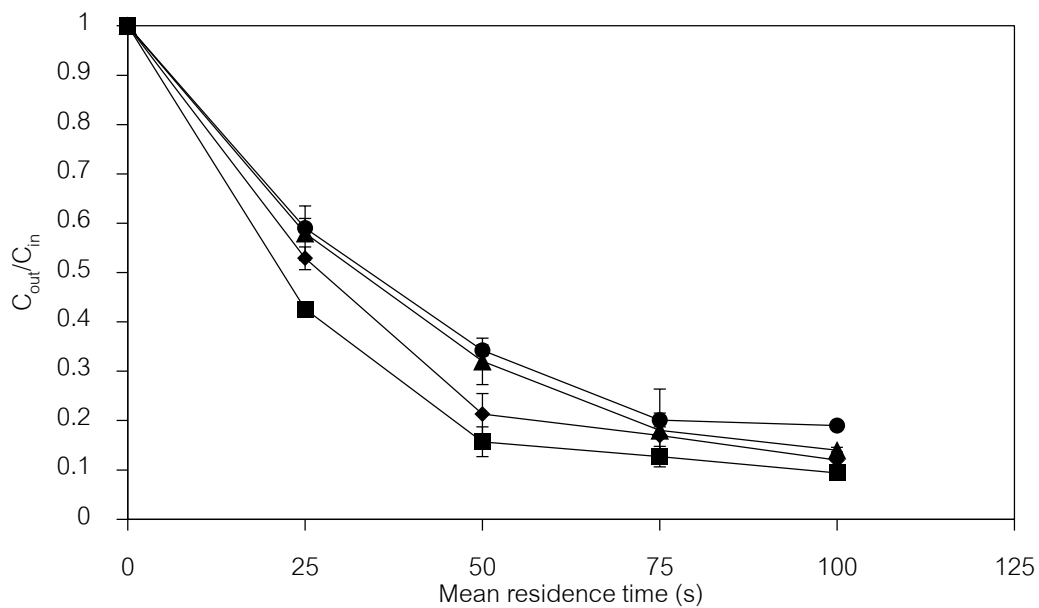


Figure 4.15 Effect of initial solution conductivity on diuron degradation: (■) No adjusted,

(◆) $\sigma = 140 \mu\text{S/cm}$, (▲) $\sigma = 500 \mu\text{S/cm}$ and (●) $\sigma = 1000 \mu\text{S/cm}$

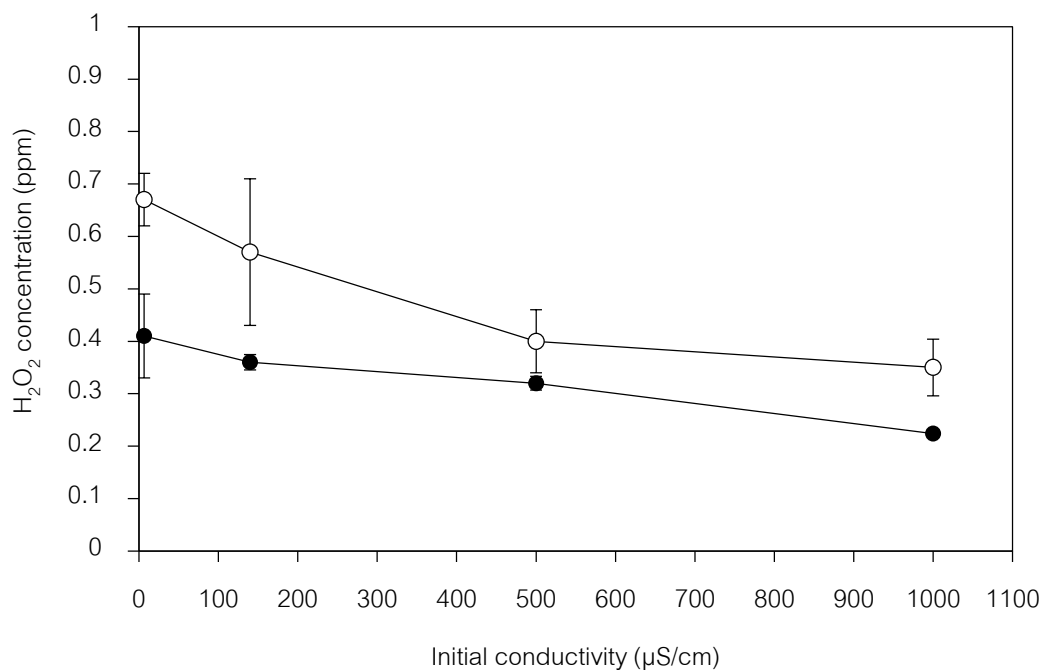


Figure 4.16 Formed hydrogen peroxide in systems: (○) in pure deionized water and (●)

in 10 ppm diuron solution

The change in either pH or conductivity of the solution ultimately affects diuron degradation because of the change in the amount of hydroxyl radicals produced. This conclusion can be corroborated by the plot in figure 4.17, which shows strong relationship between percentages of diuron degraded versus amount of hydrogen peroxide formed if no diuron is present in the solution. All data were collected using the same operating condition, i.e., applied current of 1 mA, channel thickness of 250 μm , and residence time of 100 s. As mentioned earlier, the concentration of hydrogen peroxide is an indirect representation of hydroxyl radicals produced by the system

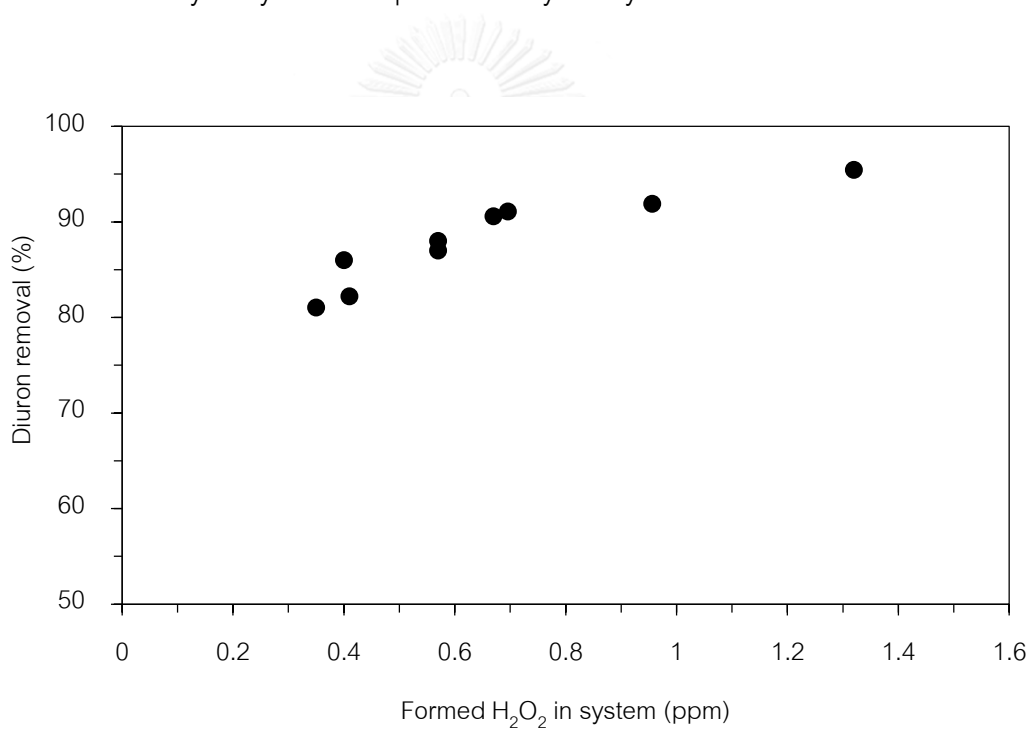


Figure 4.17 Correlation between concentrations of hydrogen peroxide detected when pure deionized water is supplied and diuron removal under the same condition

Although diuron degradation efficiency is influenced by both pH and conductivity of the solution, neither pH nor conductivity affects the order of the reaction. The pseudo first order kinetic model can still represent well the experimental data. However, the rate constant changes slightly. The rate constants for the degradation at initial pH of 3.0, 7.0, and 10.0 are 3.39×10^{-2} , 2.28×10^{-2} , $1.99 \times 10^{-2} \text{ s}^{-1}$, respectively, while that for the degradation in the solution with conductivity in the range of 6.7-1,000 $\mu\text{S/cm}$ varies from 2.69×10^{-2} to $1.88 \times 10^{-2} \text{ s}^{-1}$ as shown in table 4.4.

Table 4.4 The reaction rate constant (k) and R^2 value for the degradation of diuron under various initial solution conductivities and pHs.

Condition	Pseudo 1 st order reaction, k (s ⁻¹)	R ²
Initial solution conductivity		
▪ No addition	2.69×10^{-2}	0.90
▪ 140 $\mu\text{S/cm}$	2.34×10^{-2}	0.94
▪ 500 $\mu\text{S/cm}$	2.11×10^{-2}	0.98
▪ 1000 $\mu\text{S/cm}$	1.88×10^{-2}	0.95
Initial solution pH		
▪ 3.0	3.39×10^{-2}	0.96
▪ 7.0	2.28×10^{-2}	0.92
▪ 10.0	1.99×10^{-2}	0.92

4.1.5 Ion contamination

4.1.5.1 Effect of nitrate and sulfate ion on diuron degradation

To investigate the influence of nitrate and sulfate ion on diuron degradation, experiment was conducted by adding 0.05 M of nitrate and sulfate ion concentration in diuron solution, while no ion addition was control experimental. All conditions were conducted under 1 mA of applied current, 250 μm -thickness of microchannel and 25 - 100 s of mean residence time. It should be noted that cation didn't affect and participate to diuron degradation due to cations prefer to receive electron for reduction. Main reaction of the diuron degradation is oxidation, which is induced by hydroxyl radical. Additionally, in our experiment type of cation was fixed, is sodium ion. Generally, sodium ion could be reduced to sodium solid. However, sodium solid was not found in our experiment due to low voltage and current density were supplied.

Diuron could be degraded although nitrate and sulfate contaminated in solution. The diuron degradation slightly decreased when compared with the diuron degradation under no ion contamination, which was 91%, 79% and 76% corresponds to no ion, nitrate and sulfate ion, respectively as shown in figure 4.18. When 0.05 M of nitrate and sulfate in pure deionized water was supplied to reactor (100 s of mean residence time), the concentration of hydrogen peroxide was 0.34 and 0.14 ppm, respectively, which was lower comparing with it formed under no ion contamination in pure deionized water (0.67 ppm) as shown in figure 4.19. It indicated that production of hydroxyl radicals was low when nitrate and sulfate contaminated in solution. It has been reported that these two anions acted as hydroxyl radical scavenger to reduce hydroxyl radical via advanced oxidation process [17, 46]. However, more than 1000 times of ion concentration is higher when compared with diuron concentration (10 ppm = 0.043 mM of initial diuron concentration). Therefore, the diuron degradation should be lower than the degradation that we observed if hydroxyl radical scavenger of these anions was major role alone. It

implied that other mechanism should dominate over the hydroxyl radical scavenging of ion during EAOP in a microreactor.



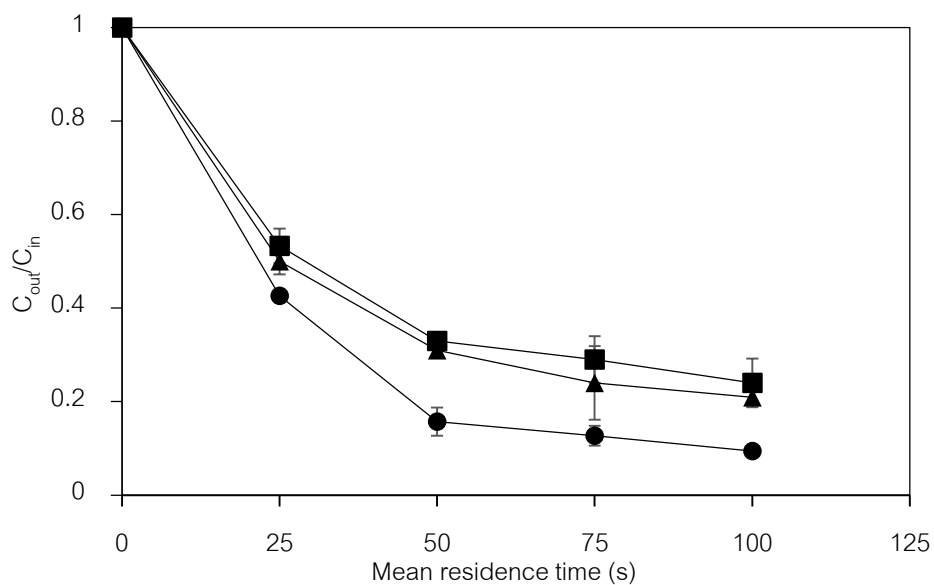


Figure 4.18 Diuron degradation under 0.05 M of nitrate and sulfate ion contamination:

(▲) = nitrate ion, (■) = sulfate ion and (●) = no ion.

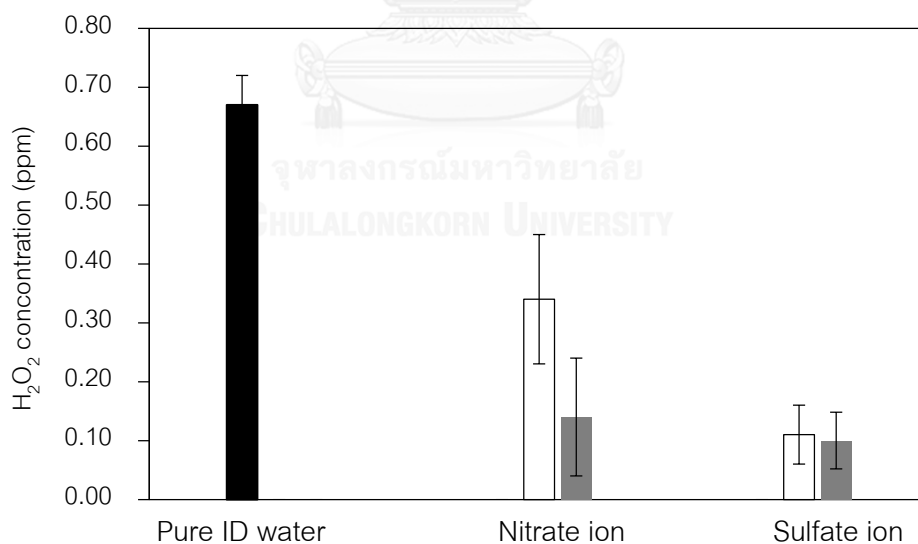


Figure 4.19 Formation of hydrogen peroxide in deionized water and diuron solution under 0.05 M of ion contamination via EAOP: (□) = in pure water, (■) = in diuron solution and (■) = no ion.

Electrosorption, which is defined as potential induced adsorption of ion onto the surface of charge electrodes, is applied to brackish water desalination and water purification process that is called “capacitive deionization (CDI)” [77]. To confirm the electrosorption mechanism in our system, another set of experimental was conducted. Firstly EAOP of 0.05M of nitrate and sulfate ion in pure deionized water was conducted. When system reached steady state condition, then 0.05M of anions concentration were switched to 0.043mM (equal to 10 ppm of initial diuron concentration). Coming out of ion concentration was collected before and after switching ion concentration under steady state condition. All conditions were conducted under 1 mA of applied current, 250 μ m-thickness of microchannel and 100 s of mean residence time. Concentration profile of nitrate ion both of before and after switching the concentration as shown in figure 4.20. The results showed that nitrate concentration decreased to 0.045 M, after switching the concentration (0.043 mM), nitrate concentration continuously decreased to 0.031 mM. However, concentration of formed hydrogen peroxide was significantly constant both of before and after switching nitrate concentration, which was 0.32 and 0.35 ppm, respectively as shown in figure 4.21. It indicated that hydroxyl radical was constantly generated both of before and after change concentration. To more understand electrosorption mechanism, another set of experiment condition was conducted, 0.043 mM of nitrate concentration in pure deionized water was supplied to reactor in the beginning of reaction. The results show that nitrate concentration rapidly decreased to 0.001 mM, while formed hydrogen peroxide was 0.63 ppm (same level as formed hydrogen peroxide in pure deionized water). The difference of coming out of nitrate ion and formed hydrogen peroxide in pure water, was observed when 0.05 M and 0.043 mM was initial feed stock due to electrosorption contributed during EAOP.

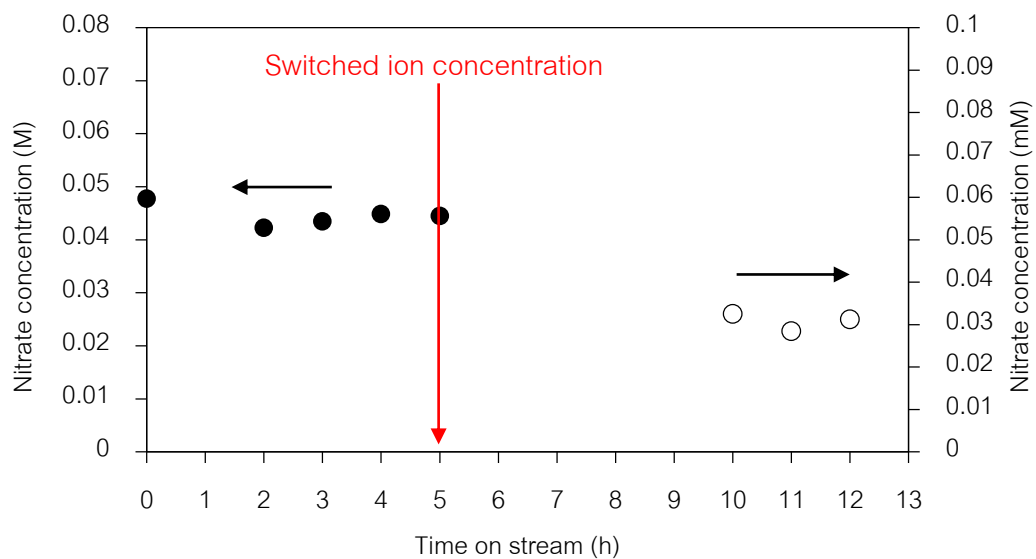


Figure 4.20 Concentration profile of nitrate ion in pure deionized water both of before (0.05 M) and after (0.043 mM) switching the ion concentration.

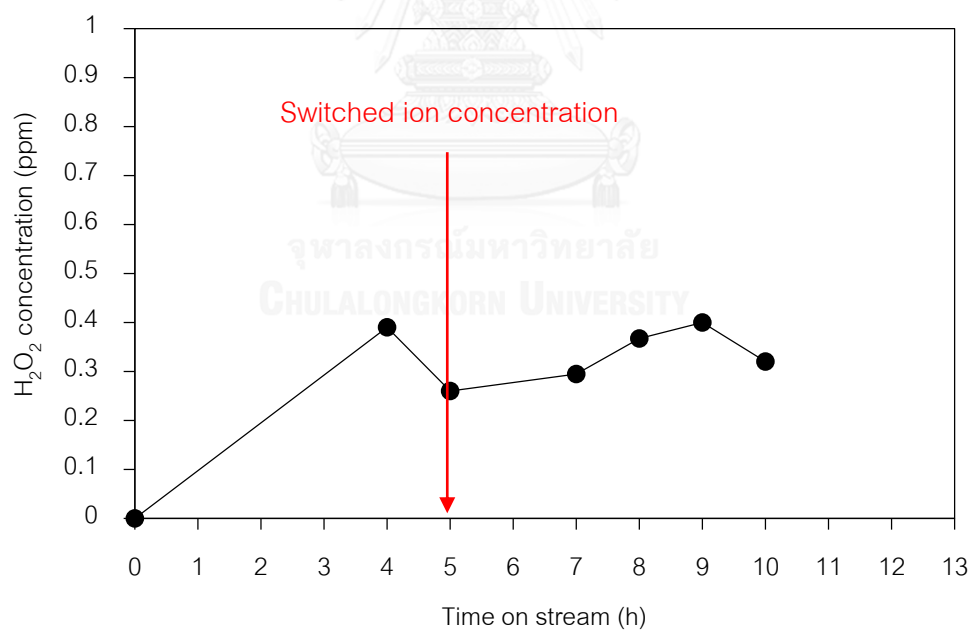


Figure 4.21 The concentration of hydrogen peroxide in pure deionized water both of before (0.05 M) and after (0.043 mM) switching the ion concentration

In case of 0.05M as initial concentration, nitrate ion is anion, partially adsorbed on anode surface by positive charge generated at electrode surface. During EAOP, the amount of anion on surface was constantly adsorbed although nitrate concentration was changed to low concentration (0.043 mM). Consequently, active site on anode were almost covered by nitrate ion as result in molecule of water partially oxidized to form hydroxyl radicals. In contrast, if 0.043 mM of nitrate concentration was supplied in the beginning, nitrate concentration rapidly decreased, while hydrogen peroxide was formed in higher concentration. It indicated that most of active site on anode uncovered by anion due to very low ion concentration was supplied. Therefore more active sites on surface were provided for dissociation of water to generate hydroxyl radicals, and recombine to form hydrogen peroxide.

However, due to outlet concentration of nitrate was lower than inlet concentration (both of before and after switching the ion concentration), the hydroxyl radical scavenger of ion still occurred to reduce ions. This behavior also was observed when solution contaminated with sulfate ion. It should be noted that nitrate ion did not reacted with diuron under no applying current, which diuron and nitrate ion were constant in controlled experiment. In the conclusion, anions adsorbed on positive charge at anode by electrosorption during EAOP in a microreactor. Anions adsorbed on anode surface, while dissociation of water partially occurred to form hydroxyl radicals at the same time. Portion of hydroxyl radicals were scavenged by anion while remain of hydroxyl radicals reacted with diuron and recombine together to form hydrogen peroxide. However, due to over 75% of diuron degradation was achieved, while high concentration of ion was supplied in diuron solution. It indicated that electrosorption was dominated over the scavenger of hydroxyl radical by anion.

As comparing between the diuron degradation under 0.05 M of nitrate and sulfate ion contamination, the diuron degradation under nitrate contamination showed higher efficiency than the degradation under sulfate ion. The formed hydrogen peroxide in nitrate solution also was higher than hydrogen peroxide formed in sulfate solution (both in pure deionized water and diuron solution) as shown in figure 4.19. It indicated that higher hydroxyl radicals were present under nitrate contamination than that were presented under sulfate contamination. It should be noted that different charge influence to adsorption capacity of ion on electrode [77]. However, our results show that the adsorption capacity of two anion are not different as same concentration. Therefore, ion concentration show more effect than charge of ion on diuron degradation under our experiment condition. It has been reported that sulfate ion has higher order reaction rate constant of hydroxyl radical scavenger than nitrate ion [17, 46], as the result in faster consumption of hydroxyl radicals.

The effect of ion concentrations on diuron degradation also was investigated. The experiments were conducted by adding 0.0013, 0.005 and 0.05 M of nitrate concentration in diuron solution. All conditions were conducted under 1 mA of applied current, 250 μm -thickness of microchannel and 25 - 100 s of mean residence time. It should be note that increasing in nitrate and sulfate concentration slightly reduced applied potential ($\sim 2.7 - 3.0$ V), which indicated that it cloud be neglect the effect of electrical potential on degradation. The diuron degradation slightly decreased with increasing nitrate concentration, which was 89%, 85% and 79% corresponds to 0.0013M, 0.005M and 0.05M of nitrate concentration, respectively as shown in figure 4.22. The formed hydrogen peroxide in pure deionized water of 0.0013 to 0.05M also were decreased 0.33 ppm to 0.11 ppm as shown in figure 4.23. It indicated that hydroxyl radical production was low when nitrate contaminated in solution increased. The increase of ion concentration resulted in increased amount of ions adsorbed on surface which the electrosorptive

capacity of electrode increased with increasing solution concentration [78], leading to low active surface area for dissociation of water to produce hydroxyl radicals. Figure 4.24 shows scheme of the electrochemical mechanism of diuron degradation under contamination of nitrate or sulfate ion via EAOPs in microreactor.



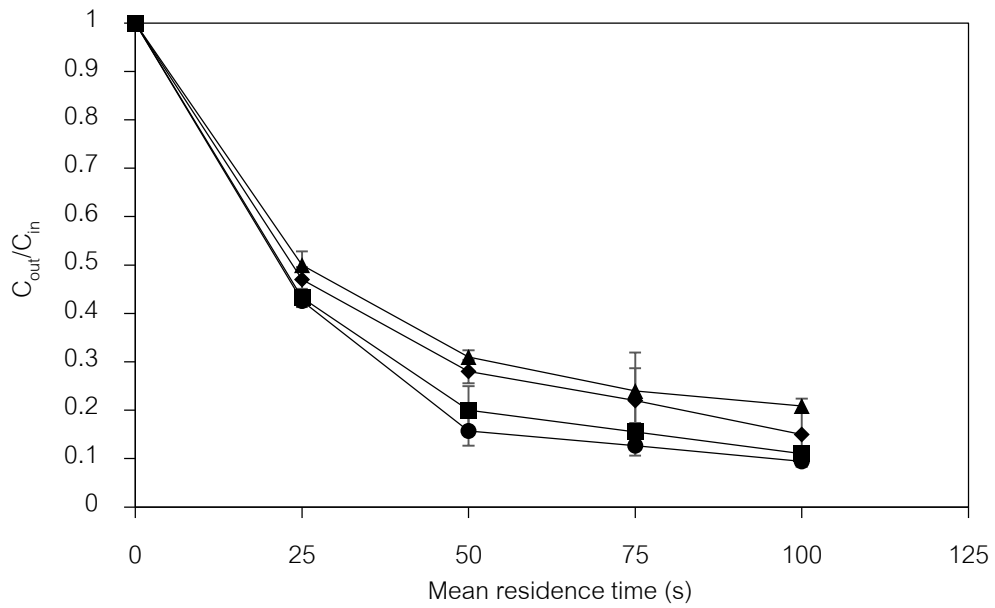


Figure 4.22 Effect of nitrate ion concentration on diuron degradation: (■) = 0.0013, (◆) = 0.005, (▲) = 0.05 M and (●) = no ion.

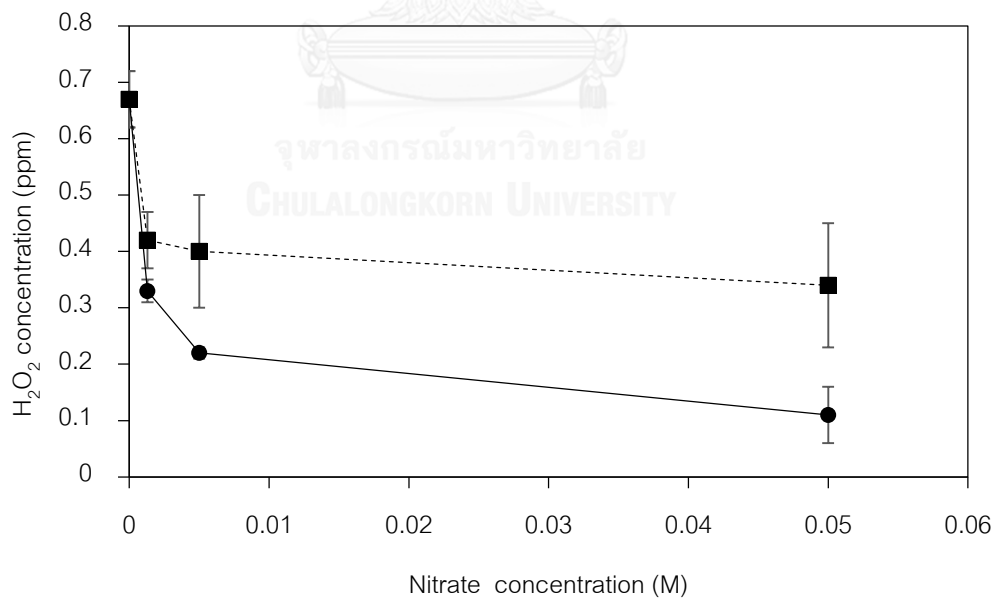


Figure 4.23 The concentration of hydrogen peroxide formed in pure water (■) and diuron solution (●) under 100 s of mean residence time

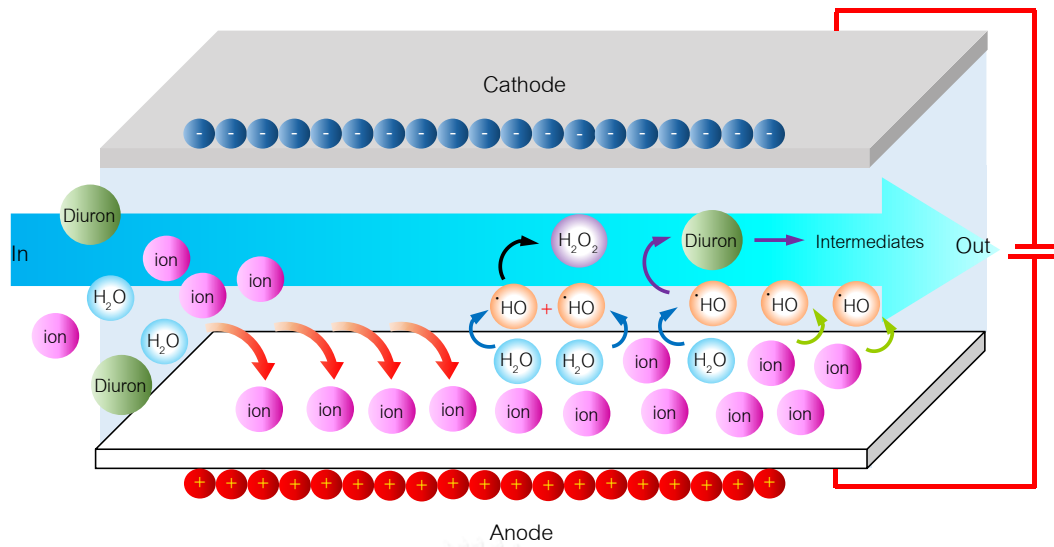
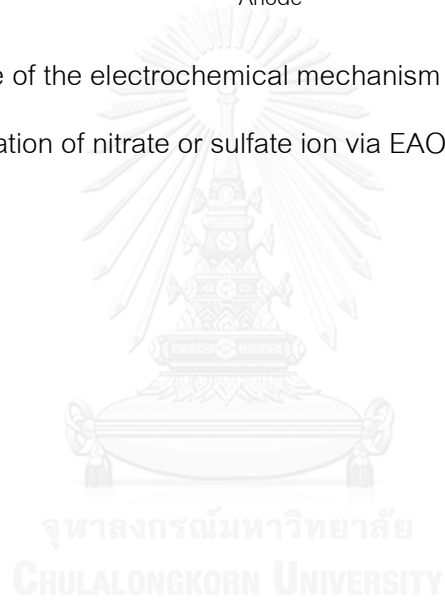


Figure 4.24 Scheme of the electrochemical mechanism of diuron degradation under contamination of nitrate or sulfate ion via EAOPs in microreactor



4.1.5.2 Effect of nitrate and sulfate ion on total organic carbon (TOC) removal

TOC of diuron degradation under ion contamination was also analysed. Diuron was degraded up to 80 %, while TOC removal still remained 54% and 51% under nitrate and sulfate ion condition respectively, which indicated that many reaction intermediates were formed as shown in figure 4.25. Under sulfate ion, TOC removal was slightly lower when compared with nitrate ion due to hydroxyl radicals were more production under nitrate contamination. As increasing nitrate ion concentration, TOC removal was slightly decreased, which the effect of low production of hydroxyl radicals and hydroxyl scavenger influenced to TOC removal as shown in figure 4.26.

The mineralization current efficiency (MCE) and the energy consumption per unit TOC (EC_{TOC}) were also calculated under nitrate and sulfate contamination via equations 4.5 and 4.7 [70-72]. For diuron degradation via EAOP under nitrate and sulfate ion contamination at the applied current of 1 mA in this work, the value of MCE decreased while that of EC_{TOC} increased with longer residence time. The results suggest that the degradation of recalcitrant intermediates requires large amount of energy for total mineralization of diuron. Table 4.5 shows values of MCE and EC_{TOC} of diuron degradation via electrochemical advanced process under contamination of nitrate and sulfate ion.

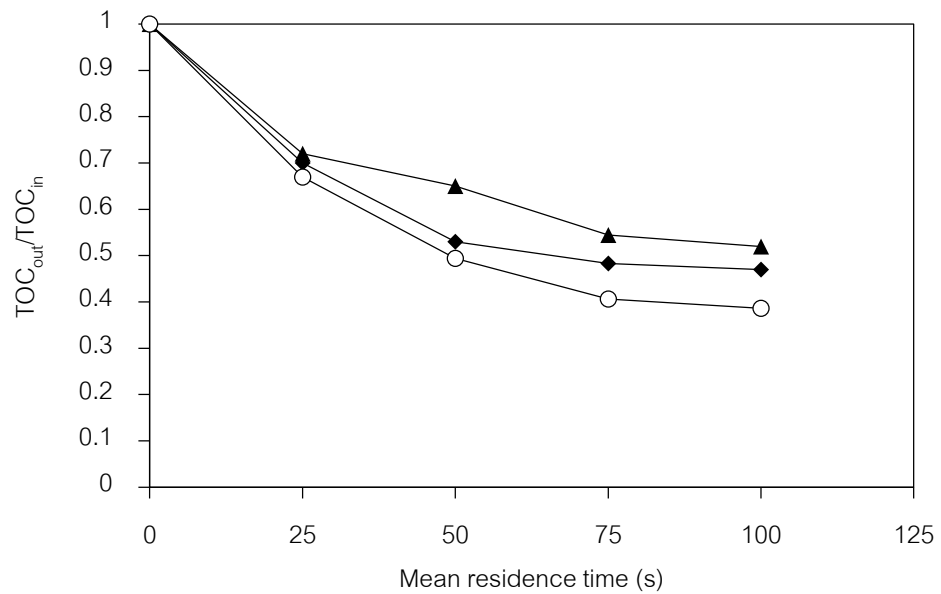


Figure 4.25 TOC removal under 0.05 M of nitrate ion (◆), sulfate ion (▲) and no ion (○) contamination

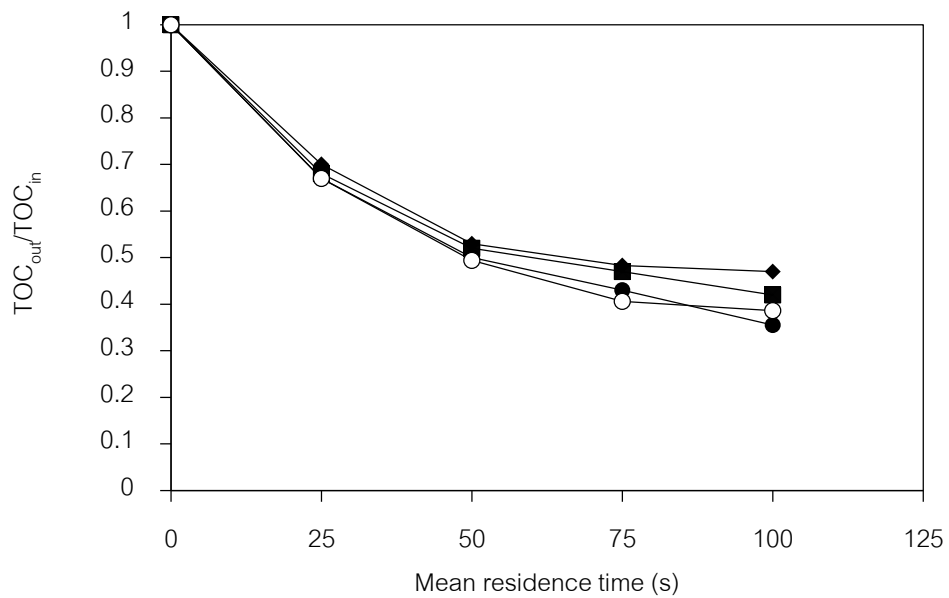


Figure 4.26 The effect of ion concentration on TOC removal: (●) = 0.0013 M, (■) = 0.005 M, (◆) = 0.05 M of nitrate concentration and (○) = no ion contamination

Table 4.5 The values of MCE and EC_{TOC} of diuron degradation via electrochemical advanced process under contamination of nitrate and sulfate ion ($I = 1$ mA and residence time = 100 s).

Condition	%MCE	EC_{TOC} (kWh·g ⁻¹ TOC)
Nitrate ion		
▪ 0.0013 M	9.30	0.36
▪ 0.005 M	8.27	0.41
▪ 0.05 M	7.36	0.46
Sulfate ion		
▪ 0.05 M	5.45	0.62

4. 2 Identification Intermediate products and reaction pathway of diuron degradation via electrochemical advanced oxidation process in a microreactor

As diuron is degraded toward its mineralization, the total organic carbon (TOC) of the solution is decreased. However, the experimental data show that the decrease in TOC is not as much as the decrease in diuron concentration (see Figure 4.27). For the degradation under the applied current of 1 mA and residence time of 100 s, about 90% of diuron is degraded, but the TOC in the solution is decreased only by about 60%. This indicates that reaction intermediates are formed. According to HPLC analysis, signals from 11 intermediate compounds were detected (see Table 4.6). Using standard reference compounds, only three intermediates could be identified and quantified, namely 3 - (3,4 -dichlorophenyl)-1-formyl-1-methylurea (compound 1, C₁), 3-(3-chlorophenyl)-1,1-dimethylurea (compound 2, C₂), and 3,4-dichloro-aniline (compound 3, C₃), respectively. For other intermediates, they were identified using LC-MS/MS, which will be discussed in the next topic. Structure of compound 1, 2 and 3 show in table 4.8.

Partial results from the quantitative analysis, from residence time of 0 to 25 s, indicated that concentrations of compound 1, 2 and 3 increased, which suggested that they were direct products of diuron degradation. As the residence time is prolonged, 3 reference compounds gradually decreased indicating further degradation. Figure 4.28 shows concentration of compound 1, compound 2 and compound 3. HPLC intensity peak of 11 intermediates are shown in figure 4.29 and 4.30 (low intensity of intermediates) show. To further understand the mechanism of diuron degradation via EAOP, the degradations of these three known intermediates were investigated using commercially available standards.

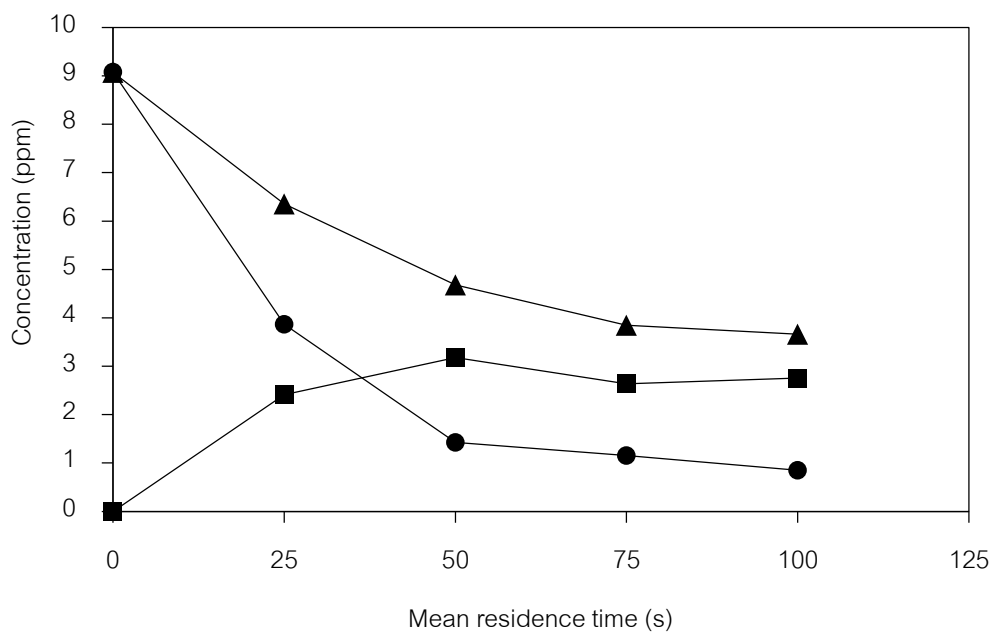


Figure 4.27 Decomposition of diuron by EAOP and evolution of the degradation intermediates under the applied current of 1 mA: (●) diuron, (■) unidentified compounds and (▲) TOC

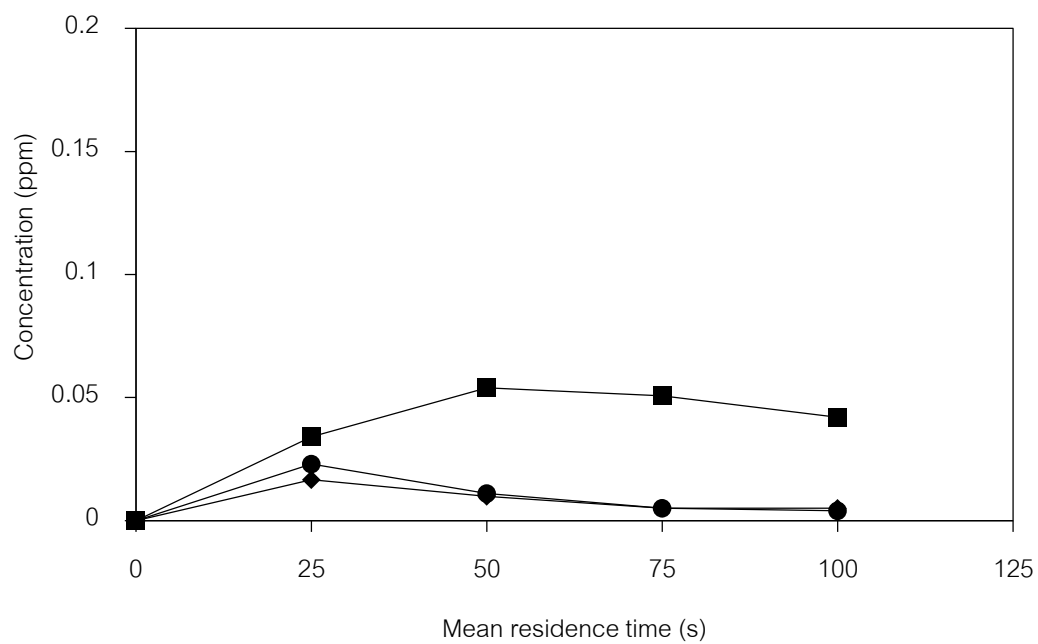


Figure 4.28 Profile of C₁, C₂ and C₃ concentration during diuron degradation via EAOP:

(●) C₁, (■) C₂ and (▲) C₃

Table 4.6 Intermediates detected from degradations of diuron and its intermediates by HPLC.



Parent compound	Retention time in HPLC chromatogram (min)																		
	1.31	1.51	1.74	1.84	2.00	2.09	2.19	2.30	2.57	2.63	2.67	3.01	3.25	3.37	3.57	3.89	4.19	4.22	
										(C ₂)					(C ₃)	(C ₁)			
Diuron	✓	✓	✓	✓	✓	✓	✓	✓	✓	✓	✓	✓	✓	✓	✓	✓	✓	✓	✓
Compound 1 (C ₁)	✓	✓	✓	✓	✓	✓	✓	✓	✓	✓	✓	✓	✓	✓	✓	✓	✓	✓	✓
Compound 2 (C ₂)	✓	✓	✓	✓	✓	✓	✓	✓	✓	✓	✓	✓	✓	✓	✓	✓	✓	✓	✓
Compound 3 (C ₃)	✓	✓	✓	✓	✓	✓	✓	✓	✓	✓	✓	✓	✓	✓	✓	✓	✓	✓	✓

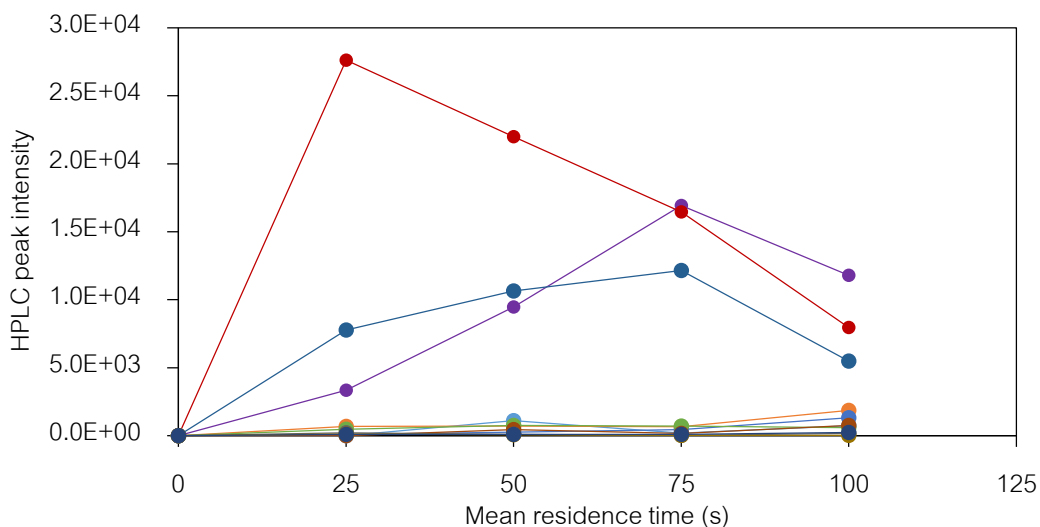


Figure 4.29 Intensity of intermediate products of diuron degradation by HPLC under no anion contamination: (●) RT = 1.51 min, (●) RT = 1.84 min, (●) RT = 2.00 min, (●) RT = 2.30 min, (●) RT = 2.57 min, (●) RT = 2.67 min (C_2), (●) RT = 3.01 min, (●) RT = 3.37 min, (●) RT = 3.57 min (C_3), (●) RT = 3.89 min (C_1) and (●) RT = 4.19 min

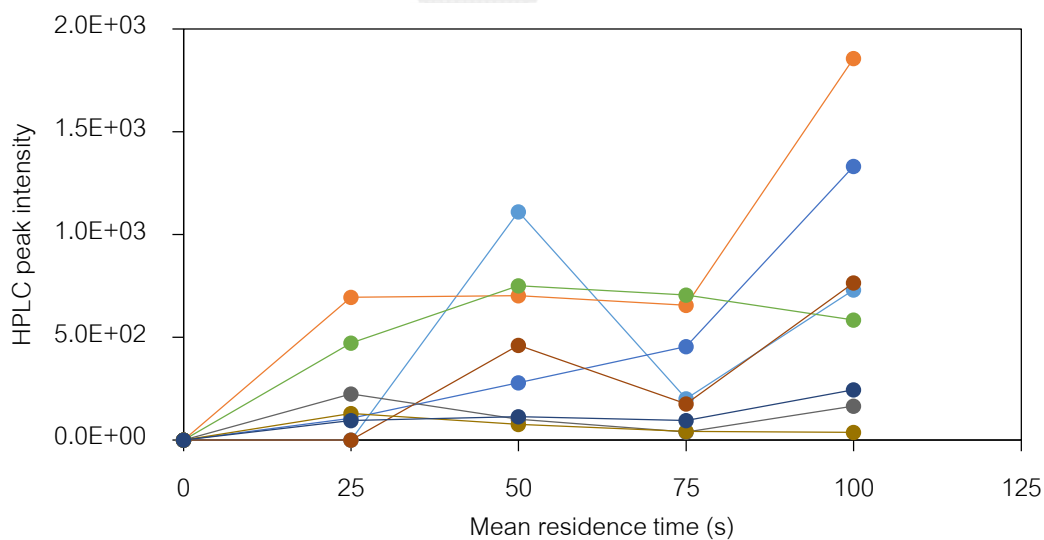


Figure 4.30 Intensity of intermediate products of diuron degradation by HPLC under no anion contamination (low intensity of intermediates): (●) RT = 1.51 min, (●) RT = 1.84 min, (●) RT = 2.57 min, (●) RT = 2.67 min (C_2), (●) RT = 3.37 min, (●) RT = 3.57 min (C_3), (●) RT = 3.89 min (C_1) and (●) RT = 4.19 min

4.2.1 The degradation of 3 reference standard compounds

To further understand the mechanism of diuron degradation via EAOP in a microreactor, the degradations of these three known intermediates were investigated using commercially available standards. The same condition with diuron degradation were also operated, which were 1 mA of applied current, 250 μm of microchannel and 25 - 100 s of residence time. Figure 4.31 shows the degradation of three standard compounds. As expected, the degradation of three compounds increased with increasing residence time.

The degradations of compound 1, 2 and 3 still follow the pseudo first order kinetic reaction, which the rate constants of 5.81×10^{-2} , 2.94×10^{-2} , and $3.98 \times 10^{-2} \text{ s}^{-1}$, respectively as shown in table 4.7. It can be seen that the degradations of these intermediates were faster than the apparent rate of diuron degradation. Furthermore, the rate constant for the degradation of 3,4-dichloro-aniline (compound 3) by EAOP in this work is two order of magnitude higher than that achieved by photocatalysis [79].

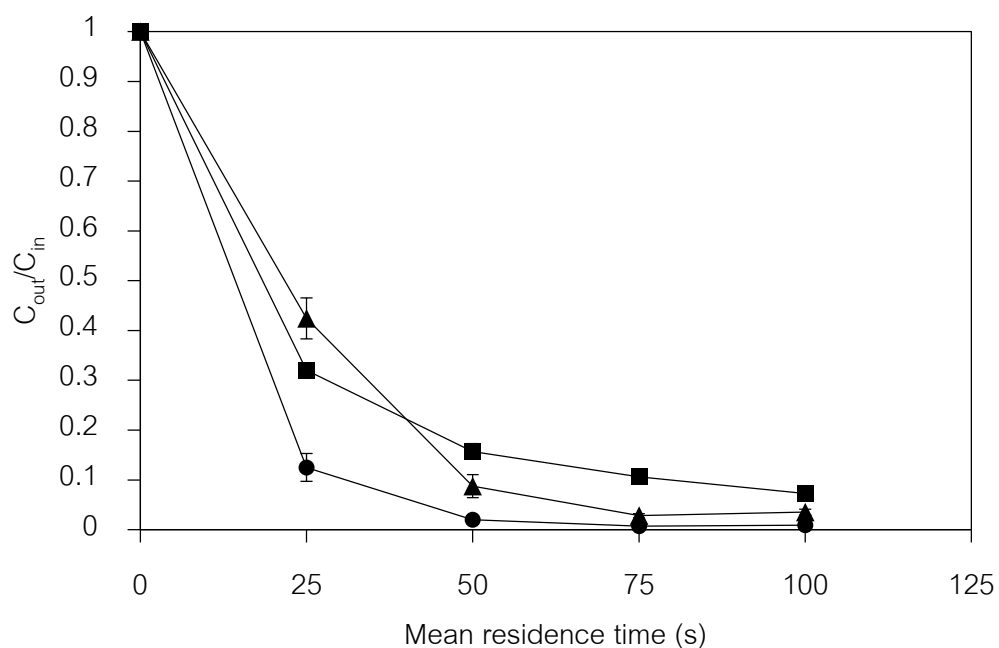


Figure 4.31 Degradation of compound 1, 2 and 3 via EAOP in a microreactor: (●) C₁, (■) C₂ and (▲) C₃

Table 4.7 Reaction rate constant (k) and R² value for the degradation of diuron and three reference compounds via EAOP in microreactor

Compound	Pseudo 1 st order reaction	
	k (s ⁻¹)	R ²
Diuron	2.69×10 ⁻²	0.90
C ₁ , 3-(3,4-dichlorophenyl)-1-formyl-1-methylurea	5.81×10 ⁻²	0.82
C ₂ , 3-(3-chlorophenyl)-1, 1-dimethylurea	2.94×10 ⁻²	0.91
C ₃ , 3,4-dichloroaniline	3.98×10 ⁻²	0.90

4.2.2 Identification of main intermediates and degradation pathway of diuron during electrochemical advanced oxidation process

In order to identify intermediate compounds that could not be determined by the conventional HPLC, LC-MS/MS was used. However, quantitative analysis could not be performed because the standard compounds were not commercially available. Identification of intermediate structures were investigated both of no anion contamination and anion contamination. All conditions were conducted by varying mean residence time in the range of 25 - 100 s at 1 mA of applied current, 250 μm -thickness of microchannel.

4.2.2.1 No anion contamination

(1) The intermediate products of diuron

According to LC-MS/MS analysis, in addition of ten compounds were identified which were 4, 5, 6, 7, 8, 9, 10, 12, 13 and 15. All identified intermediates by HPLC and LC-MS/MS under no ion condition are shown in Table 4.8. It should be noted that the 3 reference compounds already identified by the HPLC were also confirmed by LC-MS/MS analysis. Figure 4.32 shows intensity of LC-MS/MS peak of diuron degradation under no anion contamination.

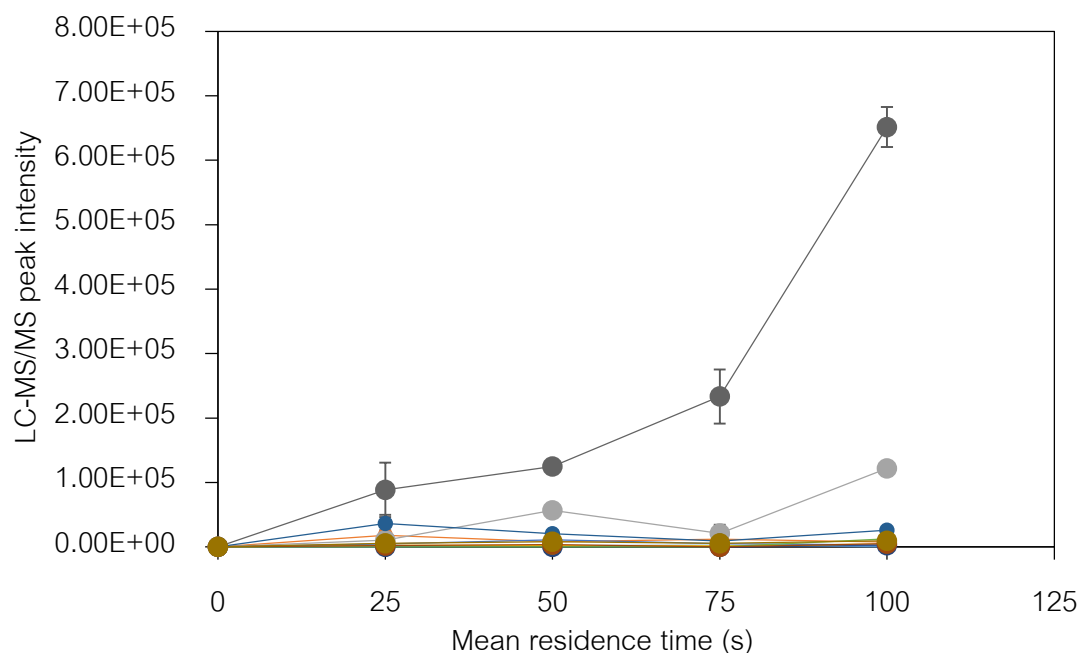


Figure 4.32 LC-MS/MS intensity of intermediate products of diuron degradation under no anion contamination (negative mode): (●) C₁, (●) C₃, (●) C₅, (●) C₆, (●) C₇, (●) C₈, (●) C₉, (●) C₁₀, (●) C₁₂, (●) C₁₃ and (●) C₁₅

As well known, hydroxyl radical, which generated via EAOP in aqueous solution, played an important role to oxidize organic compounds providing several reaction intermediates. Due to hydroxyl radical is electrophilic, the general mechanism of diuron degradation in oxidation process is reacting of hydroxyl radical with diuron molecules on both of aromatic ring and aliphatic side chain [50]. According to molecular structure of diuron, it is suggested that molecule of diuron was initially attacked by hydroxyl radical at methyl group on aliphatic side chain to formation compound **1** and **13**, which were firstly identified and classified to be primary products [1, 5]. It has been reported that C atom on methyl group is the most one of favorable position that hydroxyl radical is easier to attack first because of it has the lowest barrier energy comparing with C atom at another position [51]. After the formation of compound **1** and **13**, consequently, compound **7** was

formed by decomposition of compound **13** and hydrolysis of compound **1** [5]. Consequently, compound **9**, **10** and **12** was formed by the attack of hydroxyl radicals on alkyl side chain of their structures via demethylation process as shown in figure 4.33 [6, 8, 37, 49, 80]. The smallest detected intermediated was observed, which was 3,4-dichloroaniline (compound **3**). Explanation of formation compound **3** was cleavage of N-C bond of urea group and to form -NH_2 under the oxidation of aliphatic side chain [2]. Demathylation process of diuron degradation is one of the main pathway of diuron degradation as shown in pathway II represented in figure 4.37. Only one conjugated products were observed which was compound **15**, which was formed by organic radicals were produced and probably recombined with each other to form higher molecular mass as shown in pathway IV in figure 4.37 [81]. Due to hydroxyl radical is generated at anode surface, compound **1**, **3**, **7**, **9**, **10**, **12**, **13** and **15** are formed at anode.

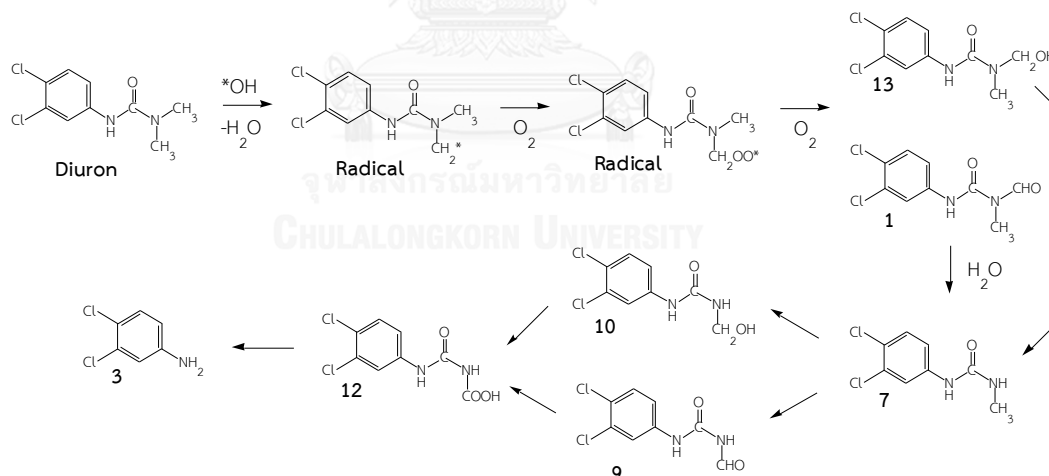


Figure 4.33 Demethylation process during degradation of diuron via EAOP

Moreover, hydroxyl radicals also promoted to form hydroxylated-products via hydroxylation of aromatic ring which is compound **6**. Compound **6** was identified by substitution of Cl by OH and releasing Cl ion simultaneously via dechlorination and

hydroxylation as shown in figure 4.34 [2, 8, 49, 50]. After the formation of compound 6, consequently, compound 5 and 8 were probably formed via demethylation process after ring hydroxylation [2]. Due to hydroxyl radical mainly induces to form compound 5, 6 and 8, these three compounds also are formed at anode. Hydroxylation of diuron is also one of the main pathway of diuron degradation as shown in pathway I in figure 4.37.

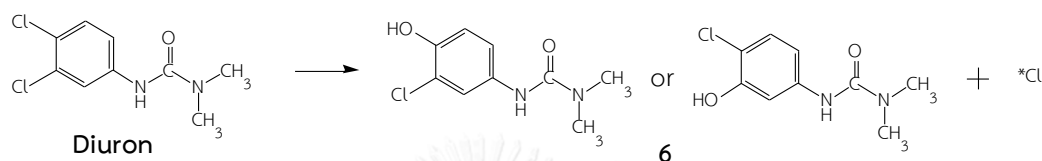


Figure 4.34 Hydroxylation of aromatic ring during degradation of diuron via EAOP

In addition, dechlorination or reduction took place by electrophilic substitution after transferring of electrons, which resulted in the formation of compound 2 at cathode, was the first reduction products as shown in figure 4.35 [8]. Consequently, compound 2 transformed to compound 4 via demethylation process, which it was formed at anode. Reduction of diuron is presented in pathway III in figure 4.37. After the demethylation, hydroxylation and reduction of diuron, the intermediates underwent to opened ring reaction and to final products (water and carbon dioxide). Thus, it could be conclude that there are 4 main pathways (demethylation, hydroxylation, dechlorination and recombination) of electrochemical diuron degradation in microreactor as shown in figure 4.37.

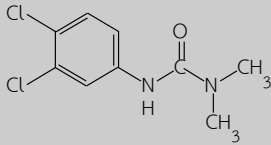
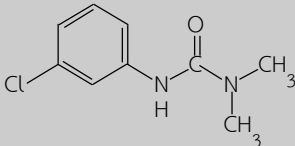
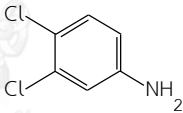
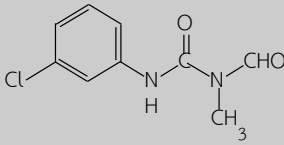
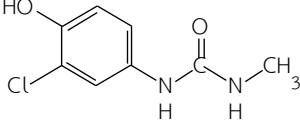
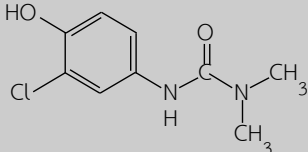


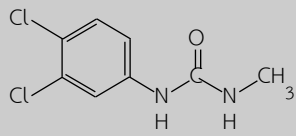
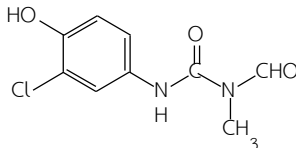
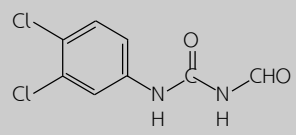
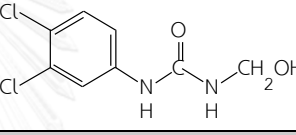
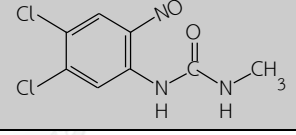
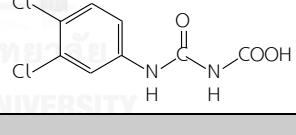
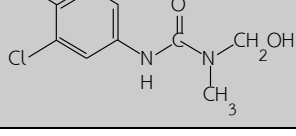
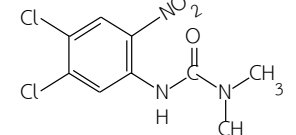
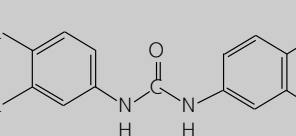
Figure 4.35 Dechlorination or reduction during degradation of diuron via EAOP [8]

A few works have been reported the formation of reaction intermediates during diuron degradation via EAOP. However, due to mechanism of intermediates formation by hydroxyl radicals is similar to other advanced oxidation processes, compound 1, 2, 3, 5, 6, 7, 9, 10, and 13 were found in electrical discharge, Fenton's reaction and photocatalytic reaction [1, 2, 6, 36, 37, 49, 55]. Additionally, compound 4, 8, 12 and 15 were reported in diuron degradation via EAOP in a microreactor in our work [82]. Due to short residence time in microreactor, compound 4, 8, 12 and 15 was probably detected in our system. Due to longer residence time in conventional reactor, these intermediate compounds could be decomposed which could not be detected.



Table 4.8 Structure of reaction intermediate products of diuron during diuron degradation via EAOP in microreactor under no ion contamination and ion contamination.

Compound	Molecular Mass (M_w)	Fragment (m/z)	Structure	Ref.
diuron	233.09			
1	247.08	160, 188, 202, 217		[8]
2	198.65	152, 154, 168, 198		[8]
3	162.02	160		[2]
4	212.37	154, 168		[82]
5	200.62	142, 199		[2]
6	214.65	168, 183		[8]

Compound	Molecular Mass (M_w)	Fragment (m/z)	Structure	Ref.
7	219.07	160, 188, 202		[37]
8	228.63	168, 183		[82]
9	232.62	160, 188, 202		[36]
10	235.07	188, 202, 233		[8]
11	248.07	189, 201, 217		
12	249.05	188, 202		[82]
13	249.05	160, 188, 202, 217		[49]
14	278.09	201, 205, 231, 233		
15	350.02	160, 188, 212		[82]

(2) The intermediate products of 3 reference standard compounds

To better understand overall degradation pathway of diuron, compound 1, 2 and 3 were also analyzed intermediate structure by LC-MS/MS during its degradation via EAOP in a microreactor. According to intermediate structures of LC-MS/MS results, it indicated that the hydroxyl radicals still mainly induced the intermediate formation.

During the degradation of compound 1, compound 3, 4, 5, 7, 8, 9, 10, 12 and 15 were identified, which formed through demethylation process [2, 8, 49, 50]. Therefore, another route to form compound 8 was probably directly aromatic ring hydroxylation of compound 1, respectively. Due to compound 4 was observed, another route to form compound 4 was directly the reduction of compound 1. Compound 2, 6 and 13 were not observed during the degradation of compound 1. It indicated that formyl group on molecule structure of compound 1 could not re-transform to methyl group. In addition, the conjugated products (compound 15) were observed [81], which indicated that the recombination reaction could also formed from the degradation of compound 1 and diuron. The overall demethylation process of diuron degradation was modified as shown in pathway II represented in figure 4.37.

During the degradation of compound 2 (reductive compound), compound 4, 5, 6 and 8 were identified, which formed via demethylation and hydroxylation process. Hydroxylation of aromatic ring of compound 2 led to formed compound 6, which was another one route of hydroxylation to form these compounds. It indicated that the substitution of Cl atom by OH to reductive compound (one Cl atom on aromatic ring) could occur, which no researcher has reported as shown in figure 4.36. Due to demethylation process also was occurred, compound 5 and 8 were formed. Compound 4 was also identified via demethylation process. Due to diuron, compound 1, 3, 7, 9, 10, 12, 13 and 15 were not observed, which indicated that substitution of Cl atom alone to aromatic ring

did not occur during EAOP. The overall reduction of diuron degradation was modified as shown in pathway III represented in figure 4.37.

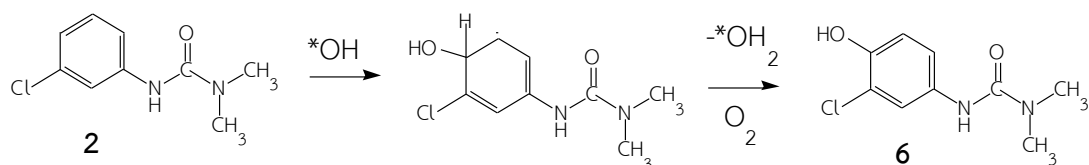


Figure 4.36 Hydroxylation of aromatic ring during degradation of compound 2 via EAOP

However, during degradation of compound 3 as reactant, no more intermediate products were identified. From HPLC result, a few intermediates were formed during the degradation of compound 3. However, due to limitation of analysis by LC-MS/MS, small molecular mass intermediates could not be detected.

(3) Overall reaction pathway

The main diuron degradation pathway were 4 routes, which were demethylation, hydroxylation, dechlorination and recombination via EAOP under no ion contamination as shown in figure 4.37. Additionally, LC-MS/MS peak intensity of compound 6 and 13 that were formed in the beginning of residence time, 0-25 s. It indicated that compound 6 and 13 were primary products [1, 2, 8, 49]. Compound 3, was a small intermediates, were formed in range 75 – 100 s of residence time due to it was eventual product and took longer time to form. Another intermediate compounds, their peak intensities were increased in first period of time and then decreased to form another intermediate products in 75 to 100s. Since the mineralization of diuron is complete, the final product of diuron are hydrochloric acid, nitric acid, carbon dioxide and water following in equation 2.5 [3]. Due to limited analysis of liquid chromatography analyzer, small acid couldn't identify. However, one evidence to prove that the formation of small acid in our system is pH of solution decreased to weak acidic solution under 100s of residence time.

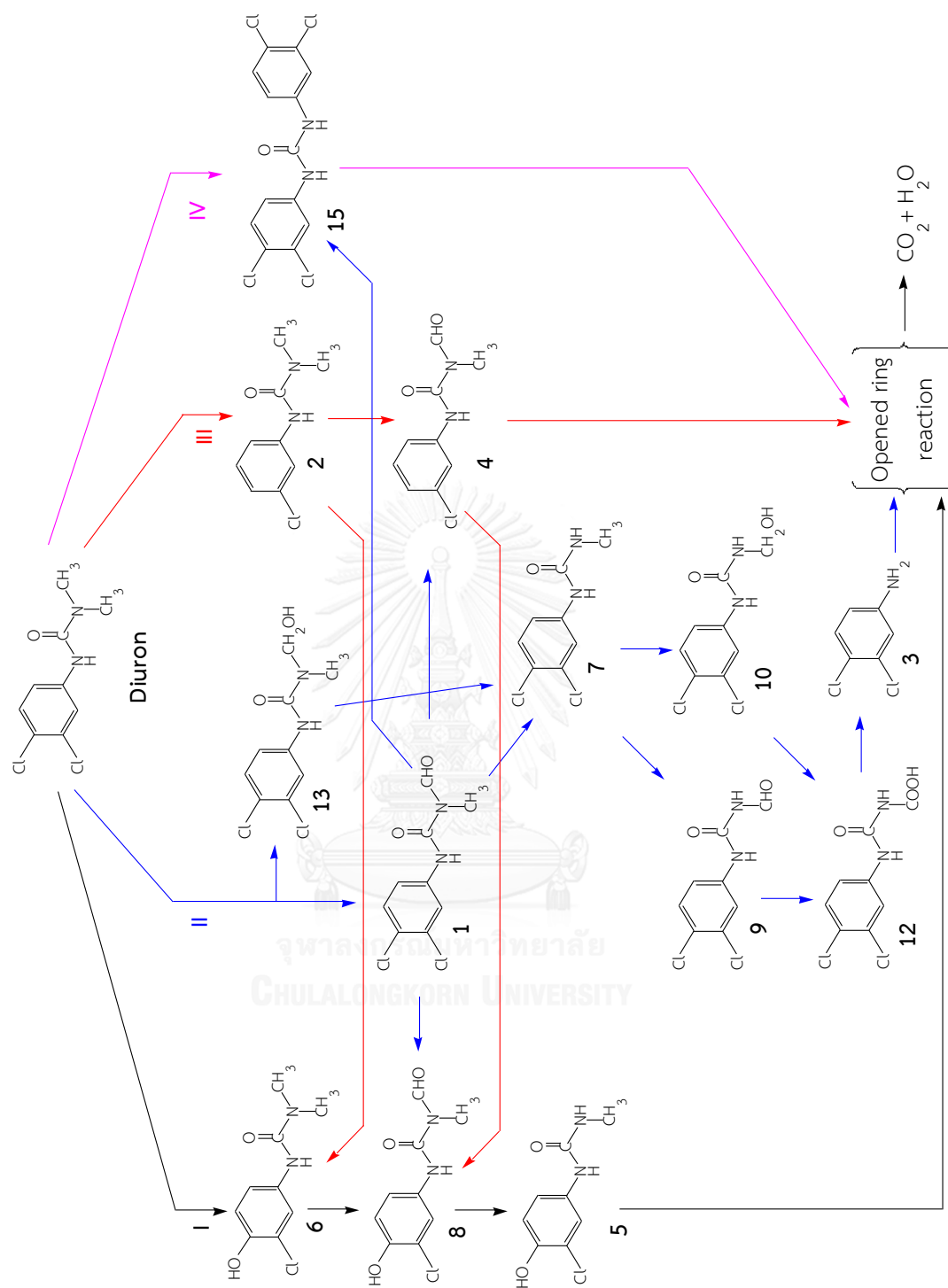


Figure 4.37 Reaction pathway of diuron degradation under no ion contamination via EAOP in a microreactor

4.2.2.2 Anion contamination

This work also studied formation of intermediate of diuron degradation in the contamination of anion. In our results, during electrochemical degradation of diuron, we found that nitrite (NO_2^-) [41] and persulfate ($S_2O_8^{2-}$) [17] could be formed via electrochemical reaction, while nitrate and sulfate ion still existed in diuron solution. Reduction of nitrate ion to nitrite ion at cathode and oxidation of sulfate ion to persulfate ion at anode are shown in equation 4.10 and 4.11. To investigate the effect of all anions (nitrate, nitrite, sulfate and persulfate ion) on the intermediate formation, the experiments were conducted by adding nitrate, nitrite, sulfate and persulfate ion into diuron solution by fixing initial solution conductivity to be 140 μ S/cm, which equaled to approximately 0.001 M of ion concentration. All experimental conditions were the same with diuron degradation under no anion contamination.



(1) Nitrate and nitrite ion contamination

Although diuron solution contaminated with nitrate and nitrite ions, all 13 intermediates were identified which are similar with that formed under diuron degradation with no ion contamination indicating 1, 2, 3, 4, 5, 6, 7, 8, 9, 10, 12, 13 and 15. It indicated that hydroxyl radicals were still mainly induced to the formation of intermediates. However, it is interested that addition of 2 nitrated-products (compound 11 and 14) were identified in the contamination of nitrate and nitrite ion. All identified intermediates under nitrate and nitrite ion contamination as shown in table 4.8. LC-MS/MS spectrum (negative mode) of compound 11 showed fragment ions at 189, 201 and 217 indicating mainly showed the

loss of $\cdot\text{H}$, $\cdot\text{NO}$, $\cdot\text{CH}_3$, $\cdot\text{NHCH}_3$ and $\cdot\text{CONHCH}_3$. Compound **11** probably was formed via nitrosation by reacting between compound **7** with peroxynitrite (ONOO^-) through nucleophilic reaction under alkaline solution (solution $\text{pH} > 8$) as shown in figure 4.38. Peroxynitrite can be produced by reaction between nitrite ion and hydrogen peroxide as shown in equation 4.12 [67], which hydrogen peroxide was also detected in our work. Due to this reaction occurred in bulk solution, compound **11** probably was formed in bulk as well. During diuron degradation under both of nitrate and nitrite ion, local measured pH of solution increased to weakly basic solution ($\text{pH} \sim 8\text{-}9.5$), which consistently peroxynitrite is stable in basic solution ($\text{pK}_a = 6.8$) [67].

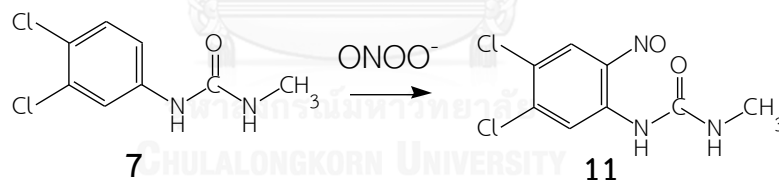


Figure 4.38 formation of compound **11**

Compound **14** also was identified in treated solution, which the fragment ions of LC-MS/MS (negative mode) shows ion at 201, 205, 231 and 233 indicating that showed the loss of $\cdot\text{NO}_2$, $\cdot\text{CH}_3$, $\cdot\text{N}(\text{CH}_3)_2$ and $\cdot\text{CON}(\text{CH}_3)_2$. The possible reaction to form compound **14** is the reaction of $\cdot\text{NO}_2$ radical attacked directly to diuron molecule via nitration as shown in figure 4.39. $\cdot\text{NO}_2$ radicals were formed at anode by reaction between hydroxyl radical and nitrite ion as shown in equation 4.13 [27, 52]. Therefore, compound **14** also formed at anode.

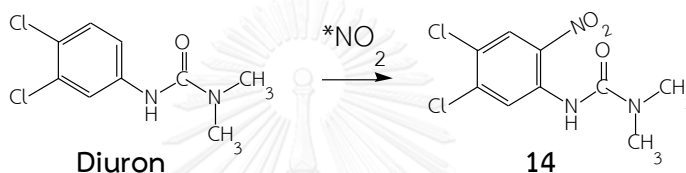


Figure 4.39 formation of compound **14**

It should be noted that compound **11** and **14** were identified under contamination nitrate and nitrite ion, which no researchers have reported. Due to low mass transfer and short residence time in microreactor, reduction of nitrate ion to nitrite ion easily occurred. Nitrite ion mainly induced to form compound **11** and **14** as the result in these compounds could be detected in our experiment. It has been reported that proxynitrite ion can promote to form nitrosophenol by nitrosation of phenol in aqueous solution at $\text{pH} \geq 8$ [67, 83]. Moreover, researchers reported that $\cdot\text{NO}_2$ induced to form other nitrated-products of photodegradation of diuron, monuron, phenol and monolinuron in the presence of nitrate and nitrite ion [26, 27, 52, 56]. Figure 4.40 and 4.41 show LC-MS/MS peak intensity of all intermediate compounds during diuron degradation under nitrate and nitrite contamination, respectively. The reaction pathway of diuron degradation under nitrate and nitrite contamination via EAOP as shown in figure 4.42.

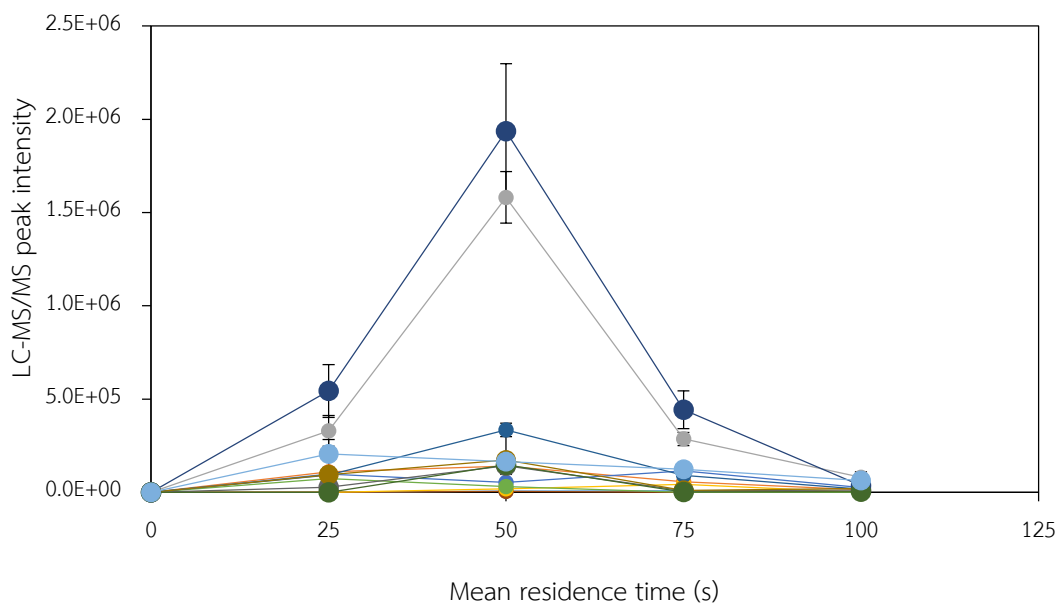


Figure 4.40 LC-MS/MS peak intensity of intermediate products under nitrate ion contamination (negative mode): (●) C₁, (●) C₃, (●) C₅, (●) C₆, (●) C₇, (●) C₈, (●) C₉, (●) C₁₀, (●) C₁₁, (●) C₁₂, (●) C₁₃, (●) C₁₄ and (●) C₁₅

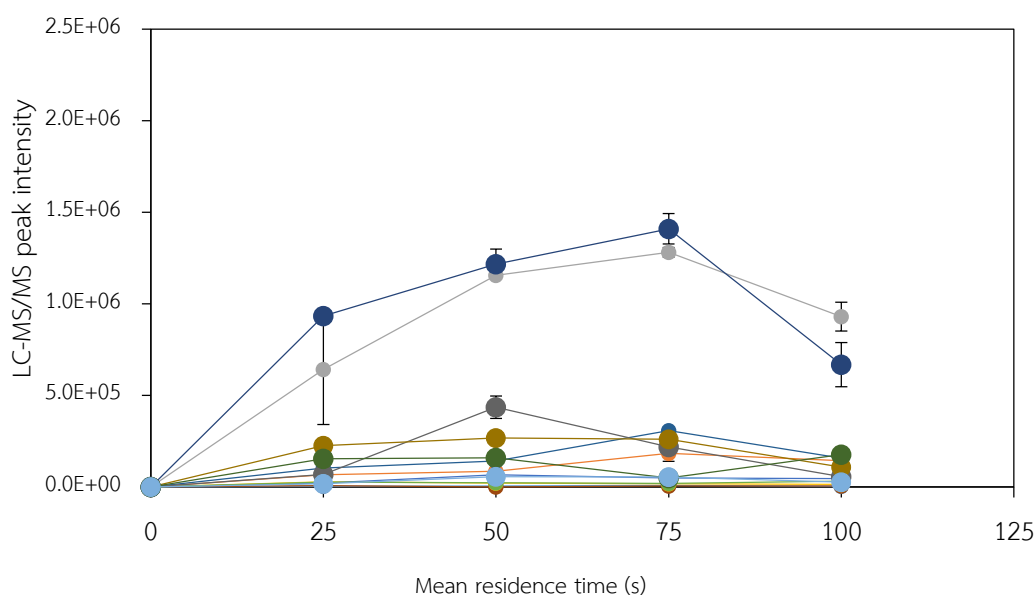
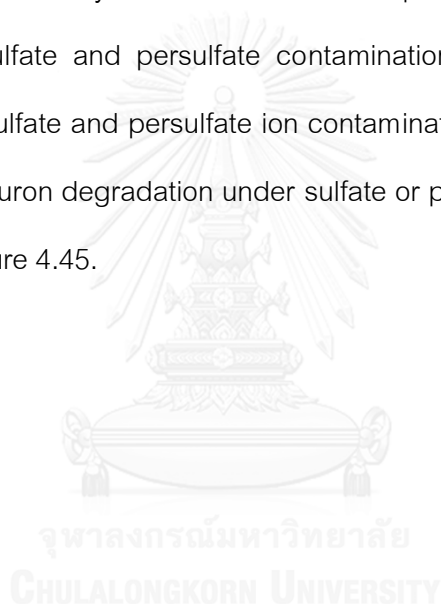


Figure 4.41 LC-MS/MS peak intensity of intermediate products under nitrite ion contamination (negative mode): (●) C₁, (●) C₃, (●) C₅, (●) C₆, (●) C₇, (●) C₈, (●) C₉, (●) C₁₀, (●) C₁₁, (●) C₁₂, (●) C₁₃, (●) C₁₄ and (●) C₁₅

(2) Sulfate and persulfate ion

According to LC-MS/MS analysis, all intermediates were identified indicating that no sulfate or persulfate participated in intermediate structure. Therefore 13 identified intermediates were also found, which were similar that were found under diuron degradation with no ion contamination including compound 1, 2, 3, 4, 5, 6, 7, 8, 9, 10, 12, 13 and 15. Therefore, hydroxyl radical is main radical inducing to form all intermediates although sulfate or persulfate ion contaminated in diuron solution. Figure 4.43 and 4.44 show LC-MS/MS peak intensity of all intermediate compound were formed during diuron degradation under sulfate and persulfate contamination, respectively. The identified intermediates under sulfate and persulfate ion contamination as shown in table 4.8. The reaction pathway of diuron degradation under sulfate or persulfate ion contamination via EAOP as shown in figure 4.45.



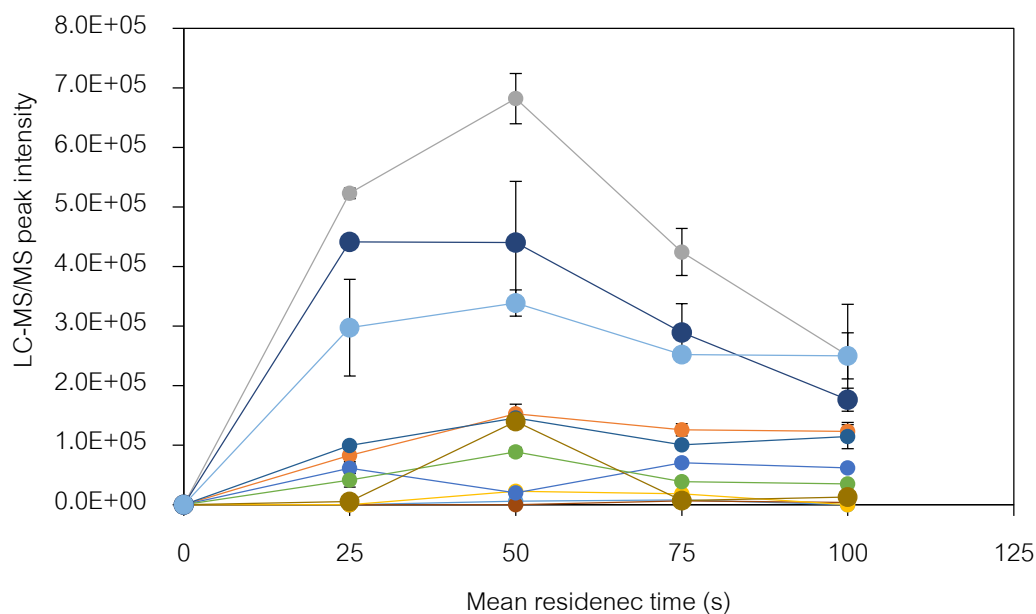


Figure 4.43 LC-MS/MS peak intensity of intermediate products under sulfate ion contamination (negative mode): (●) C_1 , (●) C_3 , (●) C_5 , (●) C_6 , (●) C_7 , (●) C_8 , (●) C_9 , (●) C_{10} , (●) C_{12} , (●) C_{13} , and (●) C_{15}

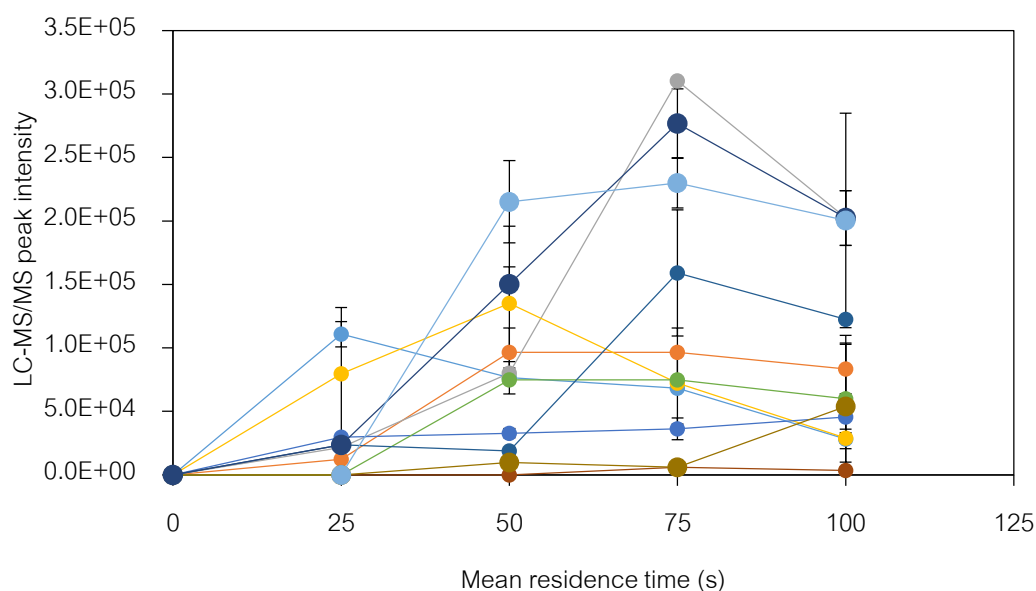


Figure 4.44 LC-MS/MS peak intensity of intermediate products under persulfate ion contamination (negative mode): (●) C_1 , (●) C_3 , (●) C_5 , (●) C_6 , (●) C_7 , (●) C_8 , (●) C_9 , (●) C_{10} , (●) C_{12} , (●) C_{13} , and (●) C_{15}

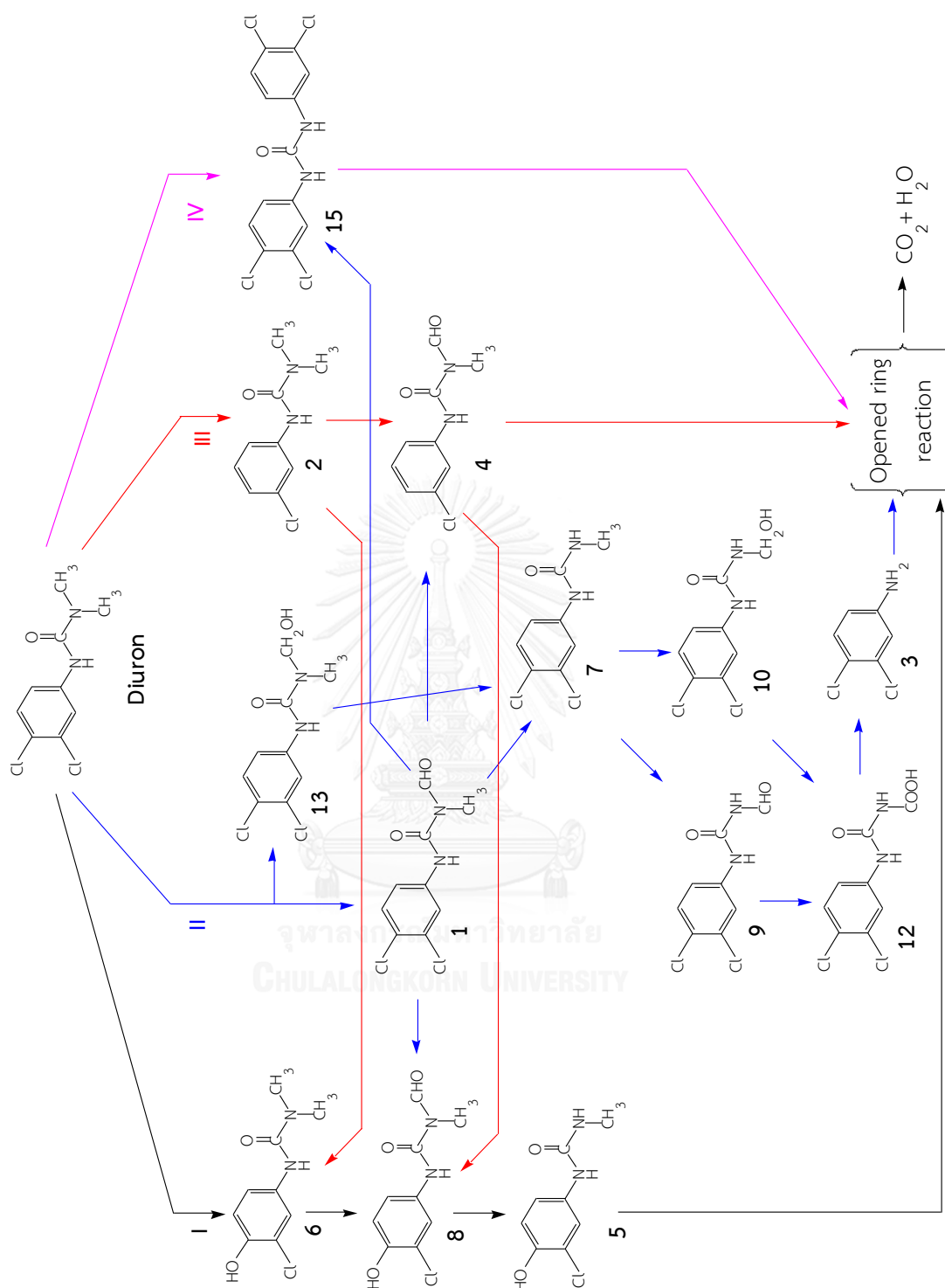


Figure 4.45 Reaction pathway of diuron degradation under sulfate and persulfate ion contamination via EAOP in microreactor

(3) Overall reaction pathway

Although, nitrate, nitrite, sulfate and persulfate contamination in diuron solution, hydroxyl radical inducing to form the main 13 intermediates. The main diuron degradation pathway were 4 routes, which were demethylation, hydroxylation, dechlorination and recombination via EAOP in our microreactor. Additionally, nitrosation and nitration route (N.II and N.I route), which led to form compound **11** and **14**, were included in overall pathway (see figure 4.42). It is should be noted that nitrated-products (compound **11** and **14**) were not found in sulfate, persulfate and no ion condition.

According to LC-MS/MS peak intensity analysis, compound **6** and **13** were formed in 25 s of residence time under all anions contaminated in solution (see figure 4.40, 4.41, 4.43 and 4.44). It indicated that compound **6** and **13** were primary products [1, 2, 8, 49]. Compound **3** were also detected in last residence time, 75 – 100 s. Due to it is small molecular mass product, which it takes longer time to form. Other compounds also showed same trend with the diuron degradation under no ion contamination.

4.3 Mathematical model and simulation for diuron degradation in EAOP microreactor

The mathematical model was developed to describe the chemical reaction in microreactor for diuron degradation and formation of intermediates via electrochemical advanced oxidation in microreactor.

4.3.1 Mathematical model for diuron degradation and reference standard compounds

The experimental data obtained at several residence times are used to fit the steady-state mathematical model of diuron degradation reaction process. Two mathematical models are constructed. The first, 'rigorous model', includes detailed diffusion and convection within the reactor. Within this model, several reaction kinetics schemes were tested, under the assumption that the reaction takes place homogeneously in the liquid phase. This investigation enabled us to find dominant reaction pathway, reaction order and to further understand the degradation behavior. It was found that the degradation of diuron via EAOP in the microreactor could be simply represented by the first-order reaction kinetics with respect to concentration of diuron [19]. In light of this finding, it was logical to construct the second mathematical model as a simple pseudo first-order kinetic model without considering transport phenomena within the reactor. This was somewhat expected development since the major advantage of microscale-based reactors is reduction of mass transfer limitations. It is a well-known fact that microreactors reduced mass transfer limitations in chemical reaction processes when maximum diffusion lengths are truly within microscale range. For a modestly fast liquid phase reaction one may expect that microchannel characteristic height in the range of 50 - 350 μm would enable a 'mass transfer-free' chemical reaction process. The reaction rate constant was found from slope in the $\ln(C_{in}/C_{out})$ versus residence time graph. Both

models show very good fit to the experimental data as shown in figure 4.46. The values of R^2 for the fitting of the degradation data under applied current of 1 mA with the rigorous and the simple models are 0.987 and 0.968, respectively. Although the rigorous model seems to give better representation of the experimental data, the fact that the simple kinetic model can represent the experimental data equally well as the rigorous model suggests that the degradation reaction process within truly microscale reactor is controlled mostly by kinetics and it is essentially low mass transfer limitation. The reaction rate constant obtained from the rigorous model is $3.39 \times 10^{-2} \text{ s}^{-1}$, while rate constant obtained from the simple model is $2.69 \times 10^{-2} \text{ s}^{-1}$. Comparing with other AOPs in conventional scale, such as electrochemical oxidation [19], photocatalytic reaction [3] or Fenton's reaction [2], the rate constant in this work is higher by approximately one to two orders of magnitude. We also found that the degradation of 3 reference standard compounds also fitted the rigorous model as shown in figure 4.47. For the degradation of 3 compounds, compound 1 is faster elimination when compared with the degradation rate of compound 2 and 3 with rate constant of 6.98×10^{-2} , 3.63×10^{-2} and $4.00 \times 10^{-2} \text{ s}^{-1}$ corresponding compound 1, 2 and 3. Therefore, the rigorous model could appropriately describe behavior of diuron and 3 reference standard compounds degradation in EAOP microreactor.

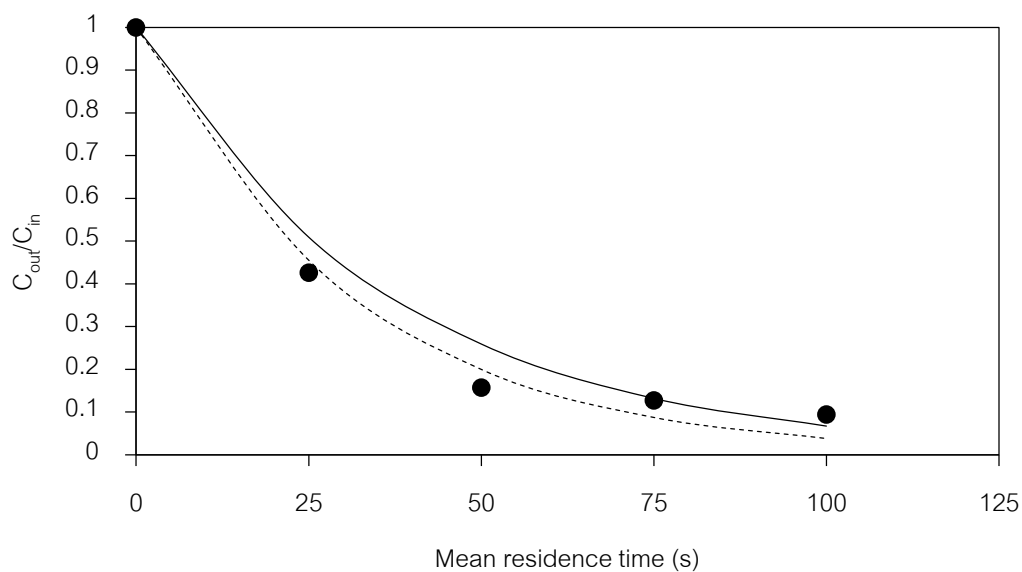


Figure 4.46 Fitting of the rigorous mathematical model and the simple kinetic model to the experimental results on the degradation of diuron: (●) exp, (—) simple model and (- - -) rigorous model

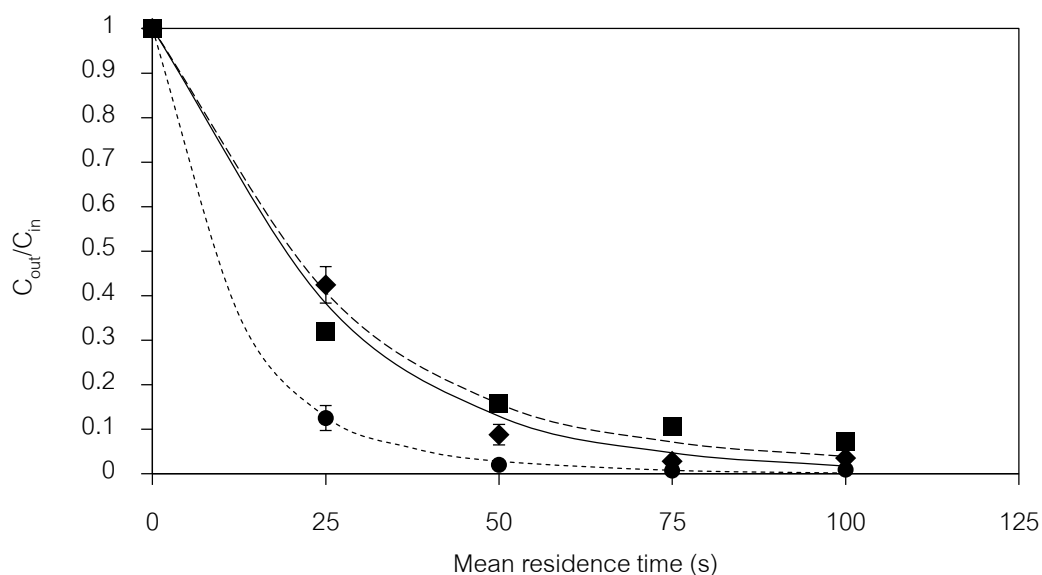


Figure 4.47 Degradations of intermediate compounds 1, 2 and 3 by EAOP under applied current of 1 mA. The marks show experimental data, while the lines represent values calculated by rigorous mathematical models: (●) compound 1, (■) compound 2 and (◆) compound 3

The model was also tested with several effects including applied current, microchannel thickness, pH and conductivity of solution. For the influence of applied current, the data obtained at mean residence times were also fitted to the rigorous model. Good fits were obtained as seen in figure 4.48. It was found that the change in the applied current does not affect the order of the reaction. The degradation still follows first-order kinetics in rigorous model with the reaction rate constant of 1.39×10^{-2} , 3.26×10^{-2} , and $4.25 \times 10^{-2} \text{ s}^{-1}$ when the applied current is 0.5, 1 and 2 mA, respectively. Not only rigorous model fitted with various applied current but also fitted thicknesses, pHs and conductivities in microreactor. The data obtained at mean residence times were also fitted to the rigorous model, which was also found that the change in the mentioned effects do not affect the order of the reaction. The degradation still follows first-order kinetics. Figure 4.49 shows the fitting of the rigorous model to the experimental results on the degradation of diuron under the change of microchannel thickness. Figure 4.50 and 4.51 show the fitting of the rigorous model to the experimental results on the degradation of diuron under the change of pH and conductivity of solution respectively. Table 4.9 shows reaction rate constants of diuron degradation predicted by rigorous model under various experimental conditions.

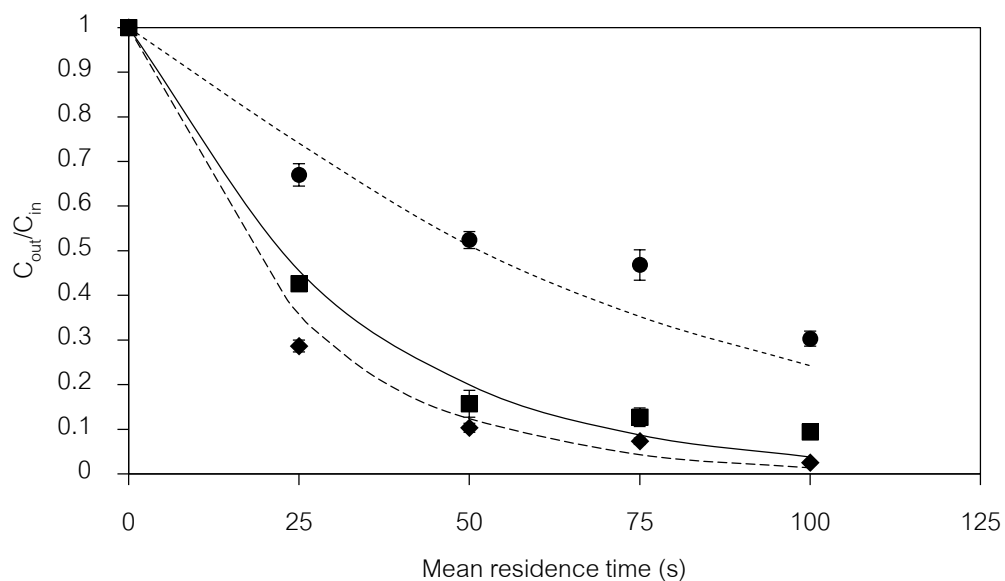


Figure 4.48 Degradation of diuron under various applied currents. The marks show experimental data, while the lines represent values calculated by rigorous mathematical models: (●) 0.5 mA, (■) 1 mA and (◆) 2 mA

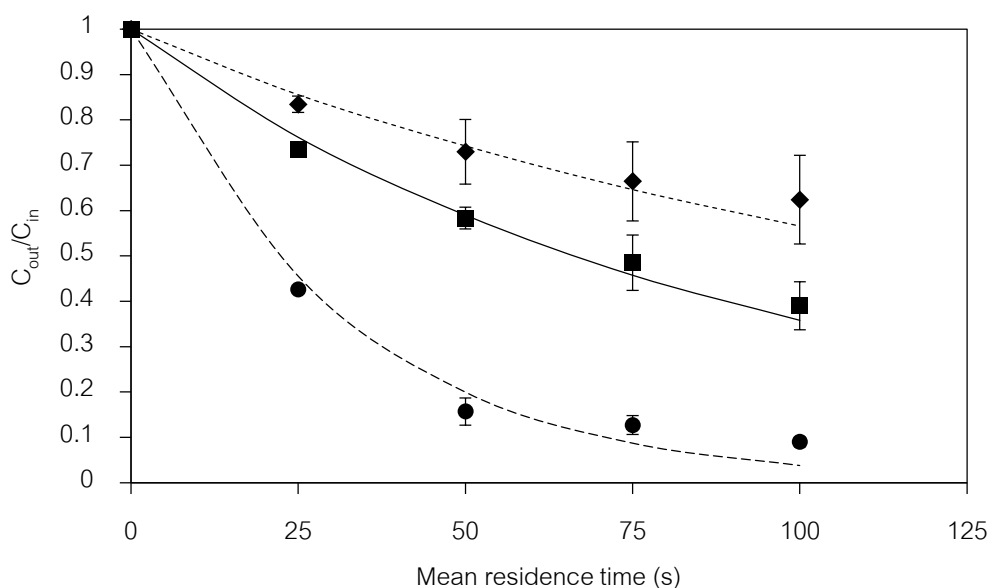


Figure 4.49 Degradation of diuron under various thicknesses. The marks show experimental data, while the lines represent values calculated by rigorous mathematical models: (●) 250 μm, (■) 500 μm and (◆) 750 μm.

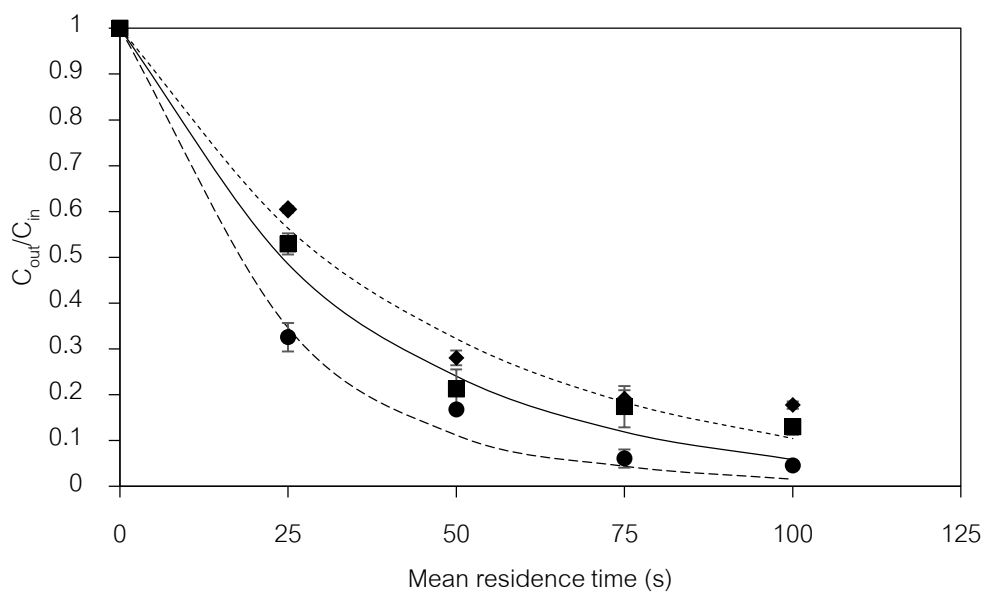


Figure 4.50 Degradation of diuron under various pHs. The marks show experimental data, while the lines represent values calculated by rigorous mathematical models: (●) pH = 3, (■) pH = 7 and (◆) pH = 10.

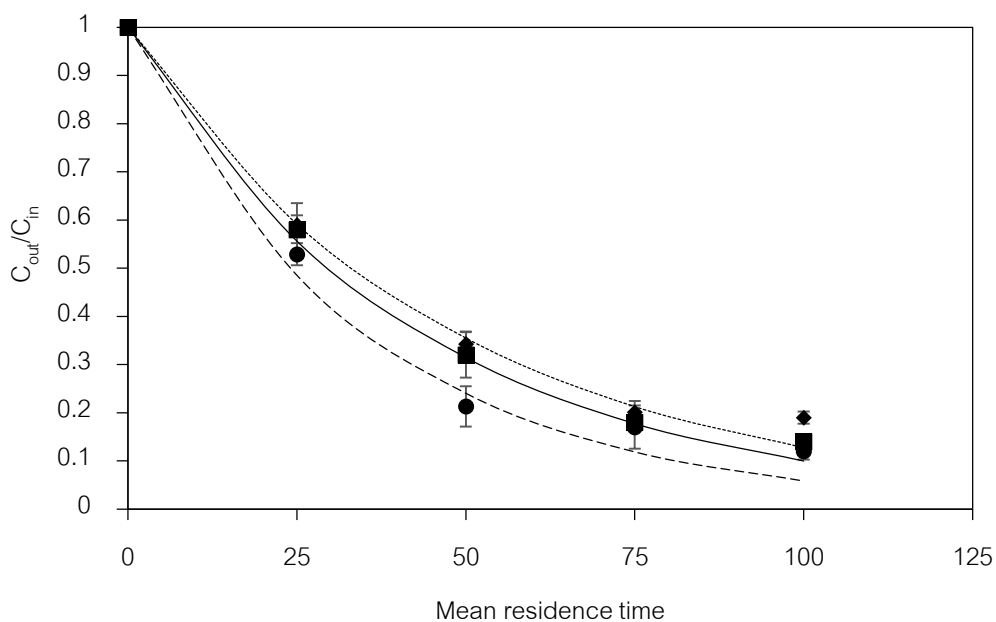


Figure 4.51 Degradation of diuron under various conductivities. The marks show experimental data, while the lines represent values calculated by rigorous mathematical models: (●) 140 $\mu\text{S/cm}$, (■) 500 $\mu\text{S/cm}$ and (◆) 1000 $\mu\text{S/cm}$.

Table 4.9 Reaction rate constants of diuron degradation predicted by rigorous model

Condition	Reaction rate constant (s ⁻¹)
Applied current (mA)	
▪ 0.5	1.39×10 ⁻²
▪ 1	3.26×10 ⁻²
▪ 2	4.25×10 ⁻²
Microchannel thickness (μm)	
▪ 250	3.39×10 ⁻²
▪ 500	0.10×10 ⁻²
▪ 750	0.06×10 ⁻²
Solution pH	
▪ 3	4.25×10 ⁻²
▪ 7	2.88×10 ⁻²
▪ 10	2.29×10 ⁻²
Solution conductivity (μS/cm)	
▪ 140	2.84×10 ⁻²
▪ 500	2.31×10 ⁻²
▪ 1000	1.88×10 ⁻²

4.3.2 Mathematical model for pathway of diuron degradation in EAOP microreactor

Partial results from the quantitative analysis by HPLC, within short residence time of 0 to 25 s, indicated that concentrations of compound 1, 2 and 3 increased, which suggests that they are direct products of diuron degradation. Nevertheless, the concentrations of the same compounds gradually decrease as the residence time is prolonged, indicating further degradation. To further understand the mechanism of diuron degradation via EAOP, the degradations of these three known intermediates were investigated using commercially available standards and developed mathematical model for pathway of diuron degradation.

In similar manner as the degradation of diuron, several products are detected from the degradations of compounds 1, 2 and 3. According to the results in Table 4.6, when compound 1 is degraded, compound 3, which is a smaller molecule, is found as one of the products. Both compound 1 and compound 3 have been observed as intermediates in the degradation of diuron. Compound 1 is formed, while compound 3 is formed by cleavage of the alkyl side chain attached to the amine group in compound 1. On the other hand, the degradation of compound 2 does not produce compound 3. There is a compound resulting from the degradation of diuron that is not the product from the degradation of compound 1, 2, or 3. Therefore, another diuron degradation route, which does not involve the formation of either compound 1 or 2, is suggested. Hence, a simple reaction pathway for diuron degradation by EAOP that can be quantitatively investigated by kinetic analysis is proposed as shown in figure 4.52, which consistent with figure 4.37. For the simulation pathway, there are 3 main routes including the formation compound 1 and 3 route, the formation compound 2 route and unidentified compound route (lumped route)

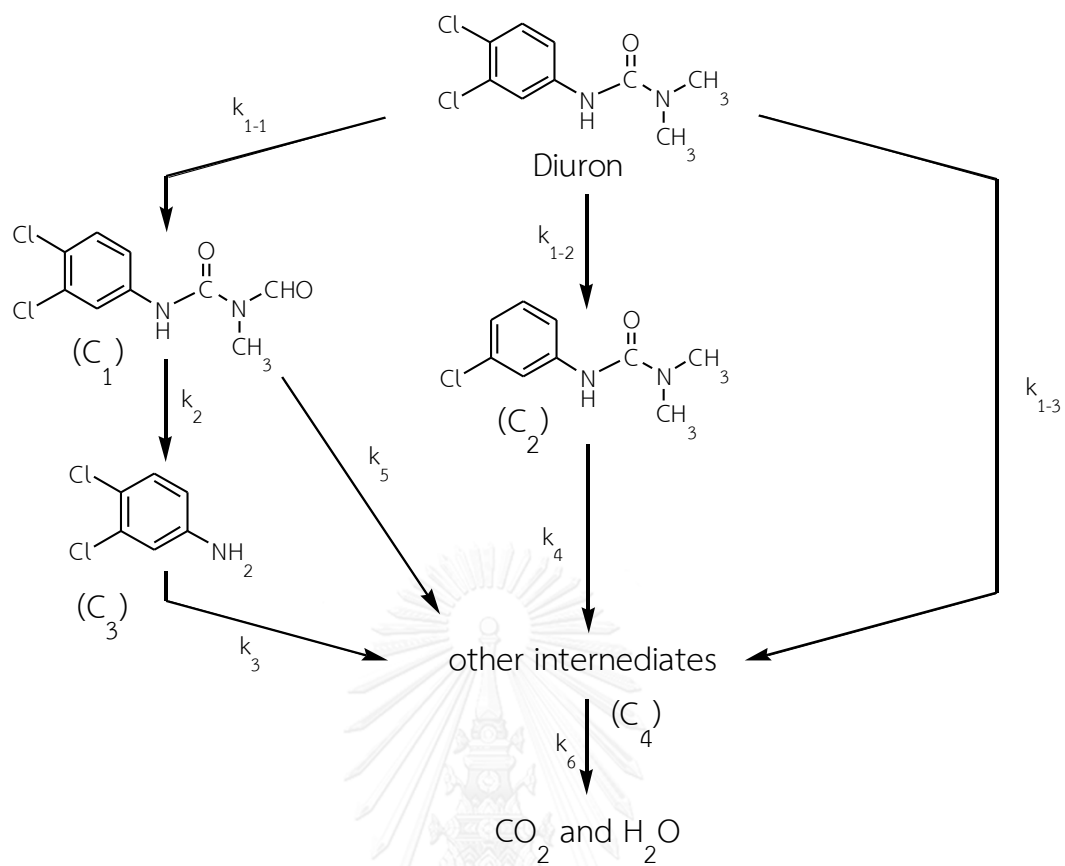


Figure 4.52 Simplified reaction pathway of diuron degradation by EAOP in microreactor

The rigorous model was developed for the degradation within a 250- μm microchannel using the applied current of 1 mA. In the model, all reactions are assumed to be first-order in the same manner as experimentally observed for diuron as well as for compound 1, 2 and 3. Rate equations for the degradations are shown in equation 4.14 - 4.18. It should be noted that concentrations of all unquantifiable intermediates were lumped together and calculated in term of organic content based on carbon balance.

$$r_{diuron} = \frac{dC_{diuron}}{dt} = -(k_{1-1} + k_{1-2} + k_{1-3})C_{diuron} \quad 4.14$$

$$r_{C_1} = \frac{dC_1}{dt} = k_{1-1}C_{diuron} - k_2C_1 - k_5C_1 \quad 4.15$$

$$r_{C_2} = \frac{dC_2}{dt} = k_{1-2}C_{diuron} - k_4C_2 \quad 4.16$$

$$r_{C_3} = \frac{dC_3}{dt} = k_2C_1 - k_3C_3 \quad 4.17$$

$$r_{C_4} = \frac{dC_4}{dt} = k_{1-3}C_{diuron} + k_4C_2 + k_3C_3 + k_5C_1 - k_6C_4 \quad 4.18$$

C_{diuron} , C_1 , C_2 , C_3 , and C_4 are concentrations of diuron, compound 1 (3-(3,4-dichlorophenyl)-1-formyl-1-methylurea), compound 2 (3-(3-chlorophenyl)-1,1-dimethylurea), compound 3 (3,4-dichloro-aniline), and combined organic content of all unquantifiable compounds, respectively. The results in figure 4.53(a) and 4.53(b) show good agreement between the calculated concentrations and the experimental data, for all measurable compounds as well as for TOC. The calculated reaction rate constants for all reactions are shown in table 4.10.

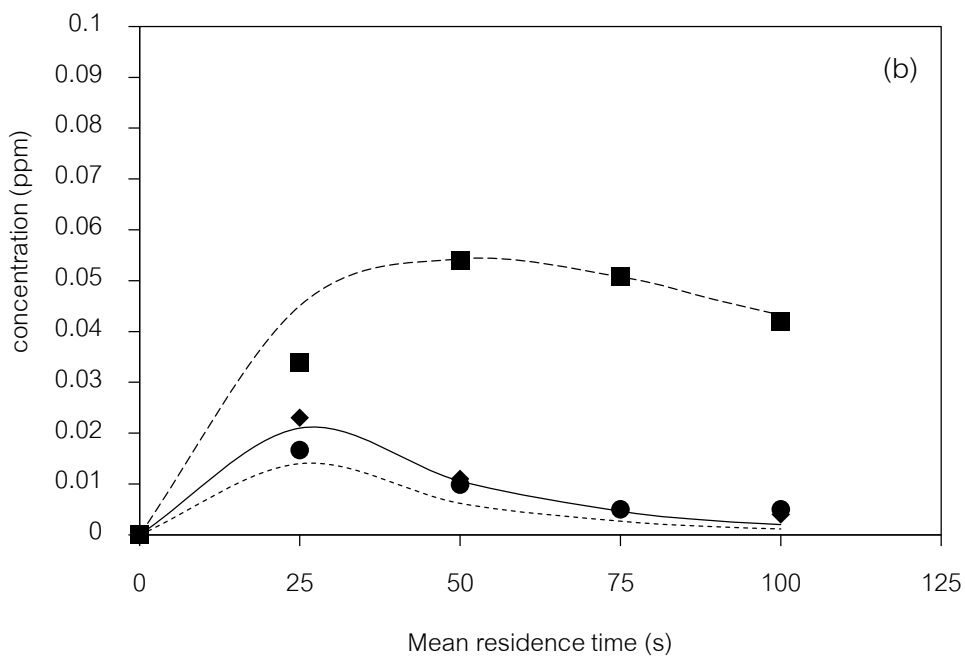
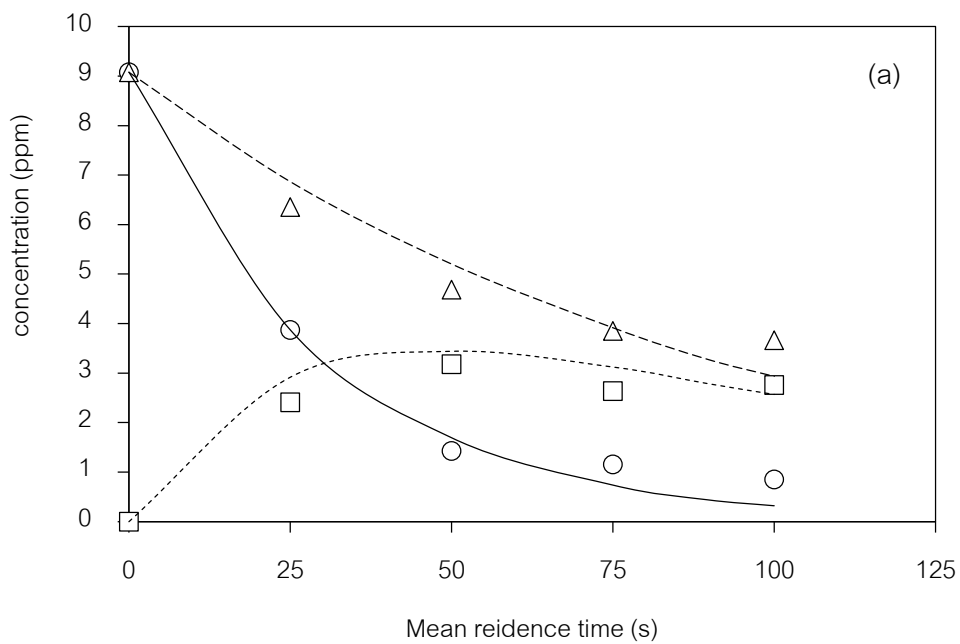


Figure 4.53 Decomposition of diuron by EAOP and evolution of the degradation intermediates under the applied current of 1 mA. The marks show experimental data, while the lines represent values calculated by the rigorous mathematical model: (a) (O) diuron, (□) C_4 and (△) TOC. (b) (●) C_1 , (■) C_2 and (◆) C_3

According to table 4.10, it can be seen that the attack by hydroxyl radicals is generally much faster than the direct reduction by electron although lots of electron are supplied to the solution. Hence, the major role of the applied current is the generation of reactive hydroxyl radicals for the degradation in similar manner as other advanced oxidation processes such as photocatalysis or Fenton's reaction. However, it is very effective in the case of the electrochemical oxidation since the current is applied directly to the solution. Generally, the attack of the hydroxyl radical on molecule of diuron and its degradation intermediates seem to be random. All degradation steps take place at roughly same rate. Nevertheless, more detailed investigations on the rate of formation of each intermediate are still needed.

Table 4.10 Reaction rate constants associated with diuron degradation pathway

Reaction	Parameter	Rate constant (s ⁻¹)
Diuron → C ₁	k ₁₋₁	6.8×10 ⁻⁴
Diuron → C ₂	k ₁₋₂	3.4×10 ⁻⁴
Diuron → other intermediates	k ₁₋₃	2.2×10 ⁻²
C ₁ → C ₃	k ₂	2.0×10 ⁻¹
C ₃ → other intermediates	k ₃	1.5×10 ⁻¹
C ₂ → other intermediates	k ₄	1.0×10 ⁻²
C ₁ → other intermediates	k ₅	2.0×10 ⁻²
other intermediates → CO ₂	k ₆	1.2×10 ⁻²

CHAPTER V

CONCLUSIONS AND RECOMMENDATIONS

5.1 Summary of results

1. Diuron degradation is enhanced via electrochemical advanced oxidation process (EAOP) in microreactor.

2. The diuron could be degraded by interaction between diuron and hydroxyl radical, while hydroxyl radical could recombine to hydrogen peroxide. Hydrogen peroxide is good representation to amount of hydroxyl radical.

3. Several parameters (e.g. residence time, thickness, initial pH, initial conductivity and anion contamination) are investigated. Most parameters influence to production hydroxyl radical.

4. Two mathematical models are developed. Although the rigorous model seems to give better representation of the experimental data, the fact that the simple kinetic model can represent the experimental data equally well as the rigorous model.

5. Several intermediates are formed during the degradation via EAOP by demethylation, hydroxylation, reduction and recombination.

6. Anion concentration influenced to type of intermediates during the degradation.

7. The simplified degradation pathway and mathematical model of diuron degradation are proposed, which show good agreement with experiment data.

5.2 Conclusions

Degradation of diuron in aqueous solution can be done using electrochemical advanced oxidation process in a microscale-based reactor. The use of microreactor greatly enhances the degradation and mineralization. Although the degradation pathway

is very complex, involving many reaction intermediates, diuron degradation takes place mainly by the interaction between diuron and hydroxyl radical generated via dissociation of water at the anode. Hydrogen peroxide is also detected in coming out solution, which is resulted by recombination of hydroxyl radical. In our works, hydrogen peroxide is good represent to quantity of hydroxyl radical in microreactor via EAOP.

Factors affecting the generation of the hydroxyl radical including residence time, initial pH and initial conductivity of the solution, applied current and anion contamination (nitrate and sulfate ion) were investigated. The increase in residence time and applied current increased the degradation of diuron, which is consistent with the increase in detected hydrogen peroxide. In the contrast of the increase of microchannel thickness, pH and conductivity decrease diuron degradation as well as detected hydrogen peroxide. In the contamination of anions, diuron degradation is decreased when compares with diuron degradation under no ion contamination due to effect of electrosorption of anion and hydroxyl radical scavenger.

The formation of reaction intermediate compound was also investigated in the presence of anion and no anion contamination. Since hydroxyl radical is dominant oxidize agent, main intermediate compounds associated with the attacking of hydroxyl radical to diuron and its intermediate are observed although anion contamination in diuron solution. Therefore, 13 intermediate compounds are identified under no anion and anion contamination. Two new nitrate intermediate compounds are identified under nitrate and nitrite ion contamination. Furthermore, the diuron degradation pathway is also proposed in the contamination of no anion and anion, which there are 4 main reactions including demethylation, hydroxylation, reduction and recombination for diuron degradation in microreactor via EAOP.

The mathematical model is developed for diuron degradation in microreactor via EAOP. Although the rigorous model seems to give better representation of the

experimental data, the fact that the simple kinetic model can represent the experimental data equally well as the rigorous model suggests that the degradation reaction process within truly microscale reactor is controlled mostly by kinetics and it is essentially low mass transfer limitation, the overall degradation process can be generally represented by a simple first-order kinetics. The model was also tested with several effects including applied current, microchannel thickness, pH and conductivity of solution, which show a good agreement with experiment results. Additionally, the simplified degradation pathway and mathematical model of diuron degradation are proposed, which show good fit with experiment data.

5.3 Recommendations

A potential area of future work for continued research on diuron degradation in microreactors via electrochemical advanced oxidation process should include an investigation on:

1. Reduction thickness of microchannel to lower 250 μm to more understand kinetic control the diuron degradation in microreactor.
2. Change solvent form water to other solvent to more understand mechanism to produce hydroxyl radical and type of intermediates.
3. The effect of temperature on diuron degradation and formation of intermediate.
4. Quantification of intermediates
5. The effect of anode and cathode type in an attempt to increase mineralization of diuron and stability of electrode.
6. The effect another of anions commonly contaminated in our environment (carbonate ion and phosphate ion).

7. Combination with another process to increase the mineralization of diuron for example Fenton's reaction.
8. The increase in production rate by numbering up.
9. In the modeling of electrochemical reaction in a microreactor should be studied including.
 - Surface reaction or reaction near anode should be considered for better understand real mechanism of EAOP during the degradation.
 - Second order reaction rate should be considered (rate reaction corresponds to concentration of diuron and hydroxyl radical). To determine the limiting reactant of diuron degradation and to confirm the order of reaction rate of diuron degradation is first order reaction.
10. Another potential area of future work for continuation of this research is toxic treated solution after diuron degradation and toxic of each formed intermediates during the degradation.

REFERENCES

- [1] Feng, J., et al., *Gas-liquid hybrid discharge-induced degradation of diuron in aqueous solution*. Journal of Hazardous Materials, 2009. **164**(2-3): p. 838-846.
- [2] Oturan, M.A., et al., *Oxidative degradation of herbicide diuron in aqueous medium by Fenton's reaction based advanced oxidation processes*. Chemical Engineering Journal, 2011. **171**(1): p. 127-135.
- [3] Katsumata, H., et al., *Photocatalytic degradation of diuron in aqueous solution by platinumized TiO₂*. Journal of Hazardous Materials, 2009. **171**(1-3): p. 1081-1087.
- [4] Carrier, M., et al., *Photocatalytic Degradation of Diuron: Experimental Analyses and Simulation of HO[•] Radical Attacks by Density Functional Theory Calculations*. The Journal of Physical Chemistry A, 2009. **113**(22): p. 6365-6374.
- [5] Macounova, K., et al., *Kinetics of photocatalytic degradation of diuron in aqueous colloidal solutions of Q-TiO₂ particles*. Journal of Photochemistry and Photobiology A: Chemistry, 2003. **156**: p. 273-282.
- [6] Malato, S., et al., *Photocatalytic Treatment of Diuron by Solar Photocatalysis: Evaluation of Main Intermediates and Toxicity*. Environmental Science & Technology, 2003. **37**(11): p. 2516-2524.
- [7] Giacomazzi, S. and N. Cochet, *Environmental impact of diuron transformation: a review*. Chemosphere, 2004. **56**(11): p. 1021-1032.
- [8] Canle López, M., et al., *Mechanisms of Direct and TiO₂-Photocatalysed UV Degradation of Phenylurea Herbicides*. ChemPhysChem, 2005. **6**(10): p. 2064-2074.
- [9] Ribeiro, A.R., et al., *An overview on the advanced oxidation processes applied for the treatment of water pollutants defined in the recently launched Directive 2013/39/EU*. Environment International, 2015. **75**(0): p. 33-51.
- [10] Sun, K., et al., *Adsorption of diuron, fluridone and norflurazon on single-walled and multi-walled carbon nanotubes*. Science of The Total Environment, 2012. **439**(0): p. 1-7.

- [11] Tixier, C., et al., *Fungal biodegradation of a phenylurea herbicide, diuron: structure and toxicity of metabolites*. Pest Management Science, 2000. **56**(5): p. 455-462.
- [12] Oturan, M.A., et al., *Kinetics of oxidative degradation/mineralization pathways of the phenylurea herbicides diuron, monuron and fenuron in water during application of the electro-Fenton process*. Applied Catalysis B: Environmental, 2010. **97**(1-2): p. 82-89.
- [13] Feng, J., et al., *Degradation of diuron in aqueous solution by ozonation*. Journal of Environmental Science and Health, Part B, 2008. **43**(7): p. 576-587.
- [14] Aquino Neto, S. and A.R. de Andrade, *Electrooxidation of glyphosate herbicide at different DSA® compositions: pH, concentration and supporting electrolyte effect*. Electrochimica Acta, 2009. **54**(7): p. 2039-2045.
- [15] Borràs, N., et al., *Degradation of Atrazine by Electrochemical Advanced Oxidation Processes Using a Boron-Doped Diamond Anode*. The Journal of Physical Chemistry A, 2010. **114**(24): p. 6613-6621.
- [16] Ramírez, C., et al., *Electrochemical oxidation of methyl orange azo dye at pilot flow plant using BDD technology*. Journal of Industrial and Engineering Chemistry, 2013. **19**(2): p. 571-579.
- [17] Fabiańska, A., et al., *Electrodegradation of ifosfamide and cyclophosphamide at BDD electrode: Decomposition pathway and its kinetics*. Chemical Engineering Journal, 2015. **276**: p. 274-282.
- [18] Pipi, A.R.F., et al., *Application of electrochemical advanced oxidation processes to the mineralization of the herbicide diuron*. Chemosphere, 2014. **109**: p. 49-55.
- [19] Bringas, E., J. Saiz, and I. Ortiz, *Kinetics of ultrasound-enhanced electrochemical oxidation of diuron on boron-doped diamond electrodes*. Chemical Engineering Journal, 2011. **172**(2-3): p. 1016-1022.
- [20] Polcaro, A.M., et al., *Electrochemical degradation of diuron and dichloroaniline at BDD electrode*. Electrochimica Acta, 2004. **49**(4): p. 649-656.

- [21] Pulkka, S., et al., *Electrochemical methods for the removal of anionic contaminants from water – A review*. Separation and Purification Technology, 2014. **132**(0): p. 252-271.
- [22] Chen, G., *Electrochemical technologies in wastewater treatment*. Separation and Purification Technology, 2004. **38**(1): p. 11-41.
- [23] Yasri, N.G., A. Yaghmour, and S. Gunasekaran, *Effective removal of organics from corn wet milling steepwater effluent by electrochemical oxidation and adsorption on 3-D granulated graphite electrode*. Journal of Environmental Chemical Engineering, 2015. **3**(2): p. 930-937.
- [24] Panizza, M. and G. Cerisola, *Direct And Mediated Anodic Oxidation of Organic Pollutants*. Chemical Reviews, 2009. **109**(12): p. 6541-6569.
- [25] Polatides, C., M. Dortsiou, and G. Kyriacou, *Electrochemical removal of nitrate ion from aqueous solution by pulsing potential electrolysis*. Electrochimica Acta, 2005. **50**(25–26): p. 5237-5241.
- [26] Boucheloukh, H., et al., *Kinetic and analytical study of the photo-induced degradation of monuron by nitrates and nitrites under irradiation or in the dark*. Photochemical & Photobiological Sciences, 2012. **11**(8): p. 1339-1345.
- [27] Nélieu, S., et al., *Nitrite and nitrate induced photodegradation of monolinuron in aqueous solution*. Environmental Chemistry Letters, 2004. **2**(2): p. 83-87.
- [28] Vione, D., et al., *Phenol photonitration upon UV irradiation of nitrite in aqueous solution II: effects of pH and TiO₂*. Chemosphere, 2001. **45**(6–7): p. 903-910.
- [29] Gavriilidis, A., et al., *Technology and Applications of Microengineered Reactors*. Chemical Engineering Research and Design, 2002. **80**(1): p. 3-30.
- [30] Anglada, Á., A. Urtiaga, and I. Ortiz, *Contributions of electrochemical oxidation to waste-water treatment: fundamentals and review of applications*. Journal of Chemical Technology & Biotechnology, 2009. **84**(12): p. 1747-1755.
- [31] Scialdone, O., et al., *Abatement of 1,1,2,2-tetrachloroethane in water by reduction at silver cathode and oxidation at boron doped diamond anode in micro reactors*. Chemical Engineering Journal, 2012. **189–190**: p. 229-236.

- [32] Scialdone, O., et al., *Anodic abatement of organic pollutants in water in micro reactors*. Journal of Electroanalytical Chemistry, 2010. **638**(2): p. 293-296.
- [33] Romero, A., et al., *Diuron abatement using activated persulphate: Effect of pH, Fe(II) and oxidant dosage*. Chemical Engineering Journal, 2010. **162**(1): p. 257-265.
- [34] Sayeh, R., et al., *Elimination of Pollutants Phenyleurea Herbicides by Advanced Oxidation Processes in Aqueous Solution*. Journal of Engineering and Applied Sciences, 2012.
- [35] Mestankova, H., et al., *Evolution of algal toxicity during (photo)oxidative degradation of diuron*. Aquatic Toxicology, 2011. **101**(2): p. 466-473.
- [36] Mazellier, P., J. Jirkovsky, and M. Bolte, *Degradation of Diuron Photoinduced by Iron(III) in Aqueous Solution*. Pesticide Science, 1997. **49**(3): p. 259-267.
- [37] Feng, J., et al., *Degradation of diuron in aqueous solution by dielectric barrier discharge*. Journal of Hazardous Materials, 2008. **154**: p. 1081-1089.
- [38] Chaplin, B.P., *Critical review of electrochemical advanced oxidation processes for water treatment applications*. Environmental Science: Processes & Impacts, 2014. **16**(6): p. 1182-1203.
- [39] Enache, T.A., et al., *Hydroxyl radicals electrochemically generated in situ on a boron-doped diamond electrode*. Electrochemistry Communications, 2009. **11**(7): p. 1342-1345.
- [40] Marselli, B., et al., *Electrogeneration of Hydroxyl Radicals on Boron-Doped Diamond Electrodes*. Journal of the Electrochemical Society, 2003. **150**(3): p. D79-D83.
- [41] Giraldo, A.L., et al., *Degradation of the antibiotic oxacillin in water by anodic oxidation with Ti/IrO₂ anodes: Evaluation of degradation routes, organic by-products and effects of water matrix components*. Chemical Engineering Journal, 2015. **279**: p. 103-114.

- [42] Scialdone, O., A. Galia, and S. Sabatino, *Electro-generation of H₂O₂ and abatement of organic pollutant in water by an electro-Fenton process in a microfluidic reactor*. *Electrochemistry Communications*, 2013. **26**: p. 45-47.
- [43] Wu, W., Z.-H. Huang, and T.-T. Lim, *Recent development of mixed metal oxide anodes for electrochemical oxidation of organic pollutants in water*. *Applied Catalysis A: General*, 2014. **480**: p. 58-78.
- [44] Dorfman, L. and G. Adams, *Reactivity of the hydroxyl radical in aqueous solutions*. 1973.
- [45] Lipczynska-Kochany, E., G. Sprah, and S. Harms, *Influence of some groundwater and surface waters constituents on the degradation of 4-chlorophenol by the Fenton reaction*. *Chemosphere*, 1995. **30**(1): p. 9-20.
- [46] Guillard, C., et al., *Influence of chemical structure of dyes, of pH and of inorganic salts on their photocatalytic degradation by TiO₂ comparison of the efficiency of powder and supported TiO₂*. *Journal of Photochemistry and Photobiology A: Chemistry*, 2003. **158**(1): p. 27-36.
- [47] Kai-Yuan, S. and B.R. Locke, *Optical and Electrical Diagnostics of the Effects of Conductivity on Liquid Phase Electrical Discharge*. *Plasma Science, IEEE Transactions on*, 2011. **39**(3): p. 883-892.
- [48] Salvestrini, S., P. Di Cerbo, and S. Capasso, *Kinetics of the chemical degradation of diuron*. *Chemosphere*, 2002. **48**(1): p. 69-73.
- [49] Farre, M.J., et al., *Evaluation of the intermediates generated during the degradation of Diuron and Linuron herbicides by the photo-Fenton reaction*. *Journal of Photochemistry and Photobiology A: Chemistry*, 2007. **189**: p. 364-373.
- [50] Amine-Khodja, A., A. Boulkamh, and P. Boule, *Photochemical behaviour of phenylurea herbicides*. *Photochemical & Photobiological Sciences*, 2004. **3**(2): p. 145-156.
- [51] Ren, X., Z. Cui, and Y. Sun, *Theoretical studies on degradation mechanism for OH-initiated reactions with diuron in water system*. *Journal of Molecular Modeling*, 2014. **20**(7): p. 1-12.

- [52] Nélieu, S., et al., *Phototransformation of monuron induced by nitrate and nitrite ions in water: Contribution of photonitration*. Journal of Photochemistry and Photobiology A: Chemistry, 2008. **193**(1): p. 1-9.
- [53] Lukes, P., et al., *Aqueous-phase chemistry and bactericidal effects from an air discharge plasma in contact with water: evidence for the formation of peroxyxynitrite through a pseudo-second-order post-discharge reaction of H₂O₂ and HNO₂*. Plasma Sources Science and Technology, 2014. **23**(1): p. 015019.
- [54] Chen, W.-H. and T.M. Young, *Influence of Nitrogen Source on NDMA Formation during Chlorination of Diuron*. Water research, 2009. **43**(12): p. 3047-3056.
- [55] Fenoll, J., et al., *Photocatalytic transformation of sixteen substituted phenylurea herbicides in aqueous semiconductor suspensions: Intermediates and degradation pathways*. Journal of Hazardous Materials, 2013. **244-245**(0): p. 370-379.
- [56] Shankar, M.V., et al., *Photo-induced degradation of diuron in aqueous solution by nitrites and nitrates: Kinetics and pathways*. Chemosphere, 2007. **66**(4): p. 767-774.
- [57] Tan, C., et al., *Heat-activated persulfate oxidation of diuron in water*. Chemical Engineering Journal, 2012. **203**(0): p. 294-300.
- [58] Tu, Q., et al., *Microfluidic Device: A Miniaturized Platform for Chemical Reactions*. Chinese Journal of Chemistry, 2013. **31**(3): p. 304-316.
- [59] Ehrfeld, W., V. Hessel, and H. Löwe, *State of the Art of Microreaction Technology*, in *Microreactors*. 2004, Wiley-VCH Verlag GmbH & Co. KGaA. p. 1-14.
- [60] Joshi, A.A., et al., *Formation of hydroxyl radicals, hydrogen peroxide and aqueous electrons by pulsed streamer corona discharge in aqueous solution*. Journal of Hazardous Materials, 1995. **41**(1): p. 3-30.
- [61] Raksatham, T., *Photoelectrocatalytic degradation of diuron on titanium film*. 2013, Chulalongkorn University: Chulalongkorn University.

- [62] Hoather, R.C. and R.F. Rackham, *Oxidised nitrogen in waters and sewage effluents observed by ultra-violet spectrophotometry*. *Analyst*, 1959. **84**(1002): p. 548-551.
- [63] ASTM International, *Standard Test Method for Sulfate Ion in Water*, in *ASTM D516-11*. 2011, West Conshohocken: PA.
- [64] Huang, K.-C., R.A. Couttenye, and G.E. Hoag, *Kinetics of heat-assisted persulfate oxidation of methyl tert-butyl ether (MTBE)*. *Chemosphere*, 2002. **49**(4): p. 413-420.
- [65] Huling, S.G., S. Ko, and B. Pivetz, *Groundwater Sampling at ISCO Sites: Binary Mixtures of Volatile Organic Compounds and Persulfate*. *Ground Water Monitoring & Remediation*, 2011. **31**(2): p. 72-79.
- [66] Wu, T. and J.D. Englehardt, *A New Method for Removal of Hydrogen Peroxide Interference in the Analysis of Chemical Oxygen Demand*. *Environmental Science & Technology*, 2012. **46**(4): p. 2291-2298.
- [67] Lukes, P., B.R. Locke, and J.-L. Brisset, *Aqueous-Phase Chemistry of Electrical Discharge Plasma in Water and in Gas-Liquid Environments*, in *Plasma Chemistry and Catalysis in Gases and Liquids*. 2012, Wiley-VCH Verlag GmbH & Co. KGaA. p. 243-308.
- [68] Baroch, P., N. Saito, and O. Takai, *Special type of plasma dielectric barrier discharge reactor for direct ozonization of water and degradation of organic pollution*. *Journal of Physics D: Applied Physics*, 2008. **41**(8): p. 085207.
- [69] Bamba, D., et al., *Photocatalytic degradation of the diuron pesticide*. *Environmental Chemistry Letters*, 2008. **6**(3): p. 163-167.
- [70] Salazar, R., et al., *Degradation of disperse azo dyes from waters by solar photoelectro-Fenton*. *Electrochimica Acta*, 2011. **56**(18): p. 6371-6379.
- [71] Ruiz, E.J., et al., *Mineralization of Acid Yellow 36 azo dye by electro-Fenton and solar photoelectro-Fenton processes with a boron-doped diamond anode*. *Chemosphere*, 2011. **82**(4): p. 495-501.

- [72] Almeida, L.C., et al., *Solar photoelectro-Fenton degradation of paracetamol using a flow plant with a Pt/air-diffusion cell coupled with a compound parabolic collector: Process optimization by response surface methodology*. Applied Catalysis B: Environmental, 2011. **103**(1–2): p. 21-30.
- [73] Krause, H., et al., *Degradation of persistent pharmaceuticals in aqueous solutions by a positive dielectric barrier discharge treatment*. Journal of Electrostatics, 2011. **69**(4): p. 333-338.
- [74] Sugiarto, A.T., et al., *Oxidative decoloration of dyes by pulsed discharge plasma in water*. Journal of Electrostatics, 2003. **58**(1–2): p. 135-145.
- [75] Wang, H.-j. and X.-y. Chen, *Kinetic analysis and energy efficiency of phenol degradation in a plasma-photocatalysis system*. Journal of Hazardous Materials, 2011. **186**(2–3): p. 1888-1892.
- [76] Konstantinou, I.K. and T.A. Albanis, *TiO₂-assisted photocatalytic degradation of azo dyes in aqueous solution: kinetic and mechanistic investigations: A review*. Applied Catalysis B: Environmental, 2004. **49**(1): p. 1-14.
- [77] Chen, Z., et al., *A study of electrosorption selectivity of anions by activated carbon electrodes in capacitive deionization*. Desalination, 2015. **369**: p. 46-50.
- [78] Mossad, M. and L. Zou, *A study of the capacitive deionisation performance under various operational conditions*. Journal of Hazardous Materials, 2012. **213–214**: p. 491-497.
- [79] Ellappan, P. and L.R. Miranda, *Two-regime kinetic study and parameter optimization of degradation of 3,4-dichloroaniline using TI–N/S catalyst under visible light*. Desalination and Water Treatment, 2014: p. 1-14.
- [80] Amir Tahmasseb, L., et al., *Ozonation of chlorophenylurea pesticides in water: reaction monitoring and degradation pathways*. Science of The Total Environment, 2002. **291**(1–3): p. 33-44.
- [81] Lányi, K., *Study of the photodegradation of urea-type herbicides by capillary gas chromatography*. Chromatographia, 2003. **57**(1): p. S235-S241.

- [82] Khongthon, W., et al., *Degradation of diuron via an electrochemical advanced oxidation process in a microscale-based reactor*. Chemical Engineering Journal, 2016. **292**: p. 298-307.
- [83] Uppu, R.M., et al., *Nitrosation by Peroxynitrite: Use of Phenol as a Probe*. Archives of Biochemistry and Biophysics, 1998. **358**(1): p. 1-16.





APPENDIX A

CALIBRATION DATA ANALYSIS

A.1 Calibration curve of diuron

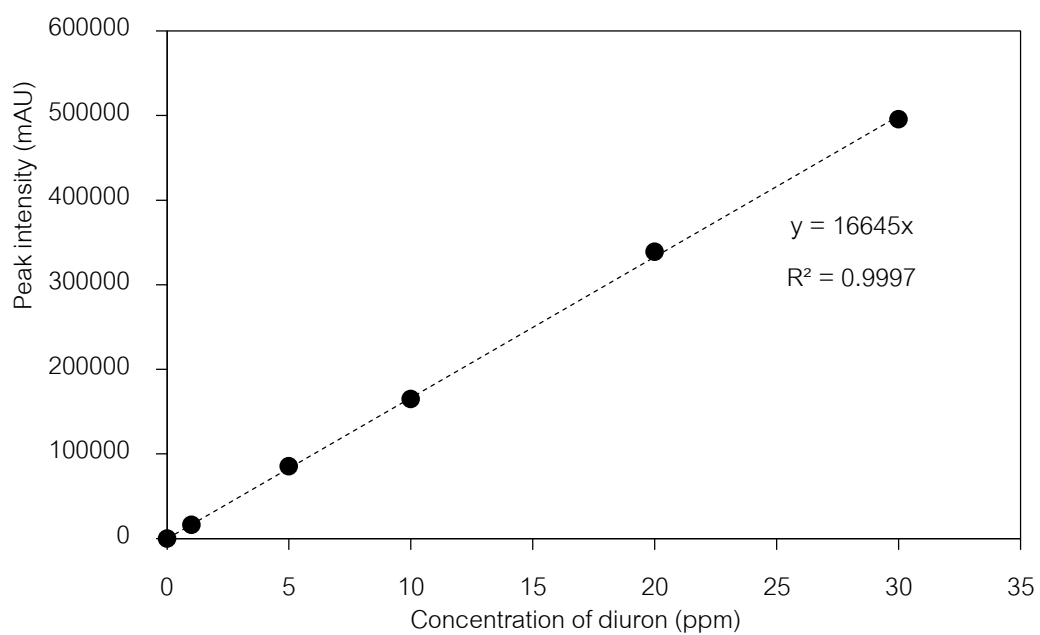


Figure A.1 Calibration curve of diuron

A.2 Calibration curve of 3-(3, 4-dichlorophenyl)-1-formyl-1-methylurea (compound 1)

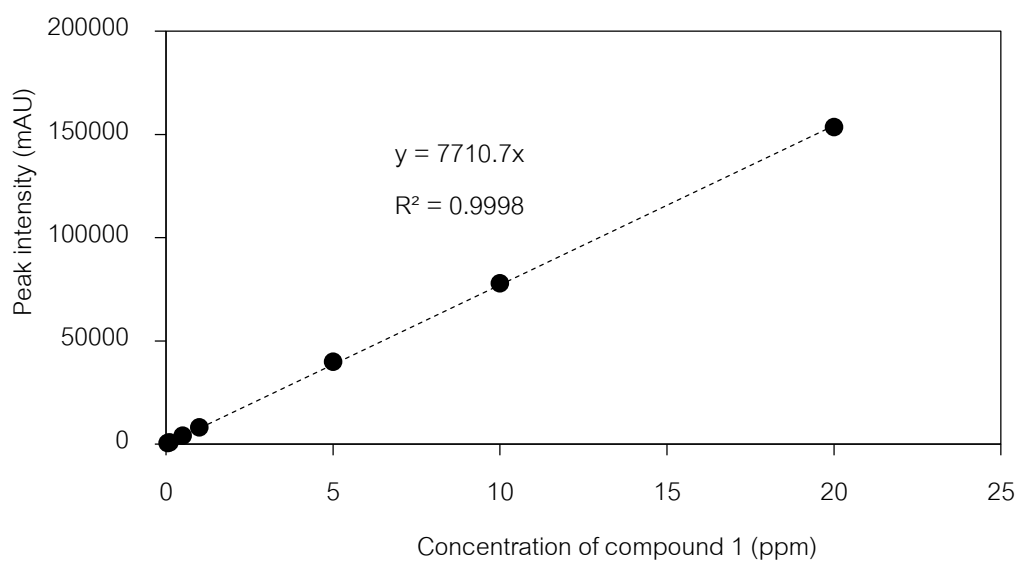


Figure A.2 Calibration curve of compound 1

A.3 Calibration curve of 3-(3-chlorophenyl)-1, 1-dimethylurea (compound 2)

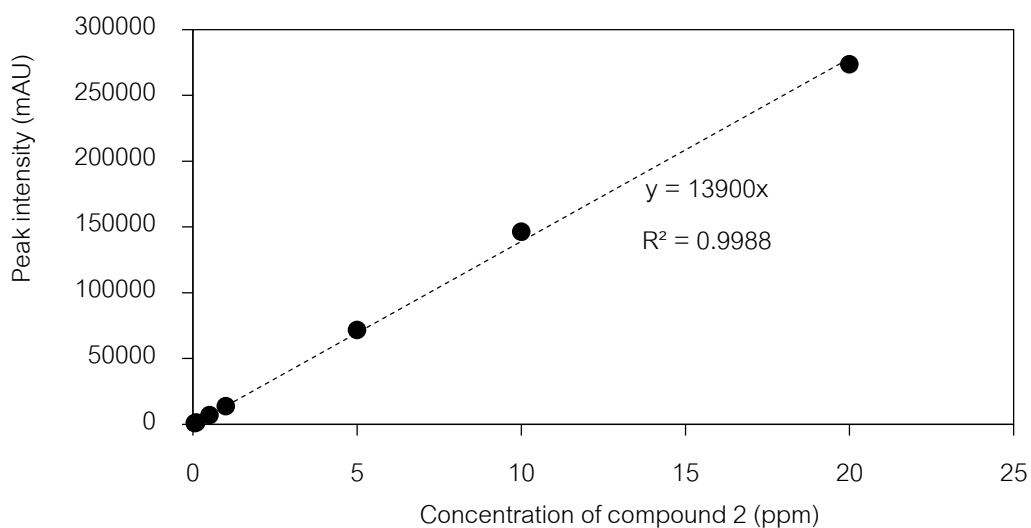


Figure A.3 Calibration curve of compound 2

A.4 Calibration curve of 3, 4-dichloro-aniline (compound 3)

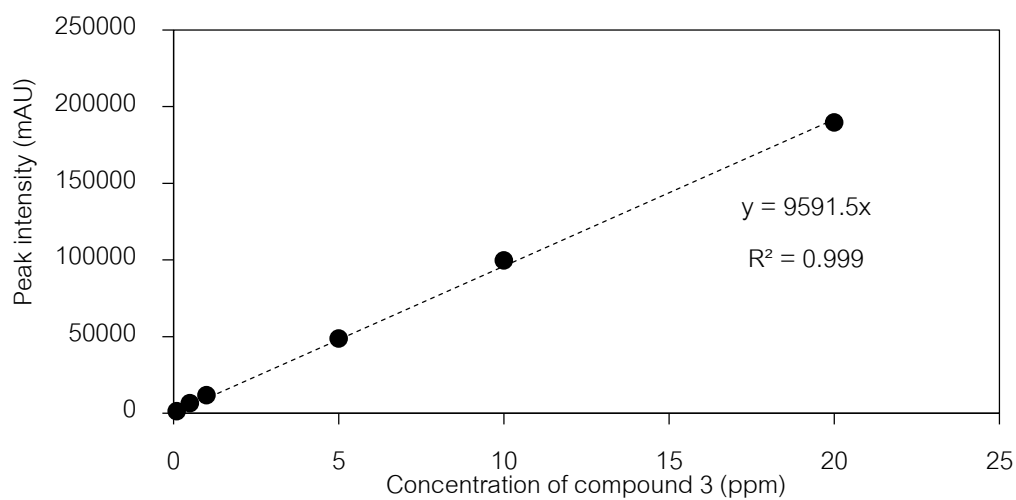


Figure A.4 Calibration curve of compound 3

A.5 Calibration curve of nitrate ion

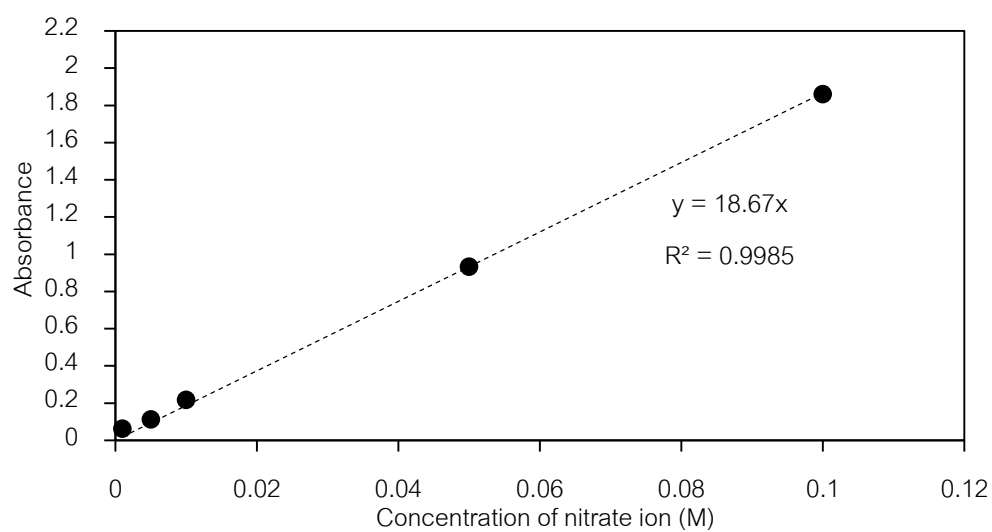


Figure A.5 Calibration curve of nitrate ion

A.6 Calibration curve of nitrite ion

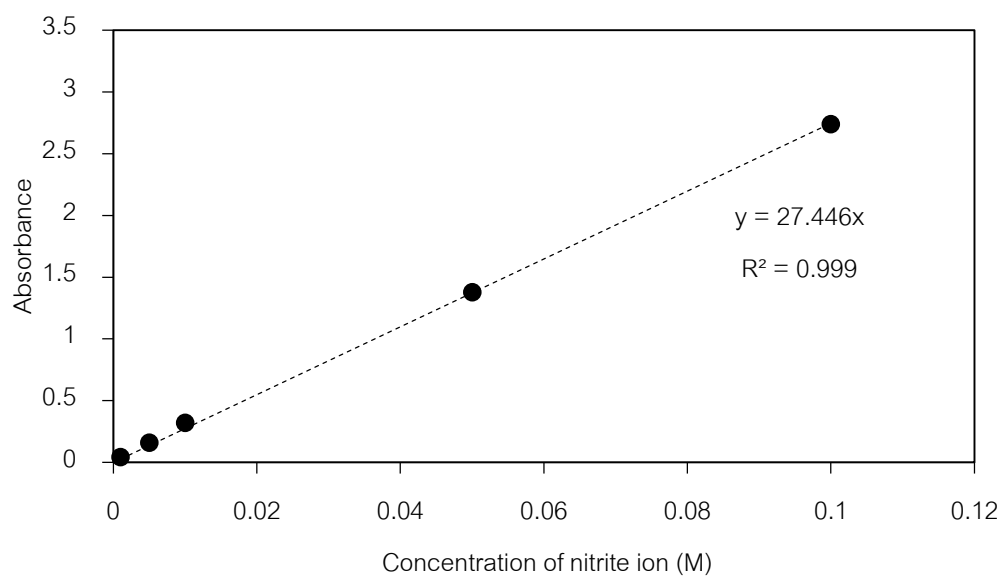


Figure A.6 Calibration curve of nitrite ion

A.7 Calibration curve of sulfate ion

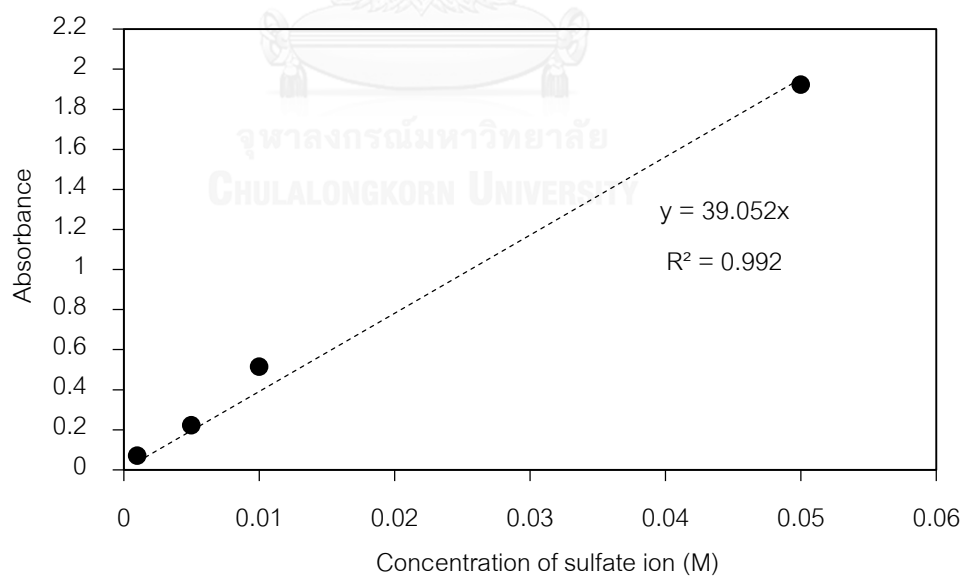


Figure A.7 Calibration curve of nitrite ion

A.8 Calibration curve of persulfate ion

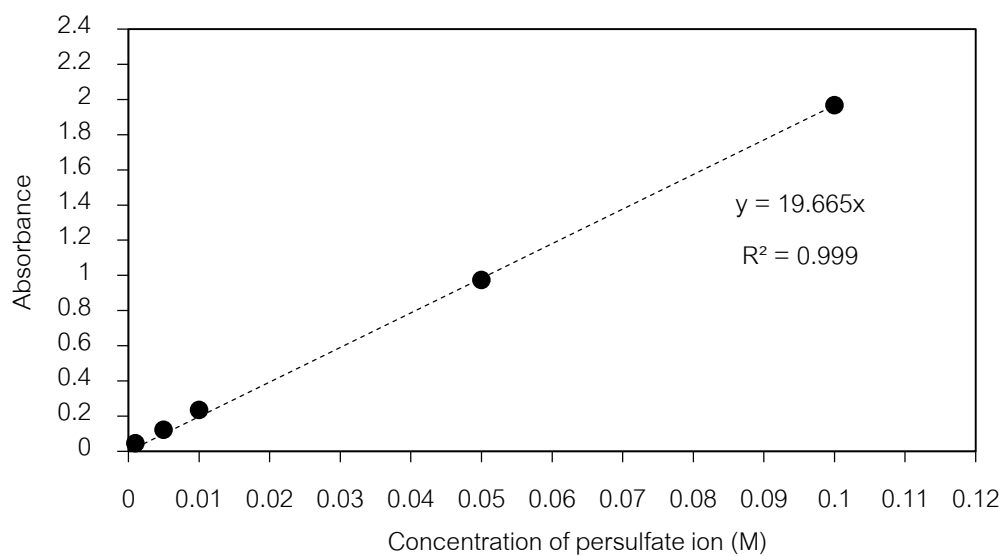


Figure A.8 Calibration curve of persulfate ion

A.9 Calibration curve of hydrogen peroxide

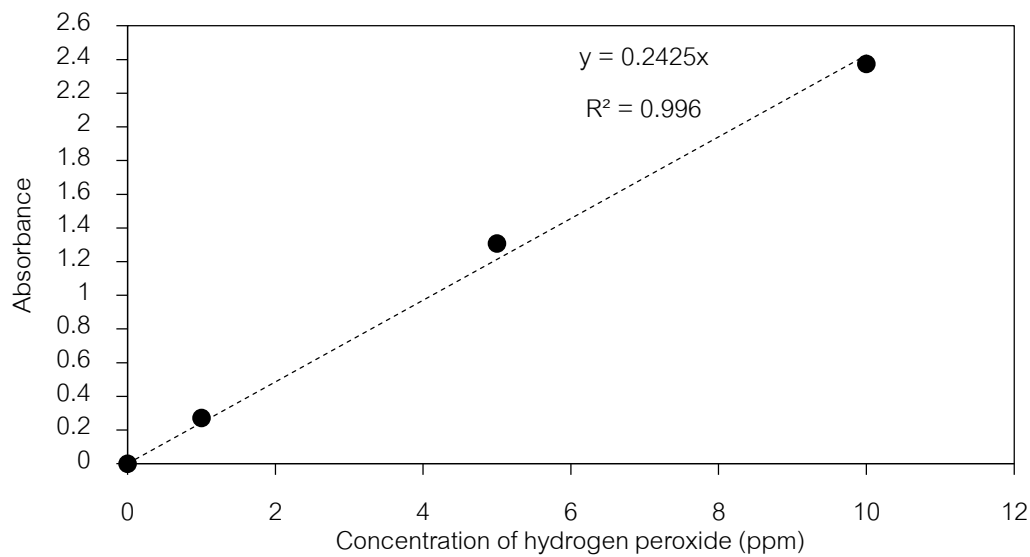


Figure A.8 Calibration curve of hydrogen peroxide

APPENDIX B

PROCEDURE OF CHEMICAL PREPARATION

B.1 Determination of hydrogen peroxide

1. Preparation of A solution

- Added 0.01 g of ammonium molybdate (99% purity, UNIVAR), 0.1 g of sodium hydroxide (98-100% purity, Loba Chemie) and 3.3 g of potassium iodide (99.5% purity, Kanto Chemical) in 50 mL of volumetric flask.
- Then added deionized water to make 50 mL of total volume.

2. Preparation of B solution

- Added 1 g of potassium hydrogen phthalate (99.8-100.2% purity, UNIVAR) in 50 mL of volumetric flask.
- Then added deionized water to make 50 mL of total volume.

3. Measurement hydrogen peroxide by UV-Visible spectrophotometer

- Sample for analyses was mixed by 1 mL of experimental sample, 1 mL of A solution and 1 mL of B solution.
- 3 mL of deionized water is used as blank.
- Detected wavelength is 350 nm.

B.2 Determination of nitrate ion

Measurement nitrate ion by UV-Visible spectrophotometer

- Sample for analyses was by mixed 0.05 mL of experimental sample and 10 mL of deionized water.
- 3 ml of deionized water is used as blank.
- Detected wavelength is 220 nm.

B.3 Determination of nitrite ion

1. Preparation of color reagent

- Added 1 g of sulfanilamide (special grade, Carlo Erba) in 10 mL of phosphoric acid (≥ 85 % wt. purity, QRec)
- Then added 0.1 of N-(1-naphthyl)ethylenediamine dihydrochloride ($>98\%$ purity, Acros organics) to the previous solution. After that added deionized water to make 100 mL of total volume.

2. Measurement nitrite ion by UV-Visible spectrophotometer

- Sample for analyses was by mixed 0.02 mL of experimental sample, 0.8 mL of color reagent and 10 mL of deionized water. Leave the sample for 2h in room temperature before measurement.
- 0.8 mL of color reagent and 10 mL of deionized water were mixed using as blank
- Detected wavelength is 543 nm.

B.4 Determination of sulfate ion

1. Preparation of conditioning reagent

- Added 37.5 g of sodium chloride (UNIVAR), 25 mL of glycerol (99.5% purity, QRec), 15 mL conc. hydrochloric acid (37% purity, QRec) and 50 mL of ethanol (99.9% purity, QRec) in beaker.
- Prepared 0.075 M of barium chloride (99% purity, UNIVAR) separately.

2. Measurement sulfate ion by UV-Visible spectrophotometer

- Sample for analyses was by mixed 0.2 mL of experimental sample, 3 mL of barium chloride and 0.025 mL of conditioning reagent. White particles was formed suddenly.
- Measured the sample by UV-Visible spectrophotometer and hold the sample for 2 min. Record the maximum absorbance.
- Detected wavelength is 420 nm.

B.5 Determination of persulfate ion

1. Preparation of reagent

- 2.5 M of hydrochloric acid (37% purity, QRec)
- 0.4 M of ferrous ammonium sulfate (99-100% purity, Loba Chemie)
- 0.6 M of ammonium thiocyanate (98% purity, UNIVAR)

2. Measurement sulfate ion by UV-Visible spectrophotometer

- Mixed 0.9 mL of 2.5 M of hydrochloric acid and 10 mL of deionized water.
- Then added 0.1 mL of experimental sample and 0.1 mL of 0.4 M of ferrous ammonium sulfate (stabilizing by adding a droplet of 2.5 M of hydrochloric acid) to previous solution.

- Leave the mixed it for 30 min in room temperature. And then added 0.2 mL of 0.6 M of ammonium thiocyanate. The sample color changed to red suddenly. After that measured the sample by UV-Visible spectrophotometer
- Detected wavelength is 450 nm.



APPENDIX C

LIQUID CHROMATOGRAPHY–MASS/MASS SPECTRUM (LC-MS/MS) DATA

C.1 LC-MS/MS spectrum of diuron (Negative mode)

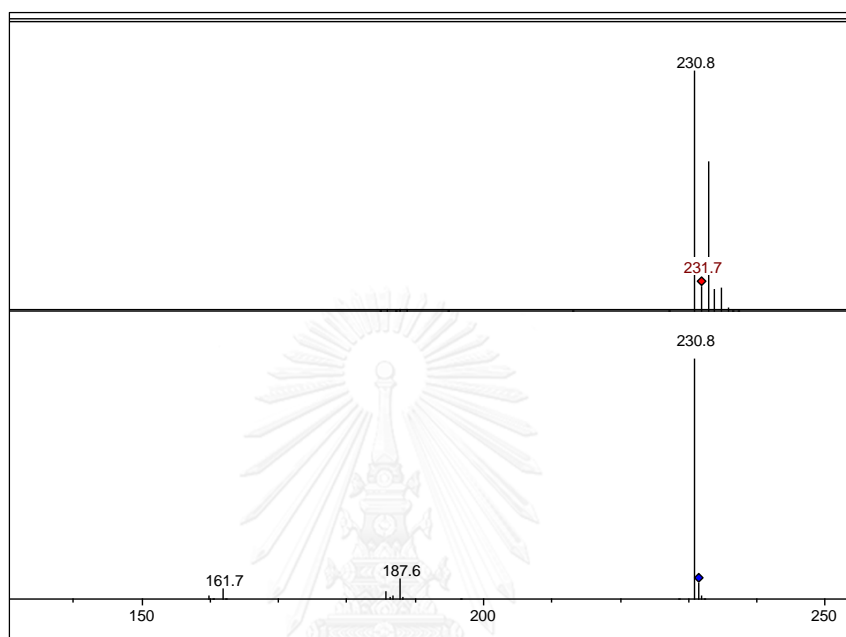


Figure C.1 LC-MS/MS spectrum of diuron

C.2 LC-MS/MS spectrum of 3-(3, 4-dichlorophenyl)-1-formyl-1-methylurea, compound 1
(Negative mode)

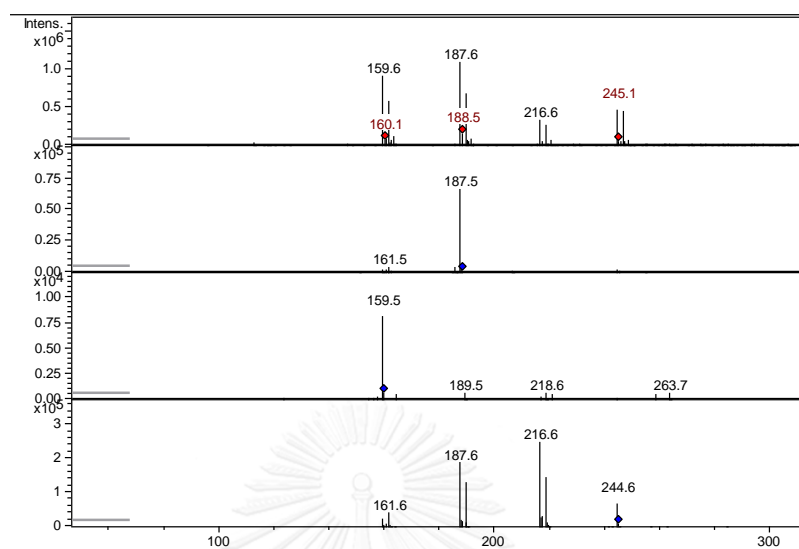


Figure C.2 LC-MS/MS spectrum of compound 1

C.3 LC-MS/MS spectrum of 3-(3-chlorophenyl)-1, 1-dimethylurea, compound 2 (Positive mode)

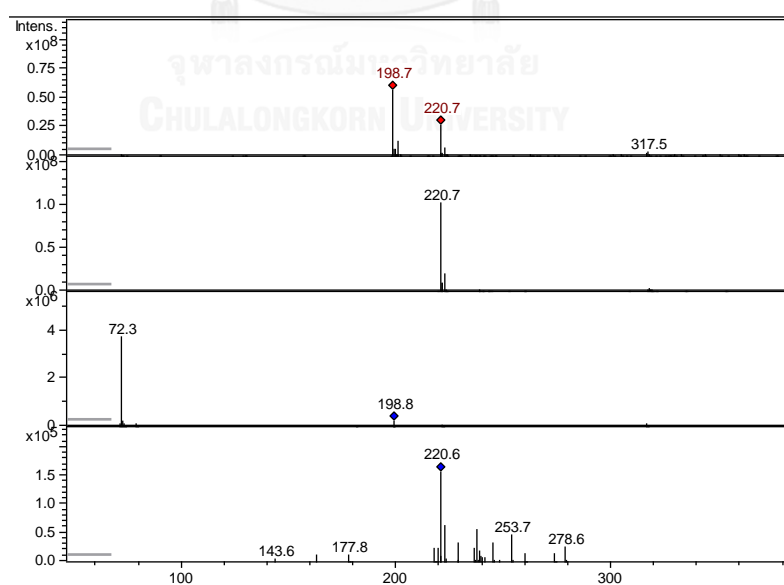


Figure C.3 LC-MS/MS spectrum of compound 2

C.4 LC-MS/MS spectrum of 3, 4-dichloro-aniline, compound 3 (Negative mode)

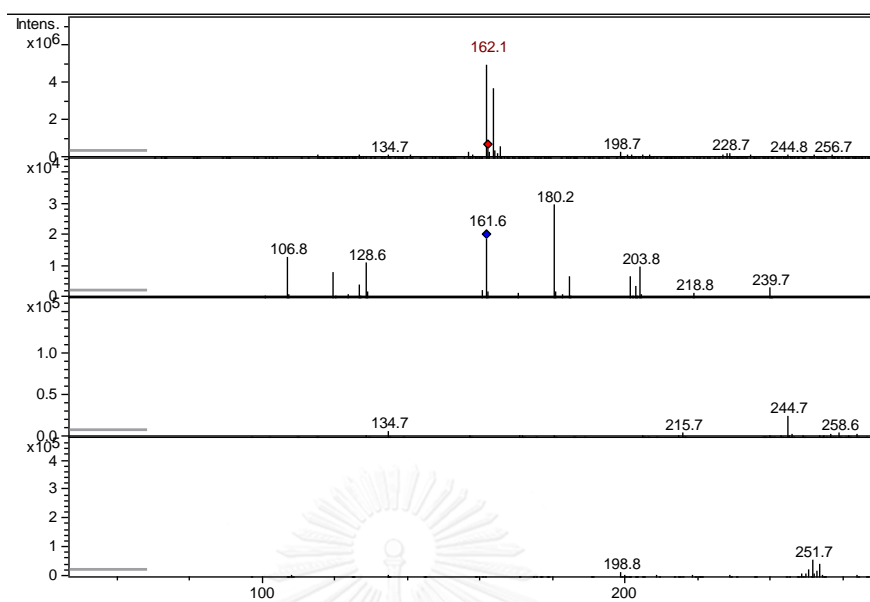


Figure C.4 LC-MS/MS spectrum of compound 3

C.5 LC-MS/MS spectrum of compound 4 (Positive mode)

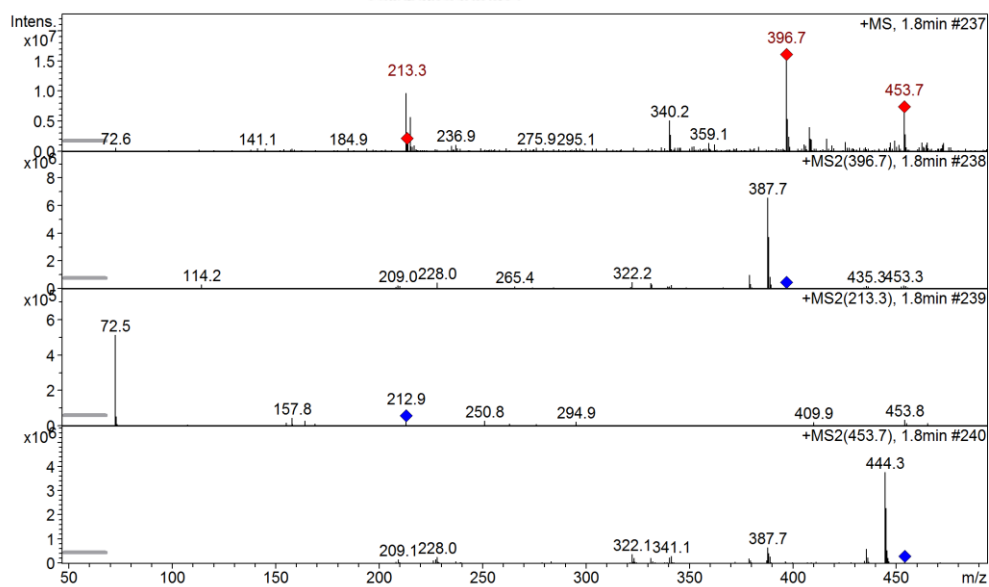


Figure C.4 LC-MS/MS spectrum of compound 4

C.6 LC-MS/MS spectrum of compound 5 (Negative mode)

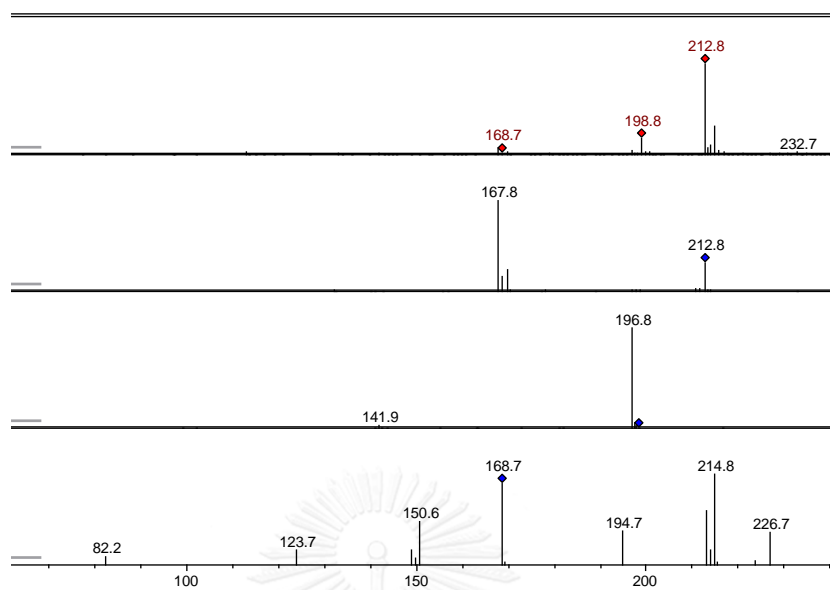


Figure C.6 LC-MS/MS spectrum of compound 5

C.7 LC-MS/MS spectrum of compound 6 (Negative mode)

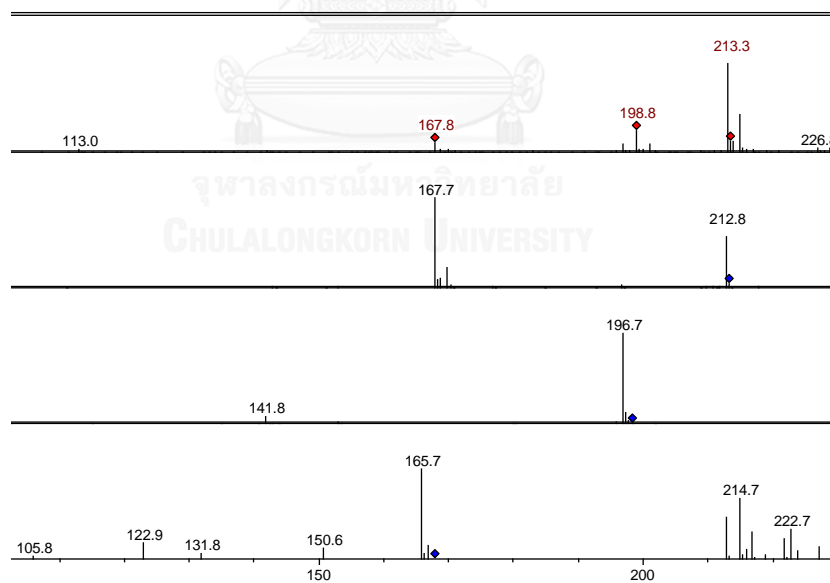


Figure C.7 LC-MS/MS spectrum of compound 6

C.8 LC-MS/MS spectrum of compound 7 (Negative mode)

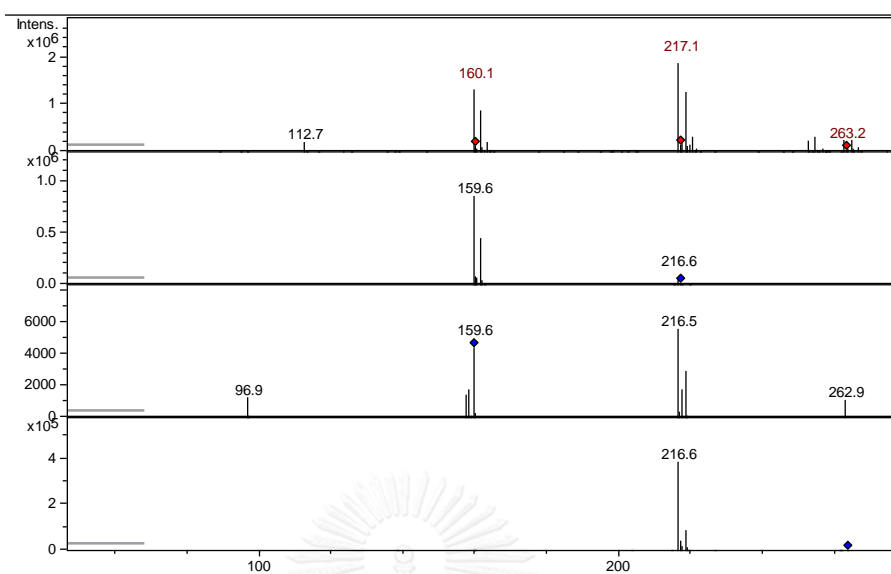


Figure C.8 LC-MS/MS spectrum of compound 7

C.9 LC-MS/MS spectrum of compound 8 (Negative mode)

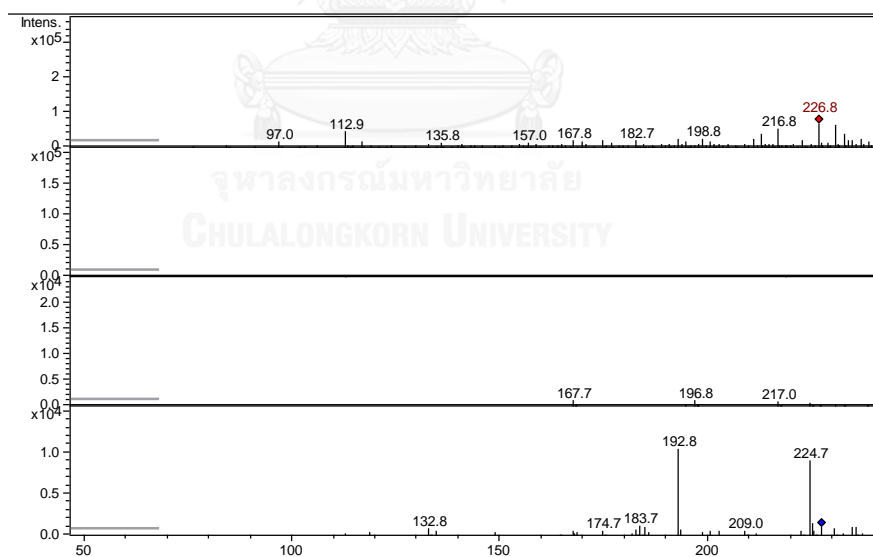


Figure C.9 LC-MS/MS spectrum of compound 8

C.10 LC-MS/MS spectrum of compound 9 (Negative mode)

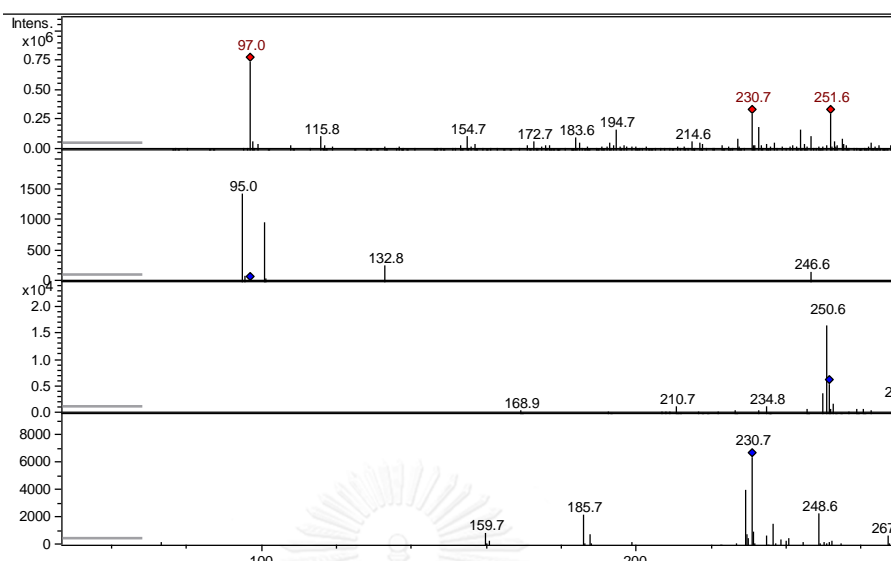


Figure C.10 LC-MS/MS spectrum of compound 9

C.11 LC-MS/MS spectrum of compound 10 (Negative mode)

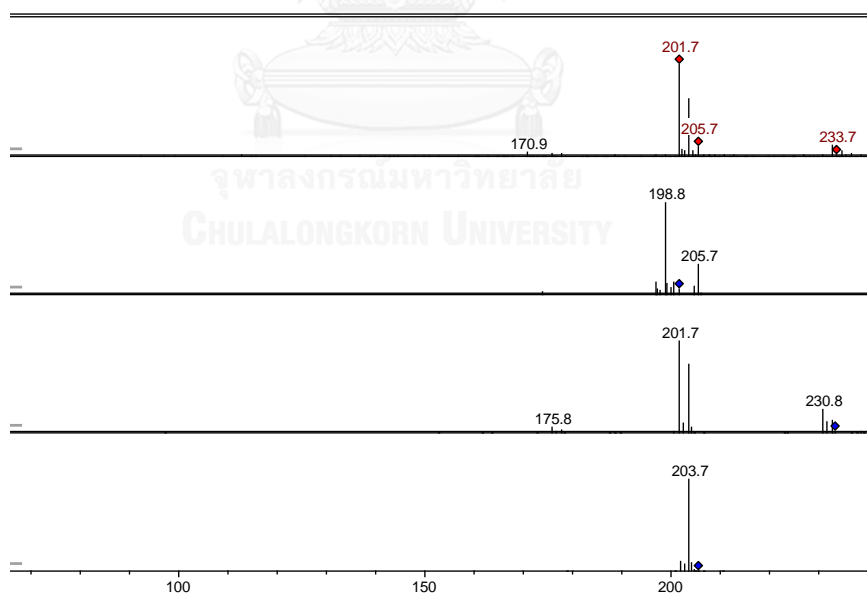


Figure C.11 LC-MS/MS spectrum of compound 10

C.12 LC-MS/MS spectrum of compound 11 (Negative mode)

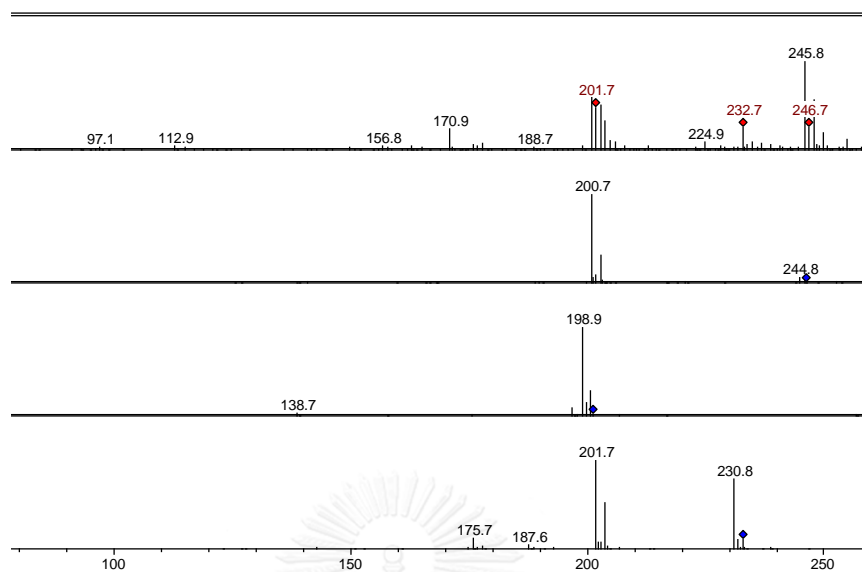


Figure C.12 LC-MS/MS spectrum of compound 11

C.13 LC-MS/MS spectrum of compound 12 (Negative mode)

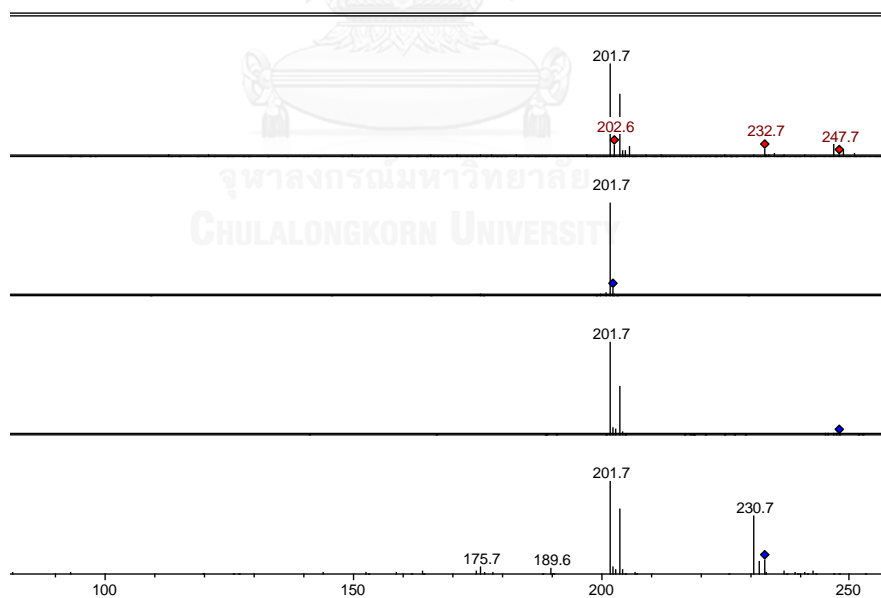


Figure C.13 LC-MS/MS spectrum of compound 12

C.14 LC-MS/MS spectrum of compound 13 (Negative mode)

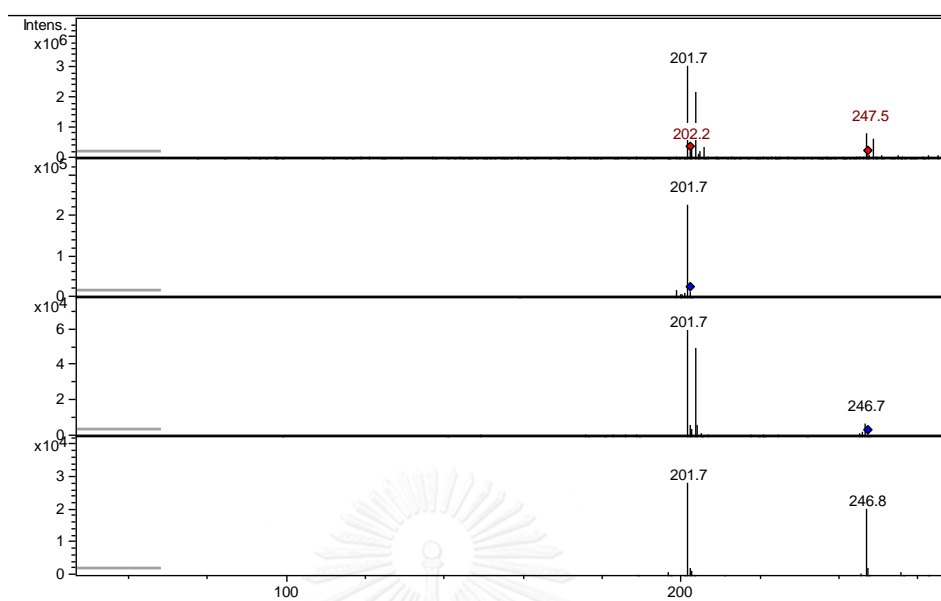
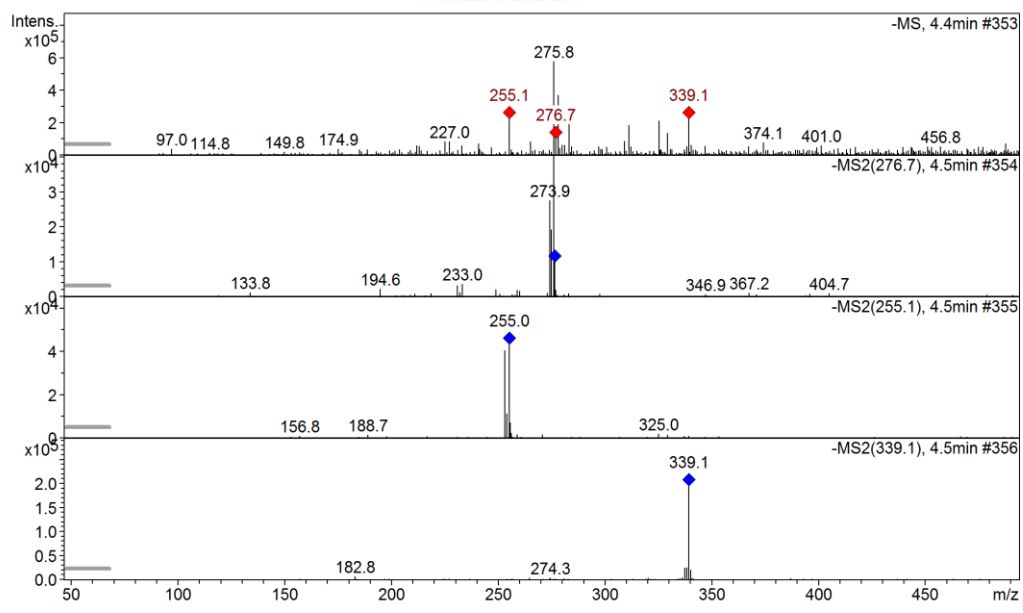


Figure C.14 LC-MS/MS spectrum of compound 13

C.15 LC-MS/MS spectrum of compound 14 (Negative mode)



C.15 LC-MS/MS spectrum of compound 14

C.16 LC-MS/MS spectrum of compound 15 (Negative mode)

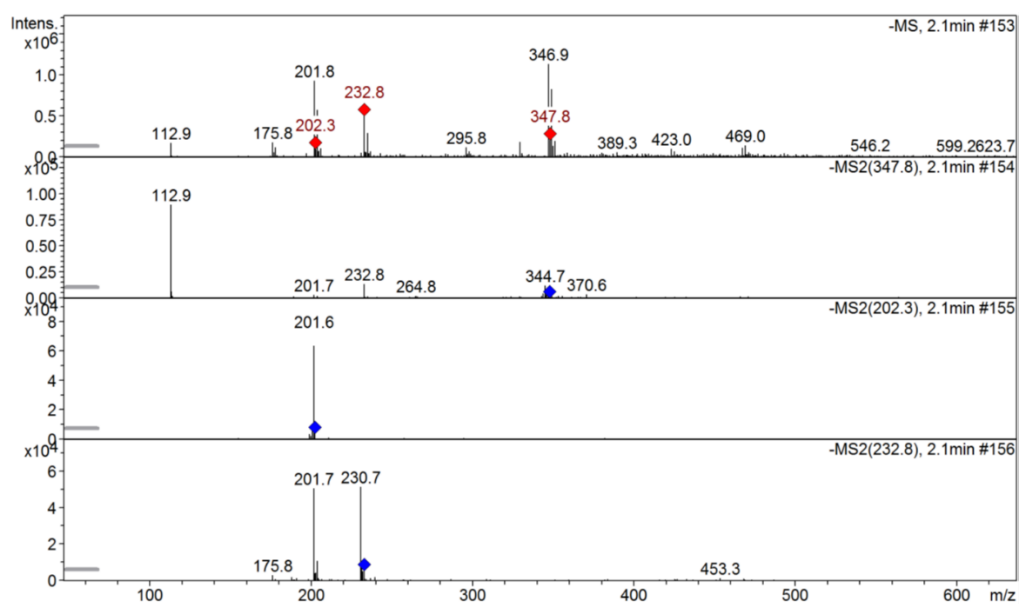


Figure C.16 LC-MS/MS spectrum of compound 15

C. 17 Procedure for analyze intermediate structure by LC-MS/MS

Example compound 1

1. For MS analysis, monoisotopic mass of compound 1 is 245.99. Under negative mode, compound 1 shows m/z peak at 245 (M-1) as shown in figure C.2.
2. Due to structure of compound 1 consists of 2Cl atoms, m/z peak always shows 2 high peaks are 245 and 243, which height of m/z peak at 243 show 2/3 of the height m/z peak of 245 due property of chlorine as shown in figure C.2.
3. For MS/MS analysis, results show fragments (m/z peak) 160, 180, 217 which indicate that loss of $C_6H_4NCl_2$, $C_7H_4ONCl_2$ and $C_8H_7ON_2Cl_2$, respectively, of from compound 1 structure as shown in figure C.1 and C.17

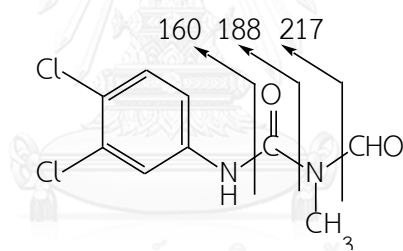


Figure C.17 Fragments of compound 1.

APPENDIX D

CALCULATION OF DIFFUSION COEFFICIENTS

Diffusion coefficient of diuron, compound 1, 2 and 3 in water at room temperature are calculated by Wilke-Chang correlation for dilute concentration in water as shown in equation D.1. Table D.1 shows diffusion coefficient of diuron, compound 1, 2 and 3 in water at room temperature (298K).

$$D_{A-B} = 7.4 \times 10^{-8} \frac{(\Psi_B M_B)^{0.5} T}{\mu \tilde{v}_A^{0.6}} \quad \text{D.1}$$

Where:	Association factor for water (Ψ_B)	is	2.6
	Room temperature (T)	is	298 K
	Viscosity of water (μ) at room temperature	is	1 cP
	Molecular of water (M_B)	is	18 g·mol ⁻¹

Molar volume of solute A (\tilde{v}_A) is depended on compound (cm³·mol⁻¹)

Table D.1 Parameters for Wilke-Chang Correlation

Compound	Molar volume ($\text{cm}^3 \cdot \text{mol}^{-1}$)	Diffusion coefficient ($\text{m}^2 \cdot \text{s}^{-1}$)
Diuron	170.1	6.92×10^{-10}
Compound 1	167.5	7.00×10^{-10}
Compound 2	158.2	7.23×10^{-10}
Compound 3	115.6	8.73×10^{-10}



APPENDIX E

INPUT PARAMETERS AND VARIABLES IN NUMERICAL MODEL

All used parameters for solving the model in diuron degradation and reaction pathway of diuron were defined as shown in table E.1 and E.2, respectively. Table E.3 and E.4 show used variables in diuron degradation and reaction pathway of diuron.

Node property settings in two physics model, defined for diuron degradation and reaction pathway of diuron, are shown in table E.5 and E.6

Table E.1 Input parameters in numerical model for diuron degradation at 100s of mean residence time

Name	Value	Description
linear velocity	2.12e-4[m/s]	average linear velocity
pressure	1[atm]	outlet pressure
C0Diuron	10[ppm]	initial concentration of diuron
DDiuron	6.92e-10[m ² /s]	diffusion of diuron
k	0.036[1/s]	reaction rate

Table E.2 Input parameters in numerical model for reaction pathway of diuron at 100s of mean residence time

Name	Value	Description
linear velocity	2.12e-4[m/s]	average linear velocity
pressure	1[atm]	outlet pressure
C0Diuron	10[ppm]	initial concentration of diuron
k1-1	6.8e-4[1/s]	reaction rate of diuron degradation for route 1
k1-2	3.4e-4[1/s]	reaction rate of diuron degradation for route 2
k1-3	3.2e-2[1/s]	reaction rate of diuron degradation for route 3
k2	2.0e-2[1/s]	reaction rate of compound 1
k3	1.5e-2[1/s]	reaction rate of compound 2
k4	1.0e-2[1/s]	reaction rate of compound 3
k5	2.0e-2[1/s]	reaction rate of other compounds
DDiuron	6.92e-10[m ² /s]	diffusion of diuron
DC1	7.00e-10[m ² /s]	diffusion of compound 1
DC2	7.23e-10[m ² /s]	diffusion of compound 2
DC3	8.73e-10[m ² /s]	diffusion of compound 3

Table E.3 Input variables in numerical model for diuron degradation at 100s of mean residence time

Name	Expression	Description
rDiuron	$k \cdot c_{\text{Diuron}}$	reaction rate of diuron
cDiuron_f	aveop1(cDiuron)	average concentration of diuron at the end of channel



Table E.4 Input variables in numerical model for reaction pathway of diuron at 100s of mean residence time

Name	Expression	Description
rDiuron	$-(k1-1+k1-2+k1-3)*cDiuron$	reaction rate of diuron
rC1	$k1-1*cDiuron-k2*cC1-k5*cC1$	reaction rate of compound 1
rC2	$k1-2*cDiuron-k4*cC2$	reaction rate of compound 2
rC3	$k2cC1-k3cC3$	reaction rate of compound 3
rC4	$k1-3*cDiuron+k3*cC3+k4*cC2+k5*cC1$ $-k6*cC4$	reaction rate of other compounds
cDiuron_f	aveop1(cDiuron)	average concentration of diuron at the end of channel
cC1_f	aveop1(cC1)	average concentration of compound 1 at the end of channel
cC2_f	aveop1(cC2)	average concentration of compound 2 at the end of channel
cC3_f	aveop1(cC3)	average concentration of compound 3 at the end of channel
cC4_f	aveop1(cC4)	average concentration of other compounds at the end of channel

Table E.5 Node properties setting in Laminar Flow Model

Physical Model	Compressibility	Incompressible flow	
		Turbulence Model Type	None
Fluid Properties	Density	From material	
		Dynamic Viscosity	From material
Wall	Boundary Condition	No slip	
Initial Values	Velocity Field, x	0 m/s	
	Velocity Field, y	0 m/s	
	Pressure	1 atm	
Inlet	Boundary condition	Laminar inflow	
		Average Velocity	Defined in Parameters
		Entrance Length	0.01 m
Outlet	Boundary condition	Pressure, no viscous stress	
		Pressure	Defined in Parameters

Table E.6 Node properties setting in Transport of Diluted Species Model

	Model Transport Mechanisms	Incompressible flow
	Dependent Variables	5 species (cCDiuron, cC1, cC2, cC3 and cC4)
Convection and Diffusion	Diffusion Coefficient	Defined in Parameters
No Flux	-	-
Initial Values	Concentration	0 for all species
Reactions	Reactions	Defined in Variables
Inflow	Concentration	<ul style="list-style-type: none"> • Diuron defined in Parameters • Other species are 0

APPENDIX F

PROCEDURE OF OPTIMIZATION OF NUMERICAL MODEL

1. Save COMSOL model as a M-file

In the COMSOL desktop, go to “File” → “Reset History” to release the history of previous programming. Then, go to “File” → “Save as Model M-File”, choose the directory and save it.

2. Modify the M-file to make it a function file for Matlab

Declare the M-file as a function with input and output variables, which would be the objective function. Then, set model parameters, which would be the reaction rate constants. Next, at the end of this file, use the syntax “mphglobal” to extract data of average concentration along the vertical cross-line at the end of reactor. Finally, compute the objective function which is sum of squares of errors between experiment data and simulated results.

3. Build a main program in Matlab

Open a new M-file and set the initial guess value. Then, use the syntax “fminsearch” to find the minimum value of objective function by varying reaction rate constants and set the options. Finally, run the major function and wait for the results.

The codes for the reaction in aqueous solution for diuron degradation and reaction pathway of diuron are similar, but in reaction pathway numerical model, more reaction of compound 1, 2 and 3 were added.

The example of MATLAB program for diuron degradation is as follow:

```
function f = diuron_1st_order_kap_100s(k)

%
% Obj_corona_1st_order_kap_100s.m
%
% Model exported on Apr 2 2013, 13:14 by COMSOL 4.2.0.150.

import com.comsol.model.*
import com.comsol.model.util.*

model = ModelUtil.create('Model');
model.modelPath('D:\Joe\COMSOL');
model.name('diuron-corona_incompress_1st_order_kap_100s.mph');
%-----
k11=k(1);
model.param.set('kap', k11);
figure(11),plot(k11,'o')
hold on
%-----
model.param.set('velocity', '2.1e-4[m/s]', 'average velocity inlet');
model.param.set('press', '1[atm]', 'pressure outlet');
model.param.set('c0Diuron', '10', 'initial concentration of Diuron');
model.param.set('DDiuron', '6.92e-10[m^2/s]', 'diff. coef. of diuron');

model.modelNode.create('mod1');

model.geom.create('geom1', 2);
model.geom('geom1').lengthUnit('mm');
model.geom('geom1').feature.create('r1', 'Rectangle');
model.geom('geom1').feature('r1').set('pos', {'0' '0'});
model.geom('geom1').feature('r1').set('size', {'21' '0.2'});
model.geom('geom1').run;
```

```

model.variable.create('var1');
model.variable('var1').model('mod1');
model.variable('var1').set('rDiuron', '-(kap)*(cDiuron)');
model.variable('var1').set('cDiuron_f', 'aveop1(cDiuron)');

model.material.create('mat1');

model.physics.create('spf', 'LaminarFlow', 'geom1');
model.physics('spf').feature.create('inl1', 'Inlet', 1);
model.physics('spf').feature('inl1').selection.set([1]);
model.physics('spf').feature.create('out1', 'Outlet', 1);
model.physics('spf').feature('out1').selection.set([4]);
model.physics.create('chds', 'DilutedSpecies', 'geom1');
model.physics('chds').feature.create('reac1', 'Reactions', 2);
model.physics('chds').feature('reac1').selection.set([1]);
model.physics('chds').feature.create('in1', 'Inflow', 1);
model.physics('chds').feature('in1').selection.set([1]);
model.physics('chds').feature.create('out1', 'Outflow', 1);
model.physics('chds').feature('out1').selection.set([4]);

model.mesh.create('mesh1', 'geom1');
model.mesh('mesh1').feature.create('size1', 'Size');
model.mesh('mesh1').feature('size1').selection.geom('geom1', 1);
model.mesh('mesh1').feature('size1').selection.set([2 3]);
model.mesh('mesh1').feature.create('fri1', 'FreeTri');
model.mesh('mesh1').feature('fri1').selection.geom('geom1', 2);
model.mesh('mesh1').feature('fri1').selection.set([1]);
model.mesh('mesh1').feature.create('bl1', 'BndLayer');
model.mesh('mesh1').feature('bl1').selection.geom('geom1', 2);
model.mesh('mesh1').feature('bl1').selection.set([1]);
model.mesh('mesh1').feature('bl1').feature.create('blp1', 'BndLayerProp');
model.mesh('mesh1').feature('bl1').feature('blp1').selection.set([2 3]);

```

```

model.mesh('mesh1').feature.create('fri2', 'FreeTri');

model.cpl.create('aveop1', 'Average', 'geom1');
model.cpl('aveop1').selection.geom('geom1', 1);
model.cpl('aveop1').selection.set([4]);

model.result.table.create('tbl1', 'Table');
model.result.table.create('tbl2', 'Table');
model.result.table.create('tbl3', 'Table');
model.result.table.create('tbl4', 'Table');
model.result.table.create('tbl5', 'Table');
model.result.table.create('tbl6', 'Table');
model.result.table.create('tbl7', 'Table');

model.view('view1').axis.set('xmin', '1.4964476823806763');
model.view('view1').axis.set('xmax', '19.503551483154297');
model.view('view1').axis.set('ymin', '-9.553997993469238');
model.view('view1').axis.set('ymax', '9.753998756408691');

model.material('mat1').name('Water');
model.material('mat1').propertyGroup('def').set('density', '1000');
model.material('mat1').propertyGroup('def').set('dynamicviscosity', '8.94e-4');

model.physics('spf').prop('CompressibilityProperty').set('Compressibility', 'Incompressible');
model.physics('spf').feature('init1').set('p', '1[atm]');
model.physics('spf').feature('inl1').set('BoundaryCondition', 'LaminarInflow');
model.physics('spf').feature('inl1').set('U0in', 'velocity');
model.physics('spf').feature('inl1').set('Uav', 'velocity');
model.physics('spf').feature('inl1').set('Lentr', '0.01');
model.physics('spf').feature('out1').set('p0', 'press');
model.physics('chds').field('concentration').component({'cDiuron'});
model.physics('chds').feature('cdm1').set('u_src', 'root.mod1.u');
model.physics('chds').feature('cdm1').set('D_0', {'DDiuron'; '0'; '0'; '0'; 'DDiuron'; '0'; '0'; '0'; 'DDiuron'});

```

```

model.physics('chds').feature('cdm1').set('DiffusionMaterialList', 'mat1');
model.physics('chds').feature('cdm1').name('Convection and Diffusion');
model.physics('chds').feature('init1').set('cDiuron', '1e-16');
model.physics('chds').feature('reac1').set('R', 'rDiuron');
model.physics('chds').feature('in1').set('c0', 'c0Diuron');

model.mesh('mesh1').feature('size').set('table', 'cfd');
model.mesh('mesh1').feature('size1').set('table', 'cfd');
model.mesh('mesh1').feature('size1').set('haut0', 3);
model.mesh('mesh1').feature('bl1').feature('blp1').set('blnlayers', '2');
model.mesh('mesh1').feature('bl1').feature('blp1').set('blhminfact', '5');
model.mesh('mesh1').run;

model.result.table('tbl1').comments('Line Integration 1 (chds.tfluxx_cCO2)');
model.result.table('tbl2').comments('Line Integration 2 (chds.tfluxx_cCO2)');
model.result.table('tbl3').comments('Line Integration 3 (chds.tfluxx_cCHCOOH)');
model.result.table('tbl4').comments('Line Integration 4 (chds.tfluxx_cHCHO)');
model.result.table('tbl5').comments('Line Integration 5 (chds.tfluxx_cCH3OH)');
model.result.table('tbl6').comments('Line Integration 6 (chds.tfluxx_cCH4)');
model.result.table('tbl7').comments('Line Integration 7 (chds.tfluxx_cH2)');

model.study.create('std1');
model.study('std1').feature.create('stat', 'Stationary');

model.sol.create('sol1');
model.sol('sol1').study('std1');
model.sol('sol1').attach('std1');
model.sol('sol1').feature.create('st1', 'StudyStep');
model.sol('sol1').feature.create('v1', 'Variables');
model.sol('sol1').feature.create('s1', 'Stationary');
model.sol('sol1').feature('s1').feature.create('fc1', 'FullyCoupled');
model.sol('sol1').feature('s1').feature.create('d1', 'Direct');
model.sol('sol1').feature('s1').feature.remove('fcDef');

```

```

model.result.dataset.create('cln1', 'CutLine2D');
model.result.dataset.create('cln2', 'CutLine2D');
model.result.dataset.create('cln3', 'CutLine2D');
model.result.create('pg1', 'PlotGroup2D');
model.result('pg1').feature.create('surf1', 'Surface');
model.result.create('pg2', 'PlotGroup2D');
model.result('pg2').feature.create('con', 'Contour');
model.result.create('pg3', 'PlotGroup2D');
model.result('pg3').feature.create('surf1', 'Surface');
model.result.create('pg4', 'PlotGroup1D');
model.result('pg4').set('probetag', 'none');
model.result('pg4').feature.create('Ingr1', 'LineGraph');
model.result.create('pg5', 'PlotGroup1D');
model.result('pg5').set('probetag', 'none');
model.result.export.create('img1', 'Image2D');
model.result.export.create('plot1', 'Plot');
model.result.export.create('data1', 'Data');

model.sol('sol1').feature('st1').name('Compile Equations: Stationary');
model.sol('sol1').feature('st1').set('studystep', 'stat');
model.sol('sol1').feature('v1').set('control', 'stat');
model.sol('sol1').feature('s1').set('control', 'stat');
model.sol('sol1').feature('s1').set('stol', '0.001');
model.sol('sol1').feature('s1').feature('fc1').set('dtech', 'hnlm');
model.sol('sol1').feature('s1').feature('fc1').set('maxiter', '5000');
model.sol('sol1').feature('s1').feature('d1').set('linsolver', 'pardiso');
model.sol('sol1').runAll;

model.result.dataset('cln1').name('Centerline');
model.result.dataset('cln1').set('genpoints', {'0' '0.1'; '21' '0.1'});
model.result.dataset('cln2').name('Cross section');
model.result.dataset('cln2').set('genpoints', {'10' '0'; '10' '0.2'});
model.result.dataset('cln3').name('End of Channel');
model.result.dataset('cln3').set('genpoints', {'21' '0'; '21' '0.2'});

```

```
model.result('pg1').name('Velocity (spf)');
model.result('pg1').set('title', 'Surface: Velocity magnitude (m/s) ');
model.result('pg1').set('frametype', 'spatial');
model.result('pg1').set('titleactive', false);
model.result('pg2').name('Pressure (spf)');
model.result('pg2').set('title', 'Contour: Pressure (Pa) ');
model.result('pg2').set('frametype', 'spatial');
model.result('pg2').set('titleactive', false);
model.result('pg2').feature('con').set('expr', 'p');
model.result('pg2').feature('con').set('unit', 'Pa');
model.result('pg2').feature('con').set('descr', 'Pressure');
model.result('pg2').feature('con').set('number', '40');
model.result('pg3').name('Concentration (chds)');
model.result('pg3').set('title', 'Surface: Concentration (mol/m<sup>3</sup>) ');
model.result('pg3').set('titleactive', false);
model.result('pg3').feature('surf1').set('expr', 'cDiuron');
model.result('pg3').feature('surf1').set('unit', 'mol/m^3');
model.result('pg3').feature('surf1').set('descr', 'Concentration');
model.result('pg4').name('Concentration profile @ centerline');
model.result('pg4').set('data', 'cin1');
model.result('pg4').set('title', 'Concentration profile');
model.result('pg4').set('titleactive', true);
model.result('pg4').set('xlabel', 'Microchannel length @ Centerline (mm)');
model.result('pg4').set('xlabelactive', true);
model.result('pg4').set('ylabel', 'Concentration (ppm)');
model.result('pg4').set('ylabelactive', true);
model.result('pg4').set('legendpos', 'upperleft');
model.result('pg4').feature('Ingr1').name('Diuron');
model.result('pg4').feature('Ingr1').set('data', 'cin1');
model.result('pg4').feature('Ingr1').set('expr', 'cDiuron');
model.result('pg4').feature('Ingr1').set('unit', 'mol/m^3');
model.result('pg4').feature('Ingr1').set('descr', 'Concentration');
model.result('pg4').feature('Ingr1').set('legend', true);
model.result('pg4').feature('Ingr1').set('legendmethod', 'manual');
```

```
model.result('pg4').feature('Ingr1').set('legends', {'Diuron'});
model.result('pg5').name('velocity profile');
model.result.export('img1').set('plotgroup', 'pg3');
model.result.export('img1').set('view', 'view1');
model.result.export('img1').set('resolution', '300');
model.result.export('img1').set('imagetype', 'jpeg');
model.result.export('img1').set('jpegfilename', 'Z:\Windows.Documents\Desktop\Concentration profile.jpg');
model.result.export('plot1').set('plotgroup', 'pg4');
model.result.export('plot1').set('plot', 'Ingr1');

%-----
%Numerical data at point a, t=100s-----
cDiuron_a=mphglobal(model,'cDiuron_f');
%Experimental data at point a, t=100s-----
cDiuron_exp_a=0.817;
%Objective function-----
f=((1*((cDiuron_a-cDiuron_exp_a)^2)));
out = model;
```

The example of objective function in MATLAB program for diuron degradation is as follow:

```
%%fminsearch: find minimum of unconstrained multivariable function using
%derivative-free method

clear all;

%Starting point
k0 = [7e-2]; %initial guest

options=optimset('Display','iter','PlotFcns',@optimplotfval,'ToX',1e-6,'Tolfun',1e-6);
[k,fval,exitflag,output]=fminsearch('corona_diuron_1st_order_kap_100s',k0,options)
```



APPENDIX G

TOXICITY TEST

The toxicity of treated solution after diuron degradation was tested. Two protocols were used to determine the toxicity that is mitotic index and aberration index. As diuron is degraded, many intermediates are formed. However, total toxicity of treated solution reduces when compared with the toxicity of pure diuron. Figure G.1 and G.2 shows mitotic index and aberration index of diuron degradation under no anion contamination and anion contamination. Controlled experiment is the toxicity of pure deionized water.

Definition of mitotic index and aberration index

1. **Mitotic index** is the sum of all undergoing mitosis cells in phase as prophase, metaphase, anaphase and telophase to the total number of cells
2. **Aberration index** is the sum of all non-undergoing mitosis cells to the total number of cells

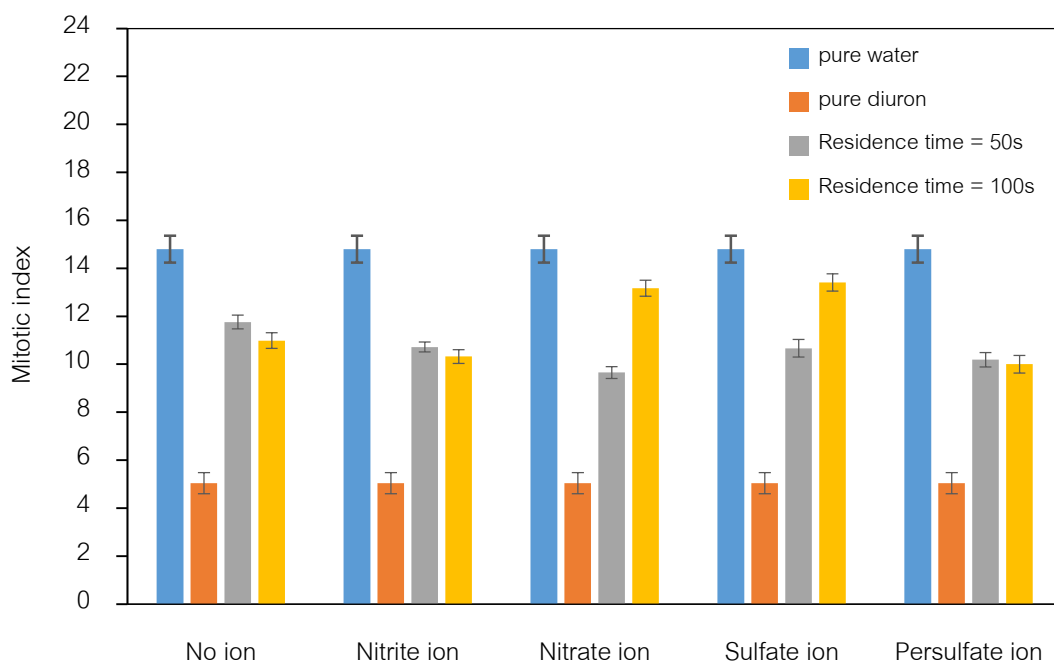


Figure G.1 Mitotic index of treated solution after diuron degradation under no anion contamination and anion contamination

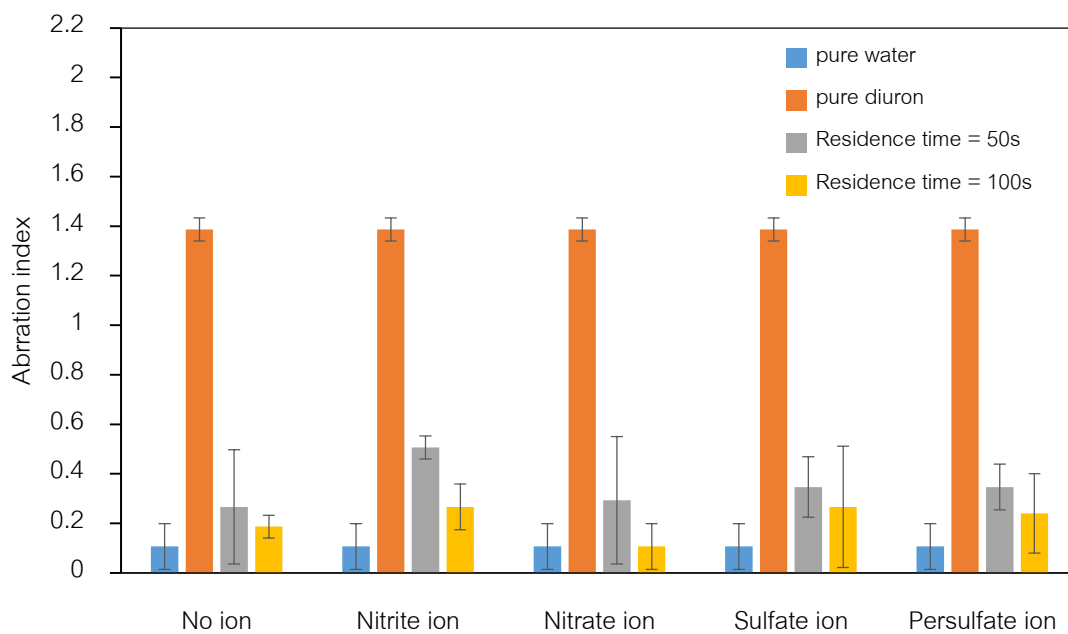


Figure G.2 Aberration index of treated solution after diuron degradation under no anion contamination and anion contamination

APPENDIX H

PUBLICATIONS

G.1 International journal

1. Worachate Khongthon, Goran Jovanovic, Alex Yokochi, Polkit Sangvanich and Varong Pavarajarn. "Degradation of diuron via an electrochemical advanced oxidation process in a microscale-based reactor". *Chemical Engineering Journal*, 2016. 292: p. 298 – 307.

2. Worachate Khongthon and Varong Pavarajarn. "Effect of nitrate and sulfate contamination on degradation of diuron via electrochemical advanced oxidation in a microreactor". *Accepted in Engineering Journal*.

G.2 International proceeding

1. Worachate Khongthon, Goran N. Jovanovic, Alex Yokochi and Varong Pavarajarn. "Degradation of diuron by corona discharge in microreactor". 9th World Congress of Chemical Engineering (WCCE9), August 18 - 23, 2013, South of Korea

2. Rungthip Noisomran, Worachate Khongthon and Varong Pavarajarn. "Photocatalytic degradation of diuron on titanium dioxide in microreactor". 9th World Congress of Chemical Engineering (WCCE9), August 18 - 23, 2013, South of Korea

3. Worachate Khongthon, Goran Jovanovic, Alex Yokochi, Polkit Sangvanichc and Varong Pavarajarn. "Effects of nitrate, nitrite, sulfate and persulfate ions on diuron degradation via corona discharge in microreactor". 2015 AIChE Annual Meeting, November 8 - 13, 2015, USA

4. Rungthip Noisomran, Worachate Khongthon, Polkit Sangvanichc and Varong Pavarajarn. "Photocatalytic degradation of diuron in microreactor". 2015 AIChE Annual Meeting, November 8 - 13, 2015, USA

VITA

Mr. Worachate Khongthon was born on June 20, 1985, in Pattani, Thailand. He received the Bachelor's Degree of Engineering with a major in Chemical Engineering from Faculty of Engineering, Prince of Songkla University, Songkhla in 2008. He continuously entered the Doctoral degree at Center Excellence in Particle Technology (CEPT), Department of Chemical Engineering, Faculty of Engineering, Chulalongkorn University, Thailand since June 2008. He also received scholarship from the Thailand Research Fund (TRF) through the Royal Golden Jubilee Ph.D. Program. During his graduate study, he spent a period of one year in School of Chemical, Bioengineering and Environmental Engineering, Oregon State University, Oregon, USA for research aboard.

